universität wien

MASTERARBEIT / MASTER'S THESIS

Titel der Masterarbeit / Title of the Master's Thesis

„ Immunomodulatory role of A20 in KRAS-driven lung adenocarcinoma“

verfasst von / submitted by

Monika Homolya

angestrebter akademischer Grad / in partial fulfillment of the requirements for the degree of

Master of Science (MSc)

Wien, 2023 / Vienna, 2023

Studienkennzahl lt. Studienblatt / degree programme code as it appears on the student record sheet:	UA 066 830
Studienrichtung lt. Studienblatt / degree programme as it appears on the student record sheet:	Masterstudium Molekulare Mikrobiologie, Mikrobielle Ökologie und Immunbiologie
Betreut von / Supervisor:	Univ.-Prof Dr. Emilio Casanova, PhD

Table of Contents

Acknowledgments

I wish to express my gratitude to Prof. Emilio Canasova for allowing me to work in his laboratory. Additionally, my heartfelt thanks go to my supervisor, Dr. Herwig Moll, for affording me the opportunity to contribute to this project and for teaching me most of the techniques. I am also appreciative of his constructive critique, patience and the scientific autonomy he granted, which allowed me to explore my curiosity and learn from my mistakes. In addition, I would like to thank Daniel and George whose' company made every day work fun and interesting. I also owe a big thank you to Margarita, who always encouraged and urged me to write my thesis. Moreover, I want to thank my friend Petra, my brother Viktor and my family for their emotional support and advice during times of need.

Last but not least I am most grateful to my partner and best friend Zoltán, for his endless support, patience and funny comments that delighted my days. Without his amazing cooking and continuous encouragement I wouldn’t have been able to write this thesis.

Abstract

Lung cancer ranks highest in global cancer mortality, with the most prevalent type lung adenocarcinoma (LUAD), comprising 40% of all lung cancer cases. Despite immune checkpoint therapy being standard for non-targetable KRAS mutant LUAD, responses are limited, underlining the need for improved prognostic markers and therapeutic strategies.

Recent findings from our laboratory have elucidated that the anti-inflammatory protein A20 acts as a tumor suppressor in both patients and experimental mouse models of KRAS-mediated LUAD. In contrast, systemic downregulation of A20 alters the tumor microenvironment to a tumor suppressive state reducing tumor growth and prolonging survival of experimental mice. To study how A20 deficient tumor cells escape the immune system we generated and characterized A20 deficient mouse tumor cells. Our data demonstrated that A20 knockout tumor cells evade immune surveillance by progressively upregulating the expression of checkpoint inhibitor Programmed Death-Ligand 1 (PD-L1) resulting in reduced $CD8^+$ T cell populations infiltrating the tumor. Conversely, mice exhibiting systemic downregulation of A20 show increased tumor infiltration of $CD4^+$ and $CD8^+$ T cells compared to control wild-type mice.

In summary, our data demonstrates that A20 features tumor suppressive properties in KRAS-driven tumor cells, whereas its expression in immune cells acts as a tumor promotor. Accordingly, adoptive transfer of immune cells with A20 downregulation could offer a safe approach to complement and enhance the treatment effectiveness for patients with KRAS-driven LUAD.

Kurzfassung

Lungenkrebs steht bei der weltweiten Krebssterblichkeit an erster Stelle, wobei der häufigste Typ, das Lungenadenokarzinom (LUAD), 40 % aller Lungenkrebsfälle ausmacht. Obwohl die Immun-Checkpoint-Therapie bei nicht zielgerichtetem LUAD mit KRAS-Mutation zum Standard gehört, ist das Ansprechen begrenzt, was den Bedarf an verbesserten prognostischen Markern und therapeutischen Strategien unterstreicht.

Jüngste Erkenntnisse aus unserem Labor haben gezeigt, dass das entzündungshemmende Protein A20 sowohl in Patienten- als auch in experimentellen Mausmodellen von KRAS-vermitteltem LUAD als Tumorsuppressor wirkt. Im Gegensatz dazu verändert die systemische Herunterregulierung von A20 die Mikroumgebung des Tumors in einen tumorsuppressiven Zustand, wodurch das Tumorwachstum reduziert und das Überleben der experimentellen Mäuse verlängert wird. Um zu untersuchen, wie A20-defiziente Tumorzellen dem Immunsystem entkommen, haben wir Tumorzellen aus A20-defizienten Mäusen erzeugt und charakterisiert. Unsere Daten zeigen, dass sich A20-Knockout-Tumorzellen der Immunüberwachung entziehen, indem sie die Expression des Checkpoint-Inhibitors Programmed Death-Ligand 1 (PD-L1) progressiv hochregulieren, was zu einer reduzierten $CD8^+$-T-Zellpopulation in den Tumoren führt. Umgekehrt zeigen Mäuse, bei denen A20 systemisch herunterreguliert wird, eine erhöhte Infiltration von $CD4^+$ und $CD8^+$ T-Zellen in den Tumor im Vergleich zu Wildtyp-Kontrollmäusen.

Zusammenfassend zeigen unsere Daten, dass A20 in KRAS-getriebenen Tumorzellen und Immunzellen eine gegensätzliche Rolle spielt, wobei die Herunterregulierung der A20-Expression in Immunzellen die Mikroumgebung des Tumors in einen tumorsuppressiven Zustand versetzen kann. Daher könnte adoptiver Transfer von Immunzellen, in denen die A20 Expression verringert wird, einen sicheren Ansatz zur Ergänzung und Verbesserung der Behandlungseffektivität für Patienten mit KRAS-getriebener LUAD darstellen.

List of Abbreviations

LUAD: Lung adenocarcinoma

KRAS: Kirsten rat sarcoma viral oncogene homolog

NSCLC: non-small cell lung cancer

A20/TNFAIP3: TNF Alpha Induced Protein 3

FDA: U.S. Food and Drug Administration

EGFR: Epidermal growth factor receptor

PD-1: Programmed Cell Death Protein 1

PD-L1: Programmed Cell Death 1 Ligand 1

GDP: Guanosine diphosphate

GTP: Guanosine triphosphate

MAPK: Mitogen-activated protein kinases

PI3K: Phosphatidylinositol 3-kinases

TME: Tumor microenvironment

DNA: Deoxyribonucleic acid

NF-κB: nuclear factor 'kappa-light-chain-enhancer' of activated B-cells

TNF-α: Tumor necrosis factor α

TNFR: TNF receptor

IFN-γ: Interferon gamma

TLR: Toll-like receptor

CD8: Cluster of differentiation 8

MHC-1 or MHC-2: Major histocompatibility complex 1 or 2

IL-6: Interleukin 6

EDTA: Ethylenediaminetetraacetic acid

DMSO: Dimethylsulfoxide

PCR: Polymerase chain reaction

FACS: Fluorescence-activated cell sorting or flow cytometry

CRISPR: Clustered regularly interspaced short palindromic repeats

Cas9: CRISPR-associated protein 9

RNA: Ribonucleic acid

JAK: Janus kinase

STAT: Signal transducer and activator of transcription

1. Introduction

1.1 Lung cancer

Lung cancer is the second most frequently diagnosed cancer globally, with estimated 19.3 million new cancer cases reported in 2020, and is the leading cause of cancer-related deaths worldwide in both sexes (Fig. 1) [1,2]. Although the overall mortality rate of lung cancer has slowly begun to decline due to better treatment options, the 5-year survival rate of lung cancer remains low, ranging from 2% to 20%, compared to other types of cancers (Fig. 2) [2–5]. This is largely due to the late diagnosis of the disease, often at advanced stages [2].

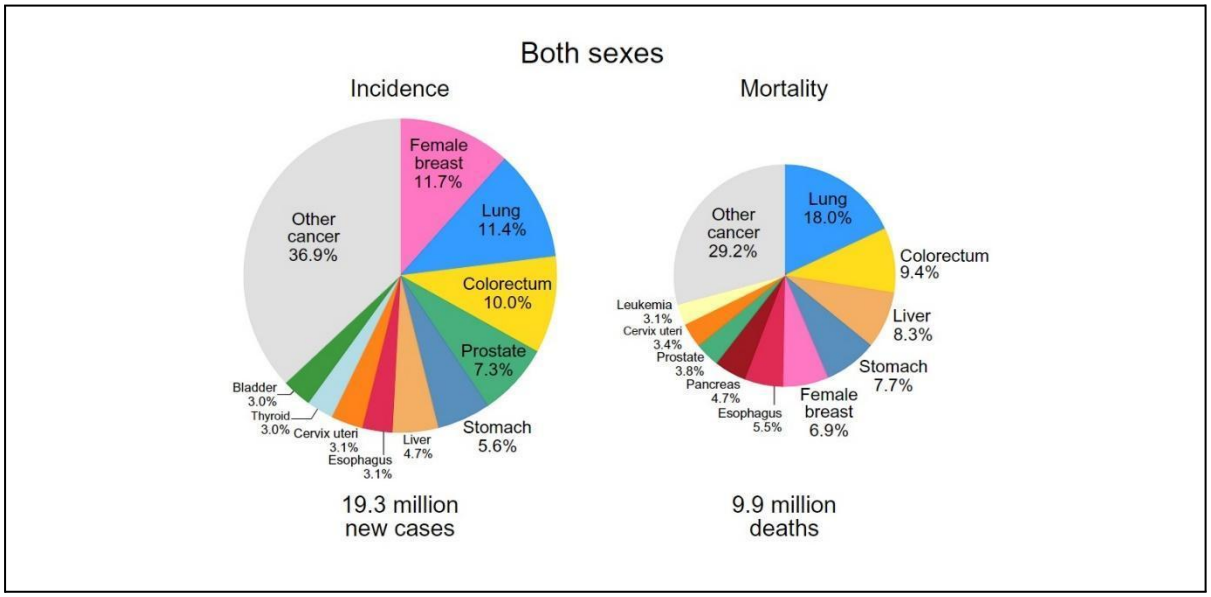

Figure 1: Incidence and mortality rates of Lung cancer worldwide. [1]

Lung cancer can be classified histologically into two main types: small-cell lung cancer and non-small cell lung cancer (NSCLC) (Fig. 3). Small-cell lung cancer, which is derived from neuroendocrine cells, accounts for approximately 15% of lung cancer cases and is characterized by smaller tumor cells and a highly aggressive nature, frequently accompanied by metastasis at the time of diagnosis [6]. Non-small cell lung cancer, accounting for 85% of cases, arises from lung epithelial cells [5,7] and can further be subdivided into three major histological subtypes: Large–cell carcinomas, Squamous-cell carcinomas and Adenocarcinomas based on cell morphology and transformed cells (Fig. 3) [4,7–9].

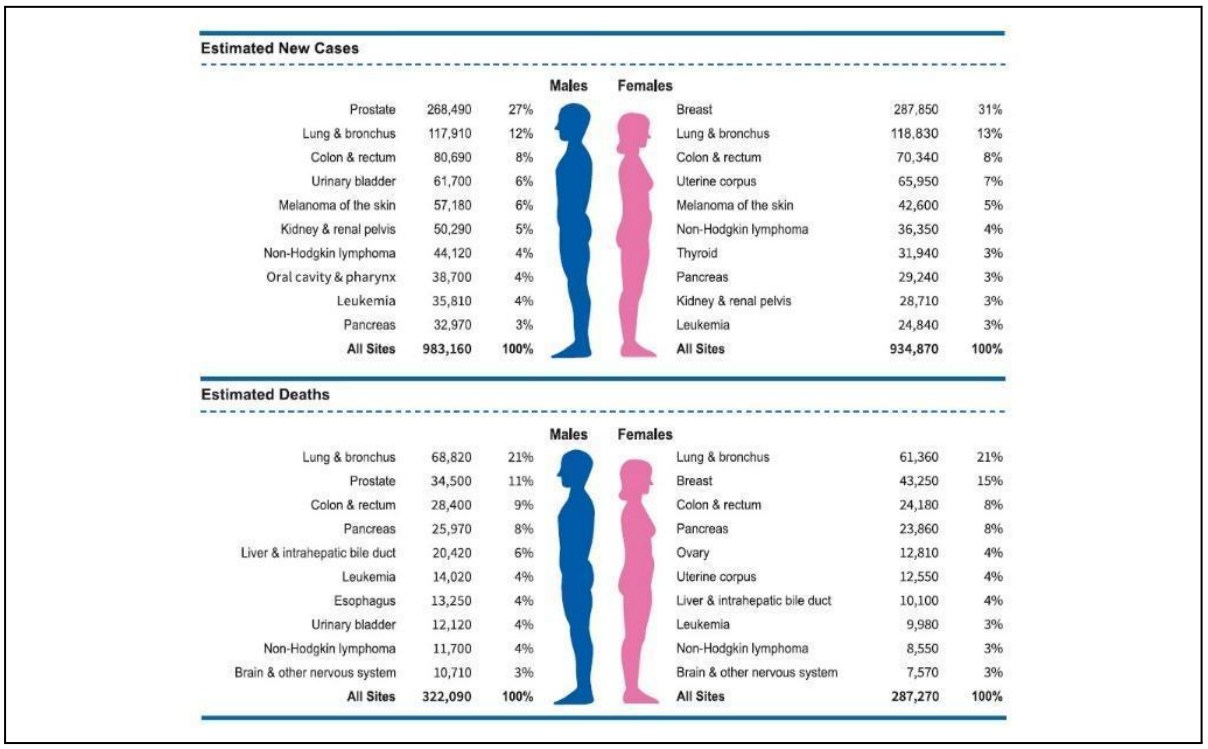

Estimated New Cases

Males			Females		
Prostate	268,490	27%	Breast	287,850	31%
Lung & bronchus	117,910	12%	Lung & bronchus	118,830	13%
Colon & rectum	80,690	8%	Colon & rectum	70,340	8%
Urinary bladder	61,700	6%	Uterine corpus	65,950	7%
Melanoma of the skin	57,180	6%	Melanoma of the skin	42,600	5%
Kidney & renal pelvis	50,290	5%	Non-Hodgkin lymphoma	36,350	4%
Non-Hodgkin lymphoma	44,120	4%	Thyroid	31,940	3%
Oral cavity & pharynx	38,700	4%	Pancreas	29,240	3%
Leukemia	35,810	4%	Kidney & renal pelvis	28,710	3%
Pancreas	32,970	3%	Leukemia	24,840	3%
All Sites	**983,160**	**100%**	**All Sites**	**934,870**	**100%**

Estimated Deaths

Males			Females		
Lung & bronchus	68,820	21%	Lung & bronchus	61,360	21%
Prostate	34,500	11%	Breast	43,250	15%
Colon & rectum	28,400	9%	Colon & rectum	24,180	8%
Pancreas	25,970	8%	Pancreas	23,860	8%
Liver & intrahepatic bile duct	20,420	6%	Ovary	12,810	4%
Leukemia	14,020	4%	Uterine corpus	12,550	4%
Esophagus	13,250	4%	Liver & intrahepatic bile duct	10,100	4%
Urinary bladder	12,120	4%	Leukemia	9,980	3%
Non-Hodgkin lymphoma	11,700	4%	Non-Hodgkin lymphoma	8,550	3%
Brain & other nervous system	10,710	3%	Brain & other nervous system	7,570	3%
All Sites	**322,090**	**100%**	**All Sites**	**287,270**	**100%**

Figure 2: Prevalence and deaths of the ten most common cancer cases in the United States according to latest statistics [2].

Lung adenocarcinoma (LUAD) is the most common type of lung cancer, accounting for around 40-47% of all lung cancers [7,9,10]. LUAD develops from type 2 alveolar cells in the lung after distinct genetic events and lead to the formation of a malignant epithelial neoplasm [7]. Lung Squamous-cell carcinoma (LUSC) develops from basal epithelial cells in the airways, while the third subtype, Large cell carcinoma (LCC), represents a more heterogeneous group of malignant neoplasms with epithelial origin [8,9].

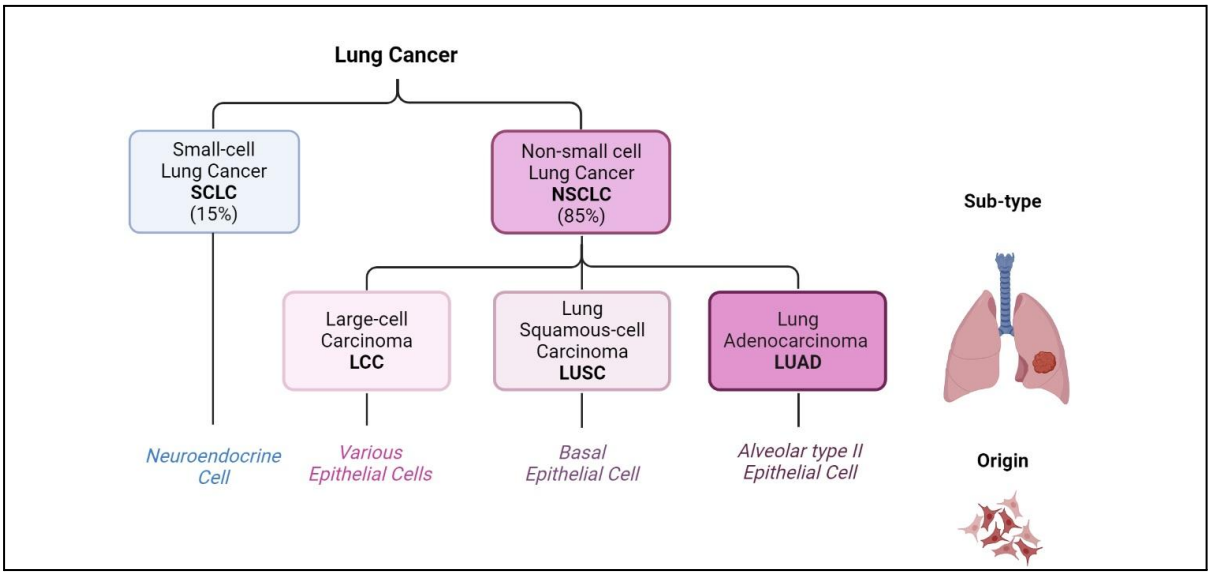

Figure 3: Lung cancer classification based on histological types and subtypes. Figure was adapted from Sánchez-Ortega et al. [7] with modifications using Bio Render [www.biorender.com]

All of these subtypes are associated with tobacco smoking, although some of the NSCLC subtypes are commonly associated with non-smoking history, such as EGFR mutant driven tumors [11,12].

1.1.1 Risk factors

The risk factors for lung cancer vary in their impact based on the individual's age, sex, genetic predisposition, geographic location, and environmental exposure [5,13,14]. Smoking is the most well-known risk factor for lung cancer. According to the International Agency for Research on Cancer, cigarette smoke contains 55 known carcinogenic substances that can cause genetic changes such as sequence alterations, methylation pattern changes, segment amplification or deletion, and chromosomal changes [5,10]. Other forms of tobacco use such as cigar and pipe smoking as well as second-hand smoke exposure also increase the risk of lung cancer development [15]. Naturally, the quantity and duration of smoking are directly proportional to the increased risk of tumor initiation and growth [15,16]. Environmental factors, such as exposure to asbestos and diesel exhaust, as well as coal mining, chimney sweeping, and painting, also increase the risk of lung cancer [17]. In addition, exposure to air pollutants, such as particulate matter, nitrogen oxides, nitrogen dioxide, sulfur oxide, arsenic, and residential radon, can increase the risk of lung cancer [17,18]. The role of genetic factors in increasing susceptibility to lung cancer was also proposed [16].

1.1.2 Staging of Non-small Cell Lung Cancer

Non-small cell lung cancer staging is a crucial process in determining the extent of cancer spread, which helps guide treatment decisions [10]. The predominant TNM classification system categorizes lung cancer into stages, based on factors such as tumor size, lymph node involvement, and metastasis (Fig. 4) [19,20]. Other factors such as histology and genetic variations of the tumor may additionally influence the selection of treatment strategies. The staging of NSCLC is generally expressed through Roman numerals, ranging from 0 to IV. A lower stage indicates a less extensive spread of the cancer and a better prognosis [19,20]. Stage 0 NSCLC, also known as carcinoma/tumor in-situ, is a preliminary stage in which the cancer is confined to the top lining of the lung or bronchus and has not metastasized.

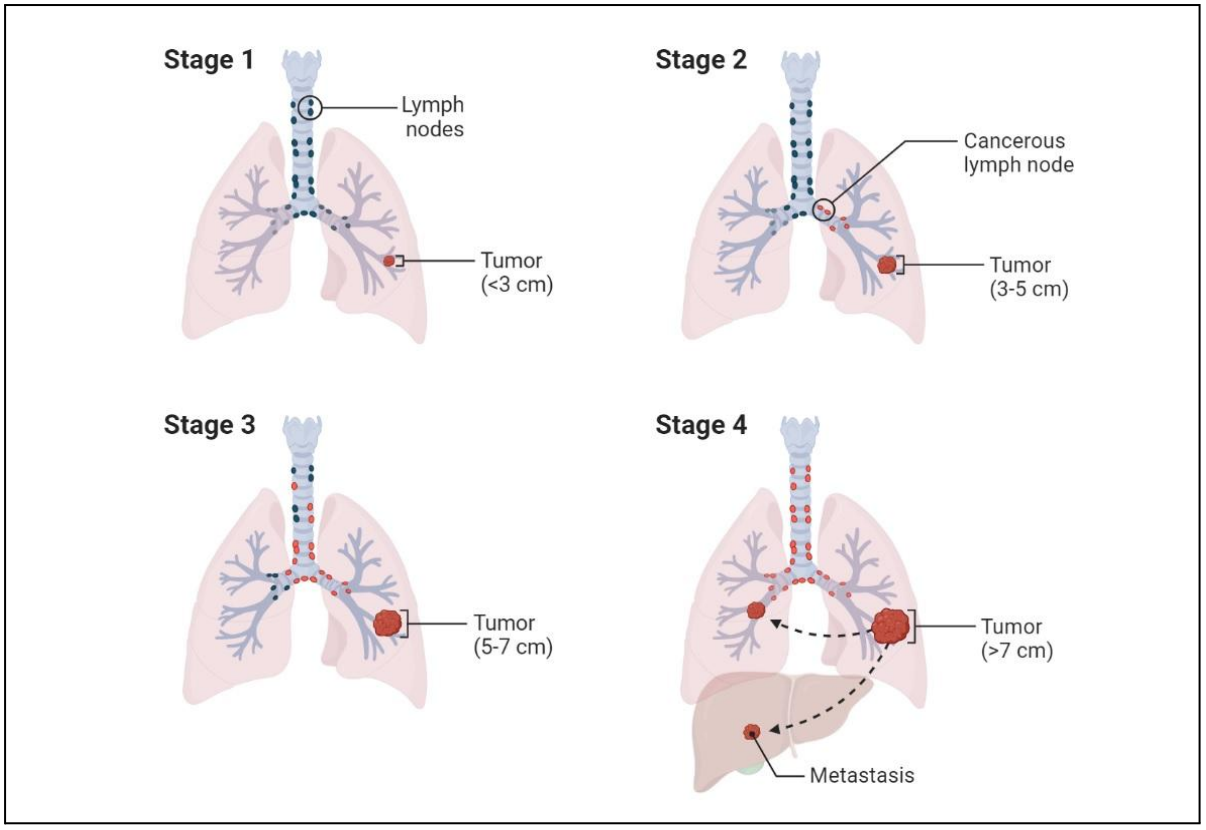

Figure 4: Staging of lung cancer. Stage 1 is localized to the lung, Stage 2 involves nearby lymph nodes, Stage 3 has further lymph node involvement and nearby tissue, and Stage 4 signifies distant metastasis to other organs. Figure made by BioRender.

Stage I NSCLC is divided into two sub-stages, 1A and 1B, based on the size of the tumor. In this stage, the cancer has not yet spread to the lymph nodes or other parts of the body. Stage II NSCLC is further divided into two sub-stages, IIA and IIB, with each sub-stage being further categorized based on the size, location, and spread of the tumor. These tumors may be larger than those in stage I and may have started to spread to nearby lymph nodes, but the cancer has not yet spread to distant organs. In Stage III NSCLC, the cancer has spread to the lymph nodes in the mediastinum (the area in the chest between the lungs) and is further classified into IIIA, IIIB, or IIIC, depending on the size, location, and extent of spread. Stage IV NSCLC is the most advanced form of the disease, in which the cancer has metastasized to other parts of the body, including the lung lining [19,20].

1.1.3 Mutational landscape of NSCLC

Cancer is a molecularly heterogeneous disease where the different clones of neoplastic cells originate from one or more altered cells and gain different types and number of mutations over time and this poses challenges for targeted therapy and other treatment approaches as well [21]. The most commonly observed activating mutations in NSCLC occur in the Kirsten rat sarcoma viral oncogene homolog (KRAS) and epidermal growth factor receptor (EGFR) (as seen in Fig. 5) [5,22,23]. Other common mutations such as alterations in the tumor suppressor gene p53 are typically found in more advanced tumors, which indicates that this plays a role in the tumor's progression rather than initiation [15].

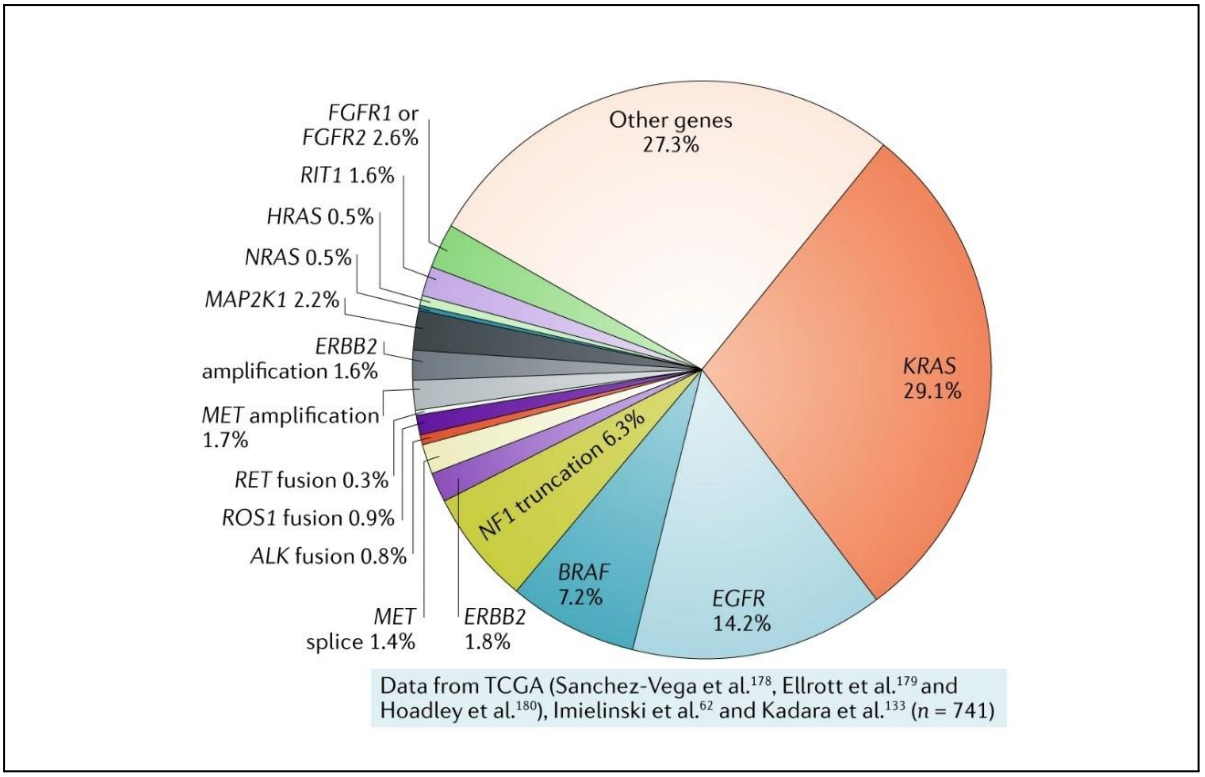

Figure 5: Mutational landscape of NSCLC in early stages. image adapted from Skoulidis et al. [22]

In addition, the most prevalent genetic alteration in the ALK transmembrane receptor tyrosine kinase gene is the EML4-ALK fusion oncogene, leading to the constitutive activation of the ALK [24]. Other less frequent but noteworthy oncogenic mutations have been identified in genes such as AKT, BRAF, PIK3, MET, ERBB2, and NRAS, accounting for less than 30% of LUAD cases in early stages [22]. In about 27% of all lung adenocarcinoma occurrences, the primary mutations are still not known (Fig. 5) [22].

1.2 RAS oncogene family

RAS proto-oncogenes are frequently mutated in a variety of human cancers such as in about 90-95% of pancreatic cancers, 40-50% of colorectal cancers and about 20-30 % of all lung cancers dependent on the study which makes it the most frequently mutated oncogene family [25–28].

The RAS family proteins are encoded by highly homologous genes with 85% sequence identity and include HRAS, NRAS, KRAS4A and KRAS4B where the lesser two are encoded by the same gene and arise from alternative RNA splicing [29]. KRAS4B is the predominant splice variant expressed in many tissues but KRAS 4A also has its functions in some tissues [30]. Members of the RAS family are receptor-coupled G-proteins, which function as a molecular binary switch by activating molecules of different signaling pathways regulating normal cell proliferation, differentiation and cell survival [29,30] (Fig. 6).

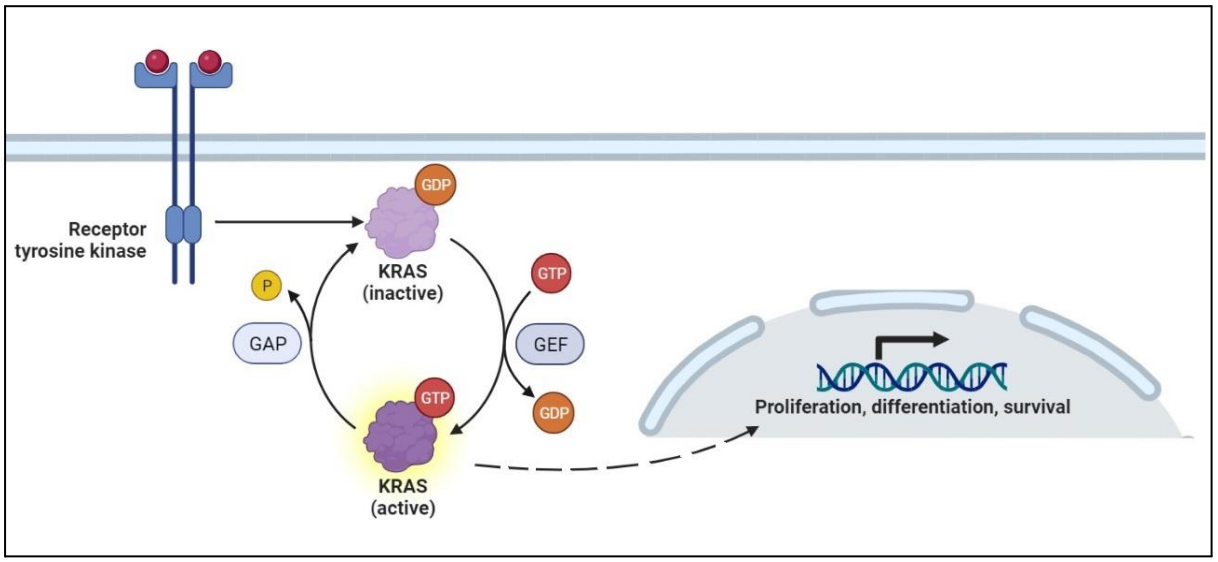

Figure 6: RAS proteins act as binary on-off switches, cycling between GDP-bound inactive states and GTP-bound active states, regulated by RasGEFs and GAPs. Mutant KRAS constitutively binds GTP and activates downstream pathways, promoting cell proliferation, survival, and metastasis. Figure generated by Biorender.

Under normal conditions where the cell is not dividing, RAS remains in an inactive state, bound to GDP. However, when external signals, like the binding of epidermal growth factor (EGF) to the transmembrane receptor tyrosine kinase (EGFR), are received, the receptor undergoes a temporary structural change and its intracellular domain becomes phosphorylated. This, in turn, recruits RAS through adaptor proteins. Guanine exchange factors (GEF) activate the inactive GDP-bound RAS by

promoting the exchange of GDP with GTP, which then triggers the activation of downstream effectors such as the MAPK and PI3K pathways. Once activated, the RAS-GTP form is inactivated by the GTPase activating protein (GAP), which stimulates the hydrolysis of GTP to GDP [31]. Oncogenic mutations of RAS frequently occur in codon 12, 13, 61 and 146 which results in high affinity binding of GTP and stimulus independent constitutively active state of the protein and loss of GTPase activity, leading to uncontrolled activation of downstream signaling pathways of cell survival, proliferation and metastasis (Fig. 6) [31,32].

1.3 KRAS oncogene

The KRAS isoform is the most frequently altered variant in the RAS family, accounting for about 86% of the mutations [28,33]. It remains the predominant oncogene mutation observed in solid tumors such as lung, colorectal, and pancreatic cancers and appearing in up to 40% of NSCLC cases [34,35]. The G>T transversion mutation, which occurs at codon 12, translates into the replacement of Glycine (G) with Cysteine (C), resulting in the KRAS G12C mutation. This mutation is the most frequently observed in lung adenocarcinoma, present in 41% of patients, and is often associated with a smoking history [33,36,37]. Other common mutations, KRAS G12V and G12D, are also frequently identified (as depicted in Fig. 7) [38]. The expression of mutant KRAS proteins remains stable across various tumor grades, indicating a dependence of these tumors on the sustained activation and signaling of KRAS, rendering it a potential therapeutic target [39,40]. Regrettably, mutated KRAS proteins present significant challenges for therapeutic intervention due to the small GTPase's exceptionally high binding affinity to GTP and the active center's shallow nature [29,32,34,40].

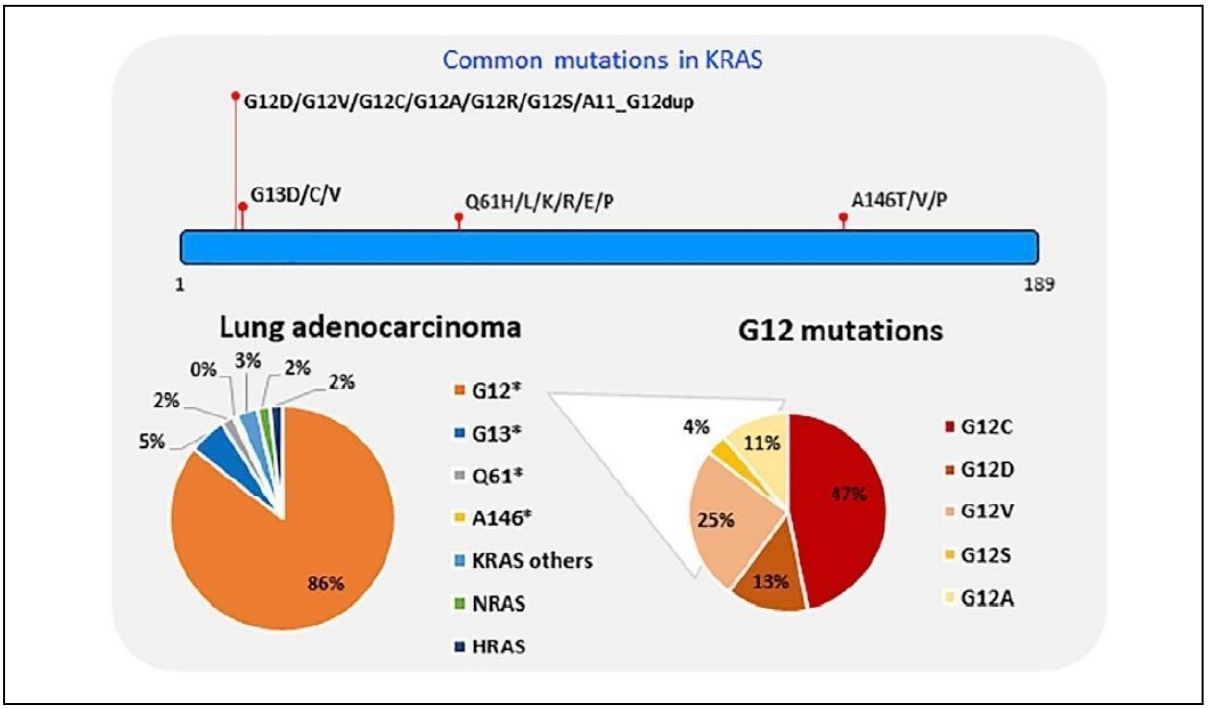

Figure 7: Frequent mutations in KRAS observed in lung adenocarcinoma (LUAD) [34]

Consequently, the design of small molecule inhibitors capable of binding to its active site to specifically block its activity is difficult. Until recently, KRAS was considered undruggable, but in 2021, selective inhibitors against the G12C mutation were approved for clinical application in a specific subset of NSCLC patients [41–43]. The mode of action of these inhibitors is predicated upon their covalent binding to the mutated cysteine of KRAS, thereby keeping the protein in an inactive GDP-bound state. However, there have been ongoing research efforts to develop KRAS-specific inhibitors and therapies against other mutant forms of KRAS, none have reached clinical use [41,44,45]. Moreover, alternate approaches such as blocking the membrane localization of KRAS or directing interventions toward downstream signaling pathways have been suggested as potential therapeutic tactics to inhibit tumor progression [46–48]. Unfortunately, these interventions failed to exhibit a substantial improvement in overall survival according to clinical investigations [49].

1.4 Treatment

The treatment of NSCLC depends on several factors including stage, resectability, performance status, histology, and genomic alterations. Treatment options can be broadly divided into five categories: surgery, chemotherapy, radiotherapy, targeted therapy, and immunotherapy [10,50].

Surgery:

In early-stage NSCLC (Stage I, and II) surgery is typically used to remove the tumor, surrounding tissue and lymph nodes [10]. In locally advanced NSCLC (Stage III), surgery may be an option in some cases if the patient is considered able to tolerate surgery.

Radiotherapy:

Radiotherapy is a commonly employed adjuvant therapy for lung cancer patients [10,51]. It is used to prevent cancer relapse following surgery, as a palliative treatment for patients who are unresponsive to surgery or chemotherapy, and in combination with chemotherapy to improve overall treatment outcomes [51]. Radiotherapy can also be used as an alternative to surgery in early-stage disease and for small tumors where surgery is not an option [10].

Chemotherapy:

Platinum-based doublet chemotherapy, involving the administration of cisplatin or carboplatin in combination with another cytotoxic agent, is a commonly employed treatment for advanced (stage IV) and unresectable tumors [10,51,52]. Adjuvant chemotherapy following surgery is utilized to eliminate any residual cancer cells in patients with stage IIA, IIB, and IIIA NSCLC. Moreover, chemotherapy is used in conjunction with radiotherapy to improve the survival rate of patients with unresectable tumors [10]. Overall, chemotherapy is an effective treatment approach for improving the length and quality of life for individuals with lung cancer at all stages [51].

Targeted therapy:

Targeted therapy is typically used for patients with advanced or metastatic NSCLC and when the tumor has a mutation that can be targeted by an approved drug [5,34].

This type of therapy involves the usage of drugs that specifically inhibit molecules and signaling pathways that are essential for the growth and survival of cancer cells.

Several drugs are approved by the FDA for targeted therapies of NSCLC, with the choice of therapy determined by the specific genetic mutations present in the tumor. Good examples are mutant components of the receptor tyrosine kinase pathway such as EGFR, ALK, ROS1 and mutant forms of KRAS [2]. Targeting therapies for KRAS mutations, a common genetic alteration found in approximately 20-25% of

lung cancer patients [2], are currently only available for the KRAS G12C mutation [53]. For treating these mutations in the second-line setting, following immunotherapy alone or combined with chemotherapy [5,52], the FDA has approved two drugs: Adagrasib and Sotorasib [41,54]. It's important to note that although targeted therapies can exhibit considerable effectiveness, cancer cells often develop resistance to these drugs over time. Therefore, continuous research is being undertaken to overcome this challenge.

Immunotherapy:

Immunotherapy-based treatment has become one of the standard treatments for lung cancer and gradually moved to the front line in the treatment of patients with advanced to early-stage diseases [55,56]. Within the tumor microenvironment during active malignancy, T cells experience continuous exposure to tumor antigens. This prolonged exposure can trigger the upregulation of inhibitory receptors, such as PD-1, on T cells, resulting in T-cell exhaustion. In NSCLC, tumor cells expressing PD-L1 interact with PD-1 on T cells, leading to early exhaustion and inactivation of T cells, thereby reducing immune-mediated killing of tumor cells [55] .

To combat T-cell exhaustion, modulation of inhibitory pathways can be achieved using monoclonal antibodies like anti-PD-1/PD-L1 [57]. These antibodies disrupt the interaction between PD-1 and PD-L1, enhancing immune activity of T cells against the tumor. Despite the approval of drugs like anti-PD-1/PD-L1 as first-line monotherapy or in combination with chemotherapy for advanced NSCLC, there remains a need for improved outcomes, as the median progression-free survival (mPFS) remains below one year [55,56].

1.5 Cancer, tumor microenvironment and inflammation

The tumor microenvironment (TME) does not only contain tumor cells harboring various genetic alterations but is also composed of stromal cells such as fibroblasts, immune cells, vascular cells and the extracellular matrix which further complicates our understanding of tumor biology [58,59]. Tumor cells interact with their surroundings so the composition of the TME and its interaction with tumor cells can either propel tumor onset and expansion or impede tumorigenesis and tumor elimination [58–60]. Typically, cancer cells employ various strategies to alter the tumor microenvironment

in their favor, facilitating their own survival, growth, migration, and evasion from the immune system. [59,61]. For instance, cancer cells may enhance the expression of checkpoint inhibitor molecules like PD-L1 to inhibit T cell function. Alternatively, they may boost the production of molecules that attract macrophages and regulatory T cells, creating an environment of immune suppression and circumventing T cell detection [60] (Fig. 8).

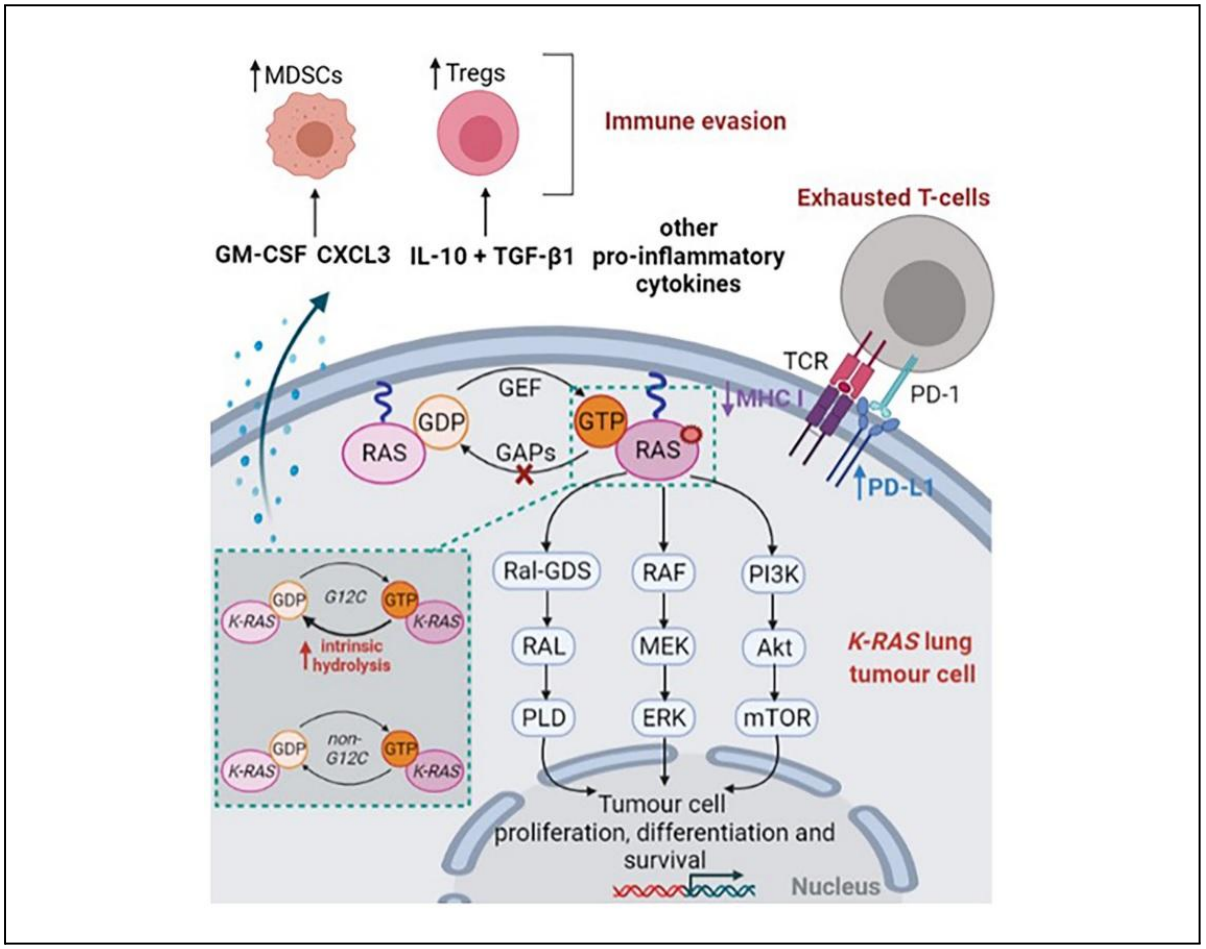

Figure 8: KRAS signaling involves the activation of downstream effector pathways, such as RAF-MEK-ERK and PI3K-AKT-mTOR, leading to cell proliferation, survival, and metastasis. Figure created with BioRender [www.biorender.com].

The persistence of chronic inflammation is one of the important characteristics of malignant tumors [62]. Smoking and other environmental factors can induce chronic inflammation in the lungs that induce DNA damage and increase the likelihood of mutations [36]. Simultaneously, newly emerged KRAS mutations can also contribute to an inflammatory microenvironment by producing pro-inflammatory cytokines and chemokines recruiting immune cells which further fuel inflammation [25,63] as mentioned above.

Hence, dysregulation of inflammation homeostasis can promote cancer initiation and progression, prompting investigations into therapeutic approaches aimed at attenuating inflammation and altering tumor-stroma interactions to favor an anti-tumorigenic microenvironment [63,64,58].

1.6 NF-κB pathway

The NF-κB proteins represent a family of inducible transcriptional factors that regulate the expression of many cellular processes including cell proliferation, survival, apoptosis, inflammatory and immune responses (Fig. 9). Nuclear factor κ B (NF-κB) was first identified in 1986 as a nuclear factor that binds to the enhancer element of the Ig κ light chain of activated B cells [65]. This small protein family includes five structurally related members: RelA (p65), RelB, c-Rel, NF-κB1 and NF-κB2 which form hetero- and homodimers and mediate transcription of target genes [66].

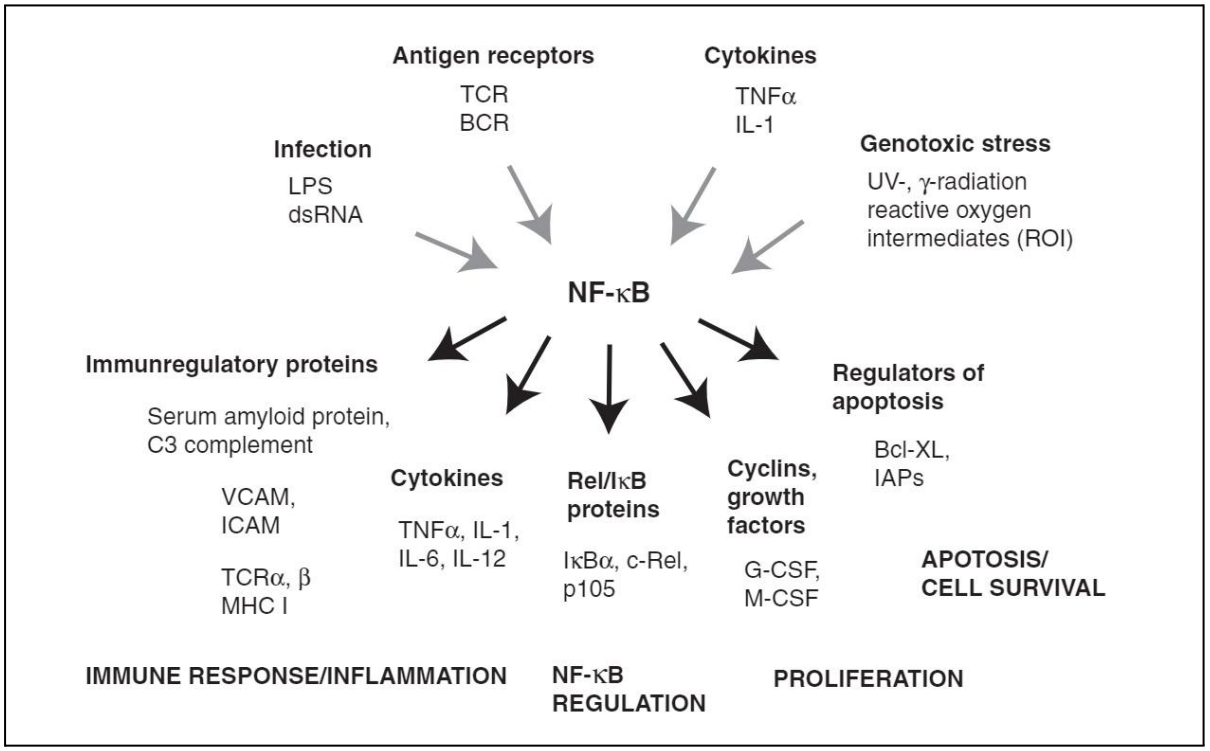

Figure 9: NF-kB signaling regulates many signaling pathways in cells and is the central regulator of inflammation and immune cell activation [65].

All members of the family share structural features on the N terminal Rel homology domain, which is required for dimerisation of the proteins and DNA binding [65]. RelA, RelB and c-Rel possess transactivation domains and are sequestered in the cytoplasm bound to inhibitory proteins of the IkB family proteins in quiescent cells. The other 2 members, NF-κB1 (p50) and NF-κB2 (p52) (synthesized as pro-forms, p105 and p100 respectively) contain inhibitory ankyrin repeats on their C terminal domain and only activate transcription if they are bound to another NF-κB transcription factor which has a transactivation domain [67].

NF-κB activation can occur through the classical/canonical pathway and the alternative/non-canonical pathways which are induced by different stimuli and differ in signaling mechanisms but both are important in the regulation of inflammation and immune regulation [68]. The canonical pathway induced by growth factors, cytokines, mitogens, microbial compounds and stress through the TNF receptor (TNFR), Pattern recognition receptors (PRRs), T cell receptor (TCR), B cell receptor (BCR) and cytokine receptors [69]. In response to the above-mentioned stimuli, the IkB kinase complex (IKK) mediates the site specific phosphorylation of the IkBa inhibitory protein that keeps the NF-κB in an inactive form (Fig. 10) [65].

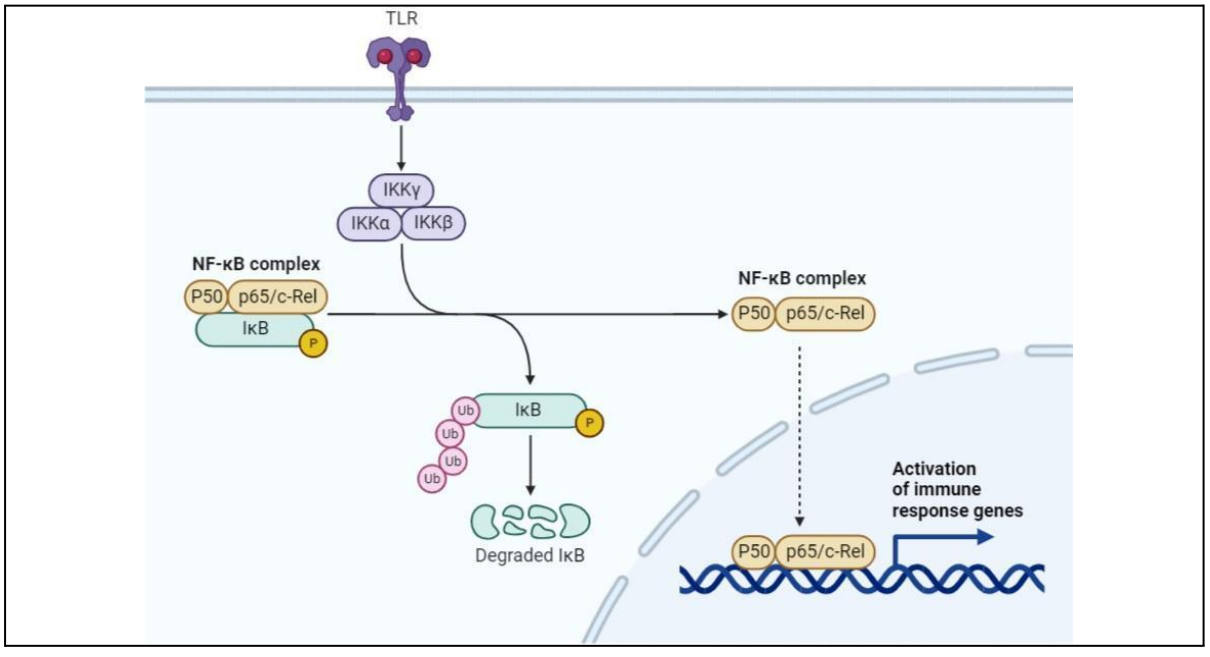

Figure 10: Classical NF-κB signaling pathway. Generated using BioRender.com [www.biorender.com]

The IKK complex is composed of two catalytic subunits IKKα and IKKβ and the third regulatory subunit IKKγ or NEMO (NF-κB essential modulator) [67] and phosphorylates

the IκBα at two N terminal serines and thus triggers its ubiquitin-mediated degradation in the proteasome. The NF-κB dimers (p50/p65) are then released from the inhibition and can translocate to the nucleus and bind to DNA elements [67].

The non-canonical pathway induced by ligands of the TNFR family, including CD40 co-receptor, Lymphotoxin Beta receptor (LTBR), Receptor activator for NF-κB (RANK) and B cell activation factor receptor (BAFFR) and its activation relies on phosphorylation and processing of the precursor p100 protein by IKKα and the NF-κB inducing kinase (NIK) [70]. While the canonical pathway is involved in most immune responses, the non-canonical pathway has a supplementary function and regulates specific adaptive responses together with the canonical pathway [71].

Several studies reported that defects in the regulation of the NF-κB pathway frequently associated with cancer initiation, progression, and resistance to treatment [72]. Enhanced activation of the NF-κB signaling pathway has been documented in various tumors, particularly lymphomas [73,74,75] and has been reported to cooperate with KRAS in lung tumorigenesis [76–78]. Therapeutic targeting of NF-κB activation is challenging due to its complex and pleiotropic role in regulating normal cellular processes. As a result, it's essential to enhance our understanding of how tumors evade inflammatory control and explore ways to address this for the enhancement of treatment strategies.

1.7 A20/ TNFAIP3: TNFα inhibitory protein 3

A20 also known as tumor necrosis factor alpha induced protein 3 (TNFAIP3) is a ubiquitin modifying enzyme and a potent anti-inflammatory protein. It was first identified in 1990 as a primary response gene in human endothelial cells following TNF stimulation and described as a protein protecting cells from TNF-induced apoptosis [79,80]. A20 is induced by several stimuli and acts as a negative regulator of both the canonical and non-canonical NF-κB pathways and suppresses NF-κB signaling downstream of TNFR, IL1R, TLR4, NLRs, CD40, TCRs and BCR thus prevents prolonged immune responses and inflammation [81–84].

A20 is a 90 kDa protein and biochemically functions as a ubiquitin modifying enzyme having both ubiquitin ligase activity and deubiquitinase activity (DUB) as depicted in Fig. 11 [83,84]. The amino terminal ovarian-tumor domain possesses DUB function which is mediated by the Cys103 residue and removes K63 ubiquitin chains

from its target proteins [85,86]. The carboxy terminal of A20 has 7 Zinc finger domains, from which the ZnF4 domain has E3 ligase activity and polyubiquitinates its substrate on K48 residues and physically can bind to K48 polyubiquitin chains, while the ZnF7 domain can bind to M1 linked chains and modulate signaling [87,88].

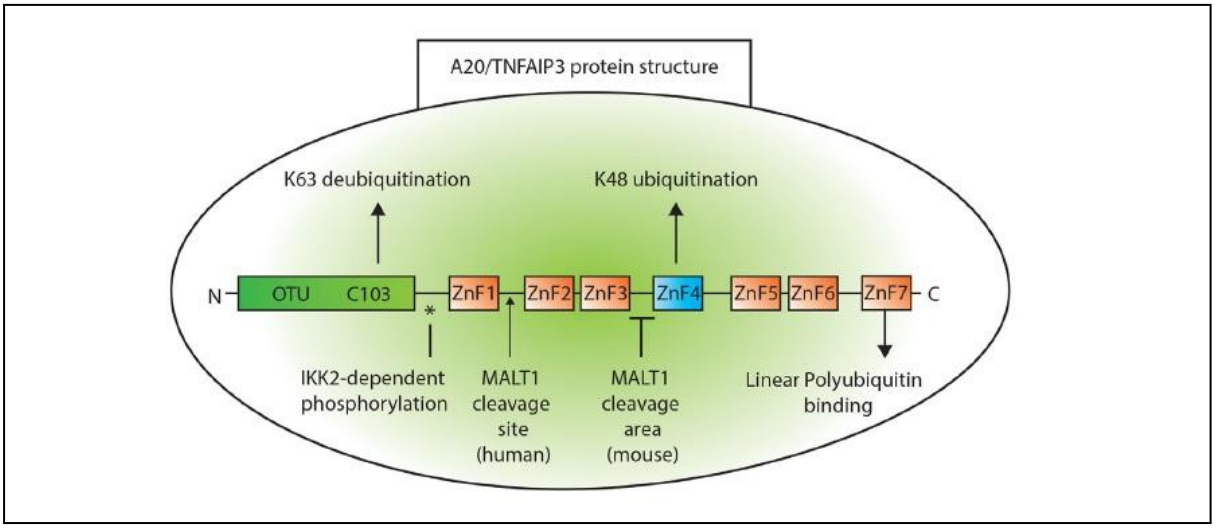

Figure 11: Structure and biochemical properties of A20/TNFAIP3 includes an N-terminal ovarian tumor (OTU) domain and seven zinc fingers (ZnF) on the C-terminal domain [84].

A20's function is best characterized on the TNF signaling pathway, where it exerts its modifying properties by enzymatic and non-enzymatic actions (Fig. 12). Upon TNFα binding to the TNFR protein complex, protein complexes RIP1 (receptor-interacting serine/threonine-protein kinase 1) and TRAF2/TRAF5 are recruited, contributing to the formation of the TNFR complex [84]. Subsequently RIP1 undergoes K63 polyubiquitination facilitated by ubiquitin-conjugating enzyme (Ubc)13 and cellular inhibitor of apoptosis protein (cIAP)1/2 and this RIP1–polyubiquitin assembly acts as a scaffold for the recruitment of transforming growth factor beta-activated kinase 1 (TAK1)-TAB2/3 complex and IKKγ (NEMO) [89]. The linear ubiquitin chain assembly complex (LUBAC) attaches M1 chain on NEMO, thereby recruiting an additional IκB kinase (IKK)-NEMO complex [84] (depicted in Fig. 12). Finally, TAK1 phosphorylates and activates IKK2, which then ultimately results in the phosphorylation and degradation of IκB thereby liberating NF-κB and facilitating its translocation into the nucleus [90].

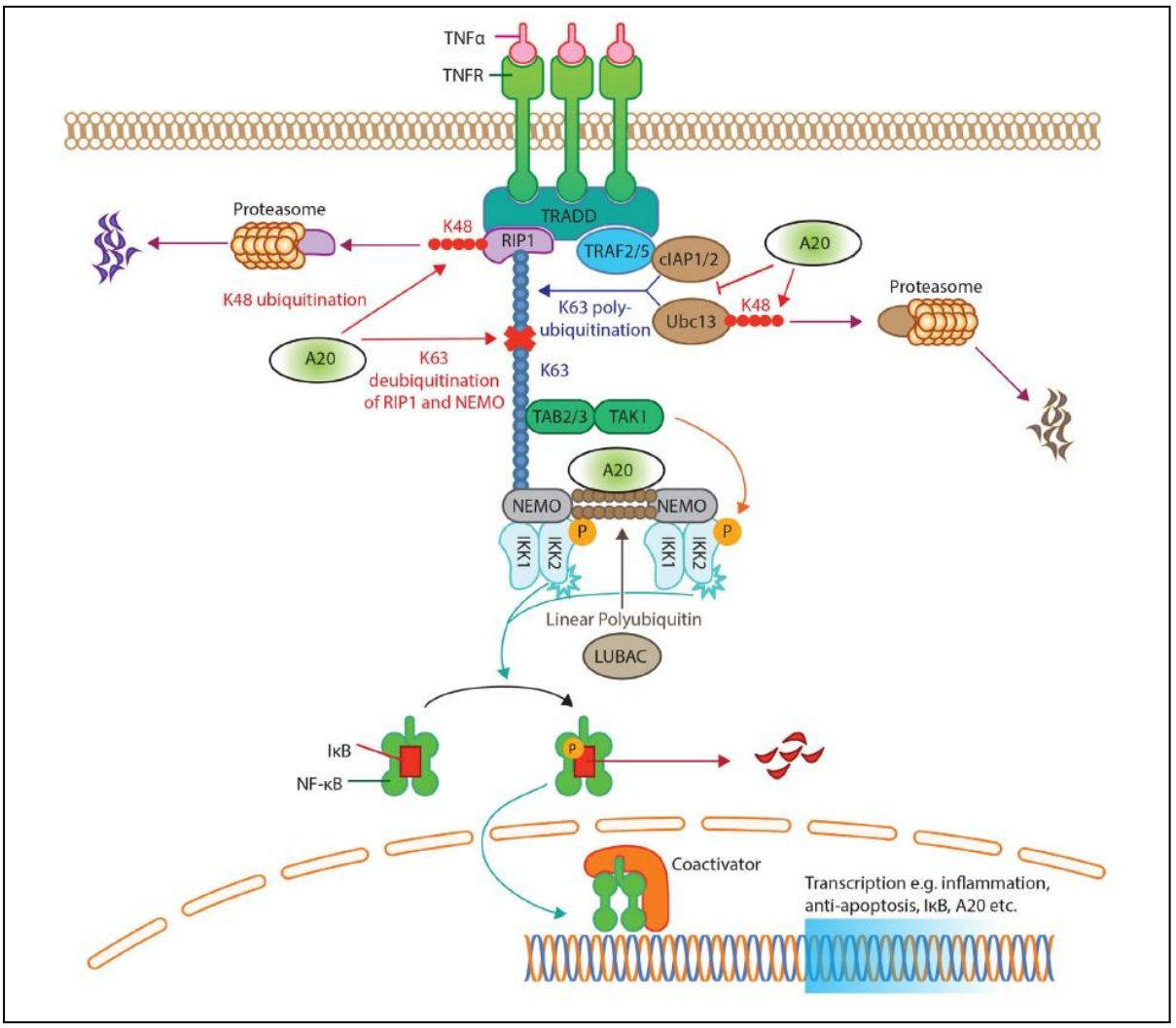

Figure 12: TNF signaling induces activation of the classical NF-κB signaling pathway which is heavily regulated by ubiquitin modifying proteins including A20 [84].

In addition to its role in counteracting NF-κB activation, A20 also has a central role in maintaining cellular equilibrium and carries out diverse functions that vary according to the specific cell type. A20's impact encompasses both positive and negative regulation of cell death [91–94], and it inhibits NLRP3 inflammasome activity [95,96], and Wnt signaling [97,98] . Additionally, it plays a role in modulating antiviral interferon signaling by targeting TBK1/IKKε [99], and control autophagy [100]. Given the wide-reaching regulatory roles of A20 within numerous cellular signaling pathways, its dysregulation has been implicated in the pathogenesis of various autoimmune and autoinflammatory disorders. Its crucial importance in regulation is reflected in the phenotype of mice with germ-line deletion in the A20/TNFAIP3 gene that develop severe multiorgan inflammation and die prematurely [101]. In contrast, A20 heterozygous (A20het or $A20^{\Delta/+}$) mice do not show an overt inflammatory phenotype

other than low-grade cerebral inflammation when unchallenged with normal circulating TNFα and IL-6 levels [102–104]. In humans, haploinsufficiency of A20/TNFAIP3 results in increased NF-κB signaling, NLRP3 inflammasome activity [95,96,105,106], and increased expression of proinflammatory cytokines, which was observed in patients with a rare, early-onset autoinflammatory syndrome ranging from very mild disease to severe multiorgan inflammation [105–110]. Several single-nucleotide polymorphisms (SNPs) in or near the A20 gene, reducing the expression levels of functional A20[111–114], have been linked to autoimmune and inflammatory diseases, including systemic lupus erythematosus (SLE), rheumatoid arthritis, psoriasis, type 1 diabetes and Crohn's disease [115,116] and it has been reported that in cancer A20 can play dual roles, either tumor suppressor or oncogene [81]. In tumors, A20 exhibits various roles across different cancer types. It is frequently inactivated through somatic mutations and/or deletions in B cell lymphomas, where it serves as a tumor suppressor [117]. Similarly, in T cell lymphomas, A20 is also considered a putative tumor suppressor [118]. A20 operates as a tumor suppressor in colorectal cancer (CRC), where reduced expression stemming from genetic and epigenetic changes is associated with unfavorable patient outcomes [119]. In hepatocellular carcinoma (HCC), varying A20 expression levels hint at its potential involvement in tumorigenesis, with higher levels linked to enhanced prognosis and overall survival, underscoring its tumor suppressor role [120]. Similarly, A20 acts as a tumor suppressor in pancreatic and lung cancer [121,122]. Conversely, A20's overexpression in breast cancer aligns with oncogenic processes, promoting proliferation, metastasis, and drug resistance [123,124] and in gastric cancer tissues, where elevated A20 mRNA levels are observed [125]. In gliomas and nasopharyngeal carcinomas A20's roles are context-dependent, exhibiting paradoxical effects under different circumstances [126,127].

Given A20's significant role in immune regulation, its function has also been explored in different immune cell types using transgenic mouse models, where conditional A20-floxed alleles enable lineage specific A20 deletion.

Silencing A20 in macrophages induces classical activation, exhibited heightened expression of costimulatory molecules (CD80, CD40, MHC-2 CD86) *in vitro*, along with increased secretion of IL-6, IL-10, TNFα, and enhanced immunostimulatory properties [128]. *In vivo* transplantation of these macrophages resulted in enhanced $CD8^+$, natural killer cell (NK), and $CD4^+$ T cell activation, leading to elevated granzyme and perforin production and enhanced immune protection of tumor

bearing experimental mice [128]. Furthermore, intratumoral injection of A20 siRNA significantly diminished the subcutaneous growth of EG.7 mouse lymphoma cells by inducing apoptosis in myeloid-derived suppressor cells (MDSCs), consequently promoting increased infiltration of cytotoxic immune cells and reduced infiltration of regulatory T cells [129]. Studies in NK cells showed that although the absence of A20 in NK cells resulted in hyperactivation, elevated cytokine and cytotoxic agent release, the majority of A20-deficient NK cells ultimately underwent apoptosis [130].

In other immune cells such as dendritic cells (DCs) it has been shown that A20 controls the maturation and activation of these cells thus maintains *in vivo* T and B cell homeostasis, preventing spontaneous autoinflammation [131]. In addition, knockdown of A20, whether *in vivo* or *in vitro*, results in the upregulation of co-stimulatory molecules and heightened production of IL-6, IL-10, and IL-12 [131]. This heightened activation in DCs leads to improved antigen presentation and amplified activation of antigen-specific cytotoxic T cells and T helper cells, while concurrently restraining regulatory T cells (Tregs) thus further limiting tumor growth in murine melanoma models [131]. Given the central role of dendritic cells in tumor recognition, clearance, and the development of immunological memory, ongoing research is actively exploring their application as potential anticancer vaccines for individuals diagnosed with non-small cell lung cancer (NSCLC)[132,133].

A20 exhibits significant expression in naive T cells, where it modulates NFκB activation driven by TCR/CD28 signaling and supports TCR-mediated survival [134]. While this regulatory role serves to prevent undesired activation, inflammation, and autoimmunity, it does dampen antitumor activity [135]. However, deletion of A20 in mature conventional $CD8^+$ T cells *in vivo* leads to sustained activation of NF-κB and increased production of IL-2 and IFN-γ due to increased sensitivity to antigen stimulation [135]. The adoptive transfer of these T cells has been shown to reduce melanoma growth in experimental mice and increased cytotoxicity and activation of bystander NK cells, further containing tumor growth[135].

Significantly, these investigations relied on highly efficient gene silencing techniques or cell type-specific deletion of A20. Genetic knockout of A20 within immune cell populations led to enhanced activation of cytotoxic cells resulting in controlling tumor growth. As a consequence, the idea of adopting A20-deficient immune cells for therapeutic purposes has been proposed as a means to diminish tumor load.

1.8 Rationale and aims of this thesis

Lung cancer continues to be the leading contributor to cancer-related deaths worldwide, exhibiting the lowest 5-year survival rate when compared to all other types of cancer [2]. The high mortality rates are largely attributable to late-stage diagnosis resulting in unfavorable prognoses.

Activating mutations in the KRAS oncogene are present in an estimated 20-30% of all lung cancer cases, however, specific inhibitors are largely non-existent in clinical practice for most KRAS mutations, with the exception of $KRAS^{G12C}$ [41,53]. Immunotherapy has significantly transformed the treatment landscape for advanced NSCLC, offering the possibility of extended survival of NSCLC of stages 1-4 [2,136]. Nonetheless, only 15-25% of patients show initial response, and eventually develop resistance [56,60,136]. This highlights the critical importance of identifying additional biomarkers that can predict treatment efficacy and potentially give a hint for combination therapies and improved therapies.

KRAS-driven LUAD is triggered by chronic inflammation, which may initiate tumorigenesis and promote cancer progression [25]. The immune-modulating enzyme A20 plays a pivotal role in promoting anti-inflammatory responses by modulating NF-κB activation [134]. Recent research in our laboratory has unveiled the tumor-suppressive potential of A20 in lung cancer cells driven by KRAS mutations. Intriguingly, in contrast to this, the downregulation of A20 within the tumor's surrounding stroma leads to a transformation of the tumor microenvironment into a state that promotes tumor suppression, resulting in significantly prolonged survival in mice harboring KRAS-driven lung tumors.

1.8.1 Preliminary data: Tumor intrinsic loss of A20

Previously we have shown that tumor intrinsic loss of A20 has an impact on lung tumor development and A20 expression levels are lower in tumor tissues compared to healthy tissues in human patients and mice [121]. Lower A20 levels also correlate with lower overall survival. Mouse LUAD cells form autochthonous lung tumor model KP ($KRAS^{G12D/+}$:$p53^{\Delta/\Delta}$), and CRISPR/Cas9 modified A20 mutated (KPA) cells did not show difference in proliferation *in vitro* and *in vivo* in immunocompromised (NSG) mice. In contrast, when transplanted into immunocompetent mice where mice bearing KPA tumors showed decreased survival, indicating A20's role as a potent tumor suppressor by altering the tumor microenvironment [121]. Further analysis of patient data revealed that A20-deleted tumors exhibited a distinct gene signature associated with low $CD8^+$ T cell abundance, which was confirmed by immunohistochemistry of human LUAD biopsies and mouse tissues. In addition, RNAseq analysis of A20-deficient mouse tumor tissue revealed an elevated interferon signature and increased expression of the T cell suppressor PD-L1 [121]. However, when using bulk RNA sequencing of tumor tissues, it becomes challenging to differentiate PD-L1 mRNA expression specifically within tumor cells from its expression in other cell types that also possess PD-L1.

Aim 1:

In order to examine the impact of A20 loss on tumor growth *in vivo* and to examine the dynamics how cancer cells evade immune recognition, our objective was to establish a KRAS mutant A20 deficient tumor cell line expressing the dTomato reporter for simplified identification of tumor cells *in vivo* (Figure 13 A and B) [137]. The A20 deficient and proficient tumor cell lines will be first verified and characterized *in vitro*. For *in vivo* characterisation, we will perform orthotopic transplant with the tumor cells into the lungs of syngeneic mice. This method enables the investigation of tumorigenesis within the context of a fully functional immune system, and enables to study how genetic changes in cancer cells influence tumor growth under natural physiological conditions [138]. Hence, we will perform Kaplan Maier survival analysis and time point analysis using flow cytometry in orthotopic mouse models to study the effects of A20 loss on tumorigenesis and immune escape mechanisms.

1.8.2 Preliminary data: A20 in the stroma

Analyzing tissue samples from KRAS mutant LUAD patients, we noticed eventually high A20 expression in cells of the tumor stroma (Fig. 13A). Double staining revealed that $CD34^{+}$ endothelial cells lining the tumor vessels were mostly negative for A20 expression (Fig. 13B), suggesting that A20 positive cells were mainly immune cells, including macrophages, monocytes and lymphocytes. In autochthonous, KRAS-driven mouse tumors [137], we also noticed infiltrating immune cells staining strongly positive for A20 (Fig. 13C). To investigate whether A20 expression in cells of the TME has implications on tumorigenesis of KRAS-driven lung tumors, we crossed $KRAS^{LSL\text{-}G12D/+}$ mice with $A20^{\Delta/+}$ and $A20^{LoxP/LoxP}$ mice. Intriguingly, following tumor induction using Ad.Cre, mice with systemic heterozygote A20 knockdown exhibited significantly increased survival as compared to their respective controls (i.e. $KRAS^{G12D/+}$, $A20^{\Delta/+}$ versus $KRAS^{G12D/+}$, $A20^{\Delta Lep/+}$ mice with ΔLep meaning deleted in lung epithelial derived tumor cells only; Fig. 13D). Notably, $KRAS^{G12D/+}$, $A20^{\Delta/+}$ mice exhibit heterozygosity of A20 in the whole body including the rising lung tumors, whereas in $KRAS^{G12D/+}$, $A20^{\Delta Lep/+}$ mice only the tumors are heterozygous for A20. However, reduced tumor burden in $A20^{\Delta/+}$ mice may be related to reduced Ad.Cre transduction efficiency caused by increased antiviral potential upon A20 knockdown [99,139]. This would result in decreased tumor initiation. To rule out this possibility, we isolated A20 wild-type mouse LUAD cells from the autochthonous lung tumor model. The resulting $KRAS^{G12D}$ mutated, p53 deficient cell line (hereafter KP cells) was then used to perform subcutaneous and orthotopic transplantations of KP cells [138]. In both models, we noticed impaired tumor growth when transplanted into $A20^{\Delta/+}$ mice, as evaluated by significantly decreased tumor mass in $A20^{\Delta/+}$ recipients compared to their wild-type controls (Fig. 13E) and increased survival in Kaplan Maier analysis (Fig. 13F). Hence, systemic knockdown of A20, including in the tumor stroma, significantly impaired development of KRAS-driven lung tumors.

Based on these observations we hypothesized that the reduction of A20 primarily in immune cells initiates a sequence of intracellular processes that subsequently enhance the suppression of tumor growth.

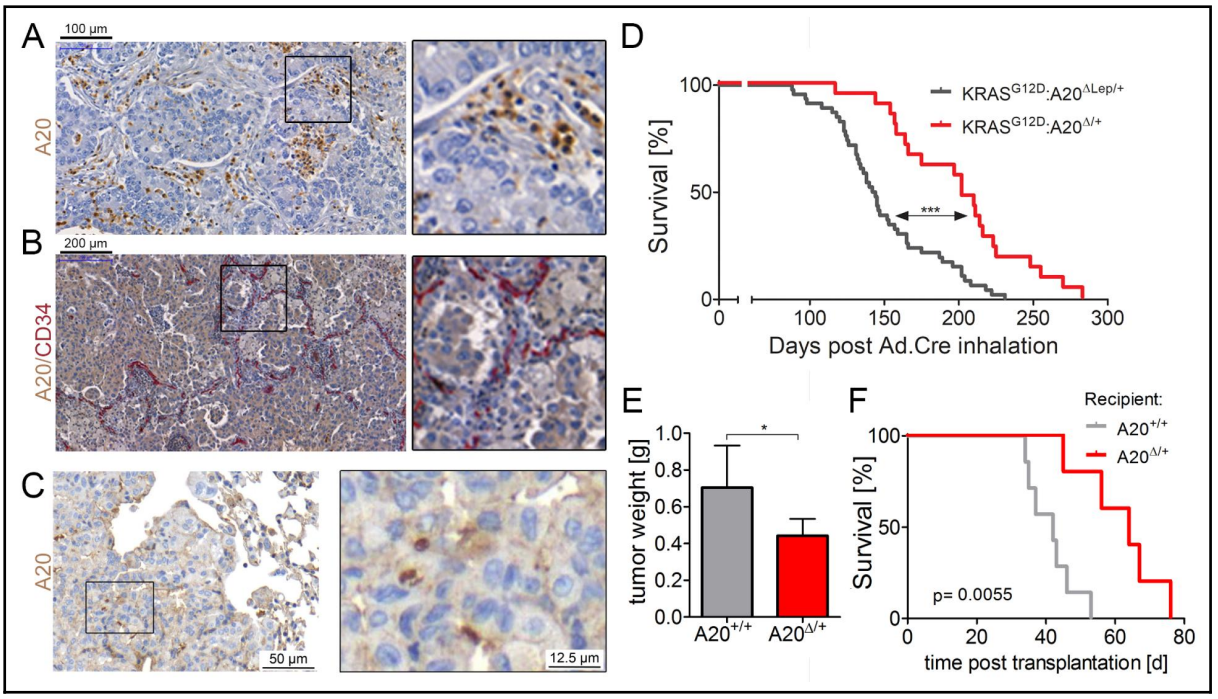

*Figure 13: **(A)** Representative image of a KRAS mutated LUAD biopsy stained for A20 and with **(B)** co-staining for CD34. **(C)** Picture of an autochthonous mouse lung tumor 10 weeks post tumor initiation and stained for A20. **(D)** Survival analysis of KRAS$^{G12D/+}$:A20$^{\Delta Lep/+}$ mice compared to whole body heterozygous A20 knockout KRAS$^{G12D/+}$:A20$^{\Delta/+}$ mice. **(E)** Tumor weight 4 weeks after subcutaneous transplantation of KP mouse lung tumor cells into syngeneic c and A20$^{\Delta/+}$ mice. **(F)** Survival analysis of wild-type versus A20$^{\Delta/+}$ mice following orthotopic engraftment of KP cells into the lungs.*

Aim 2:

The goal of the study is to further elucidate these alterations in the lung tumor microenvironment in response to partial A20 knockdown as in A20 heterozygous mice and upon conditional A20 knockout. Systemic knockout will be achieved using the Tamoxifen/Cre^{ERT2} system (A20$^{fl/fl}$:Cre^{ERT2}). Subsequently, we will test whether A20 knockout/knockdown enhances anti-tumorigenic potential to restrain growth of KRAS-driven lung tumors and identify immune cell populations that are most significantly contributing to restrain tumor growth.

Therefore, KPr cells will be transplanted intratracheally into syngeneic recipient mice (A20 heterozygous, A20$^{fl/fl}$:Cre^{ERT2} and respective control mice). Subsequently we will harvest lungs of recipient mice after different time points and determine alterations by flow cytometry using markers for myeloid and lymphoid subsets and by RNA-seq and subsequent bioinformatics integration of the data.

In summary, the reduction of A20 in specific immune cell populations, resulting in heightened activity and improved antitumor efficacy, would present a promising

approach to enhance the effectiveness of adoptive cell therapy when used in conjunction with other treatments, thereby could complement established therapeutic approaches.

2. Materials and Methods

2.1 *In vivo* experimental methods

2.1.1 Mouse models

Animal husbandry and mouse experiments were approved by the Austrian Federal Ministry of Science, Research, and Economy. The experiments were conducted according to the Protection of Animal Acts. Mice were generated and maintained on a C57BL/6 background. We closely monitored the body weight of the animals throughout the experiment, and when it dropped by 20%, the mice were humanely euthanized. Mice lines were acquired from The Jackson Laboratory and from Charles River Laboratories and bred in house.

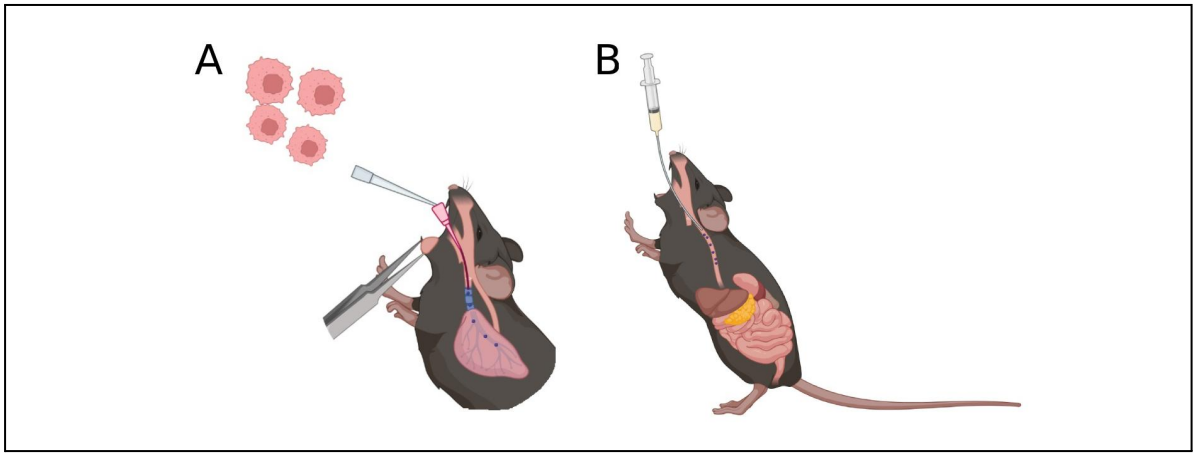

Figure 14: Mouse tumor models. ***(A)*** *orthotopic transplantation of Tumor cell lines into the lungs of mice.* ***(B)*** *Gavage feeding of animals for in vivo treatment. Figure generated using Biorender.*

Autochthonous tumor model

Mice heterozygous for the mutant KRAS G12D is under the control of a stop cassette flanked by loxP sites and p53 $KRAS^{LSL\text{-}G12D/+}$:$p53^{loxP/loxP}$ were crossed to $ROSA26^{LSL\text{-}dTomato}$ mice [140]. Mice were inhaled with Adenovirus which expresses the Cre recombinase under the promoter of the Surfactant C protein (Spc) that is only expressed in type II alveolar type cells (Fig. 15). Following virus inhalation, the recombination process triggers the expression of the KRAS G12D mutation, leading

to the activation of the dTomato reporter gene and the disruption of the p53 gene in transformed tumor cells [137].

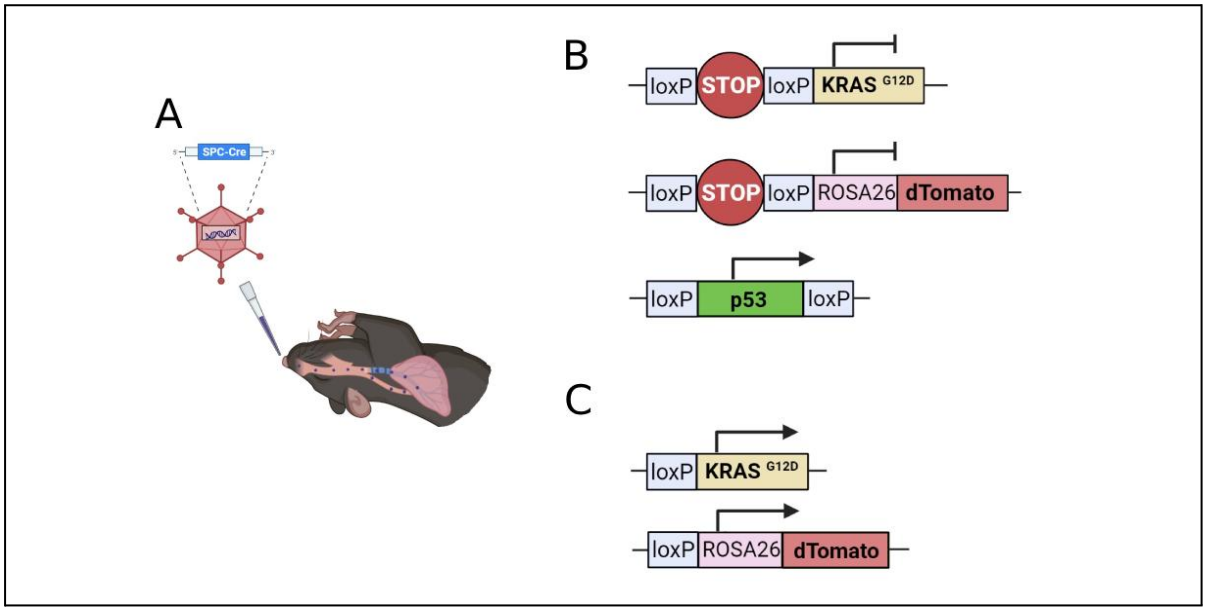

Figure 15: Autochthonous tumor model of KRAS-driven lung adenocarcinoma. ***(A)*** *Transgenic mice are inhaled with Cre recombinase expressing Adenovirus, where the Cre is expressed under the promoter of the surfactant protein C, that is only active in type 2 lung epithelial cells.* ***(B)*** *The KRAS G12D mutation and the dTomato reporter is expressed and the p53 gene is disrupted in transformed tumor cells* ***(C)*** *after Virus inhalation [137].*

Orthotopic transplantation model

Wild-type C57BL/6J mice were obtained from Jacksons Labs and bred to mice carrying heterozygous deletion of the A20/TNFAIP3 gene ($A20^{\Delta/+}$ mice). Before transplantation, the mice were anesthetized with Ketamine- Xylazine mixture (Table 1.) 10 µl/g body weight via subcutaneous injection. The cells were resuspended in antibiotic and serum-free RPMI 1640 supplemented with 0.01 mM EDTA and were transplanted intratracheally into anesthetized mice using a catheter with a blunted needle (BD Bioscience) in 50 µl final volume per mouse [138].

Reagents	Volume	Concentration
PBS	45 mL	
Ketamine (100 mg/mL)	5 mL	9.43 mg/mL
Xylazine (20 mg/mL)	3 mL	1.13 mg/mL

Table 1. Reagents for anesthesia.

Inducible systemic knockout model

To generate full body A20 knockout mice, $A20^{fl/fl}$ mice were crossed with transgenic ROSA26-Cre^{ERT2} mice and treated with Tamoxifen at the age of 8 weeks.
Tamoxifen was dissolved in DMSO, aliquoted and frozen in 50 mg/ml stocks. One stock was freshly diluted to 10 mg/ml in sunflower oil, stored at 4°C and used for up to one week. Mice received 1-10 mg/ml tamoxifen in 100 µl doze by oral gavage over a certain period of time (2-7 days). To determine the efficiency of the recombination, DNA was isolated from the lungs, spleen and tail after the treatment and the recombination efficiency of the exon 2 in the TNFAIP3 gene was tested with PCR using the genotyping primers.

2.1.2 Genotyping and PCR

Toes of mice were clipped and the tissues were lysed in a 150 µl DNA lysis buffer with Chelex 100 beads (Bio Rad)(Table 2.) and incubated OVN at 56°C on a thermo shaker. Supernatants of the samples were used for PCR reactions (Table 3-7).

Chelex DNA Extraction lysis buffer	250 ml
Chelex 100	50g
Tris pH 8	10 mM
EDTA	1 mM

Table 2. Contents of the lysis buffer used for DNA extraction from mouse tissue.

PCR Reagents	Volume
Primer mix (Fw and Rev, 10 µM)	1 µL
5x GoTaq buffer	5 µL
dNTPs (5 mM)	1 µL
GoTaq DNA Polymerase	0,1 µL
H_2O	17,9 µL
DNA	1,5 µL

Table 3. Reagents used for PCR.

temperature	time	cycle
95°C	3 min	
95°C	30 sec	x 38
58°C	30 sec	
72°C	45 sec	
72°C	10 min	
4°C	∞	

Table 4. PCR program setting for A20 and R26-Cre^{ERT2}.

Reagents	Amount
Agarose	4 g
1x TAE	200 mL
SYBR safe	4 µL

Table 5. Reagents used for gel electrophoresis.

Agarose gel electrophoresis

For determining the DAN product sizes, agarose powder was dissolved and heated up in 1x TAE buffer to get a 2% concentrated solution. SYBR safe dye was added to the hand warm agarose solution, gently mixed and poured into running chambers to solidify. After removing the combs, the gel was placed in the Gel electrophoresis chamber in 1x TAE buffer. The PCR products and a 1kb marker were loaded into the wells on the gel and the machine was turned on to 120 Volts. After about 40 minutes, the gel was taken out and imaged using the ChemiDoc Touch Imaging System (Bio-Rad).

Product sizes

Gene	Size [bp]
A20 WT	250
A20 fl	420
A20 delt	650
Rosa-Cre^{ERT2}	500

Table 6. Genotyping PCR product sizes.

Genotyping primers	Primer sequences
A20 delta Rev	TGTCTGCTGATGCCATTTTGAC
A20 wt Fw	AGTCTGGGACTGGATGTAGC
A20 wt Rev	CTGGCTAAGGCCTTGATACC
Rosa26-Cre^{ERT2} Fw	GTAACTGTGGACAGAGGAGCCATAAC
Rosa26-Cre^{ERT2} Rev	GGGAAACCATTTCCGGTTATTCAAC

Table 7. Primers used for genotyping.

2.2 *In vitro* work

2.2.1 Cell lines

The KPr cells (KRAS$^{LSL\text{-}G12D/+}$:p53$^{\Delta/\Delta}$:tdTom) cell line was isolated from autochthonous mouse models of lung tumors following Ad.Cre inhalation. Recombination is induced in the type II alveolar cells leading to the expression of mutant KRAS, dTomato reporter and homozygous knockdown of p53. dTomato expressing KP tumor cells were isolated at endpoint post inhalation where the mice lost 20% of the initial body weight.

2.2.2. Culturing mammalian cells

Culturing conditions

Tumor cell lines were cultured in standard RPMI 1640 medium, supplemented with 10% FBS, 1% L-glutamine and 1% PenStrep (Gibco ™) while the standard medium for primary lymphoid cells (splenocytes) was RPMI 1640 supplemented with 10% FBS, 1% L-glutamine and 1% PenStrep, 0,1 mM Non-essential amino acids (Gibco) 0,1 mM β-MeOH and 1 mM sodium pyruvate. Live cells were counted using CASY/trypan blue (10µl cell suspension + 10µl trypan blue) using a cell counter machine.

Passaging cells

Cells were washed with sterile 1x PBS and detached from the culture plate by incubating the cells with trypsin 0.05% EDTA (Gibco ™) at 37°C, 5% CO_2 in a humid incubator for 5 minutes. The detached cells were resuspended in complete medium, containing 10% FBS and centrifuged at 300 xg for 3 minutes. The cells were resuspended in 1-2 ml of standard medium, counted and reseeded at desired density on tissue culture treated petri dishes.

Freezing cells

Isolated primary cells, including lung cells and splenocytes or tumor cell lines were harvested and collected by centrifugation. The cell pellets were resuspended in 1 ml of freezing medium that consisted of RPMI 1640 supplemented with 20% FBS and 10% DMSO. Cell suspensions were transferred into pre-labeled cryovials and subsequently to -80°C within a cryo box. The aliquots were removed from the cryo boxes after one week and transferred into liquid Nitrogen for long term storage.

Thawing cell lines

Aliquots of frozen cell lines were thawed and quickly transferred into 14 ml falcon tubes, containing 9 ml of complete medium. The cell suspension was centrifuged at 300 xg for 3 minutes and the cell pellet was resuspended in 1 ml fresh complete medium, plated on 10 cm petri dishes and cultured as described previously.

2.2.3 Genetic modification of cultured cells with CRISPR/Cas9

KPr cells were cultured in RPMI1640 (Gibco, RPMI medium with L-glutamine and 25 mM) medium supplemented with 10% FBS and 1% P/S and $5x10^4$ cells were seeded into wells of a 24 well plate one day before transfection. Then 500 ng from the plasmids were mixed with 100 µl Optimem and 0,5 µl Plusreagent in eppendorf tubes and incubated for 5 minutes at room temperature (RT). 2 µl of Lipofectamine LTX was added to each tube, mixed briefly and incubated for 25 minutes at RT that allows the plasmids to be packed in liposomes. In the meantime the medium on the cells was changed to RPMI 1640 +10% FBS (Gibco, Cat# 10500-064), L-glutamine to remove the antibiotics and the transfection reaction mix was added to the cells dropwise. The cells were transfected with a plasmid encoding the Cas9 protein and the guideRNA (Table 9.) with puromycin resistance gene pSpCas9(BB)-2A-puro-A20 while the negative cells were transfected with empty backbone plasmid pSpCas9(BB)-2A-puro (Fig. S1) and the positive control cells were transfected with pSpCas9(BB)-2A-GFP plasmid encoding GFP instead of puromycin resistance cassette (Fig. S2).

The cells were incubated for 24 hours and examined under fluorescent microscope to check if the control cells express GFP and thus determine the efficiency of the transfection. From the next day, cells were incubated in 13 µg/ml Puromycin for 3-4 days to negatively select the untransfected cells. One third of the positively selected transfected cell pool was frozen, the other was used for DNA isolation and the leftover was diluted and seeded into 96 well plates in a way that every second well would contain 1 cell in 100 µl medium. Single cell clones were expanded gradually and transferred into bigger plates.

2.2.4 DNA isolation from cells

Cells were trypsinized, washed 2 times with 1x PBS and collected by centrifugation at 800-1200 xg for 5 minutes. The cell pellet was resuspended in 200 µl of DNA lysis buffer (Table 8.) to which 30 µg/ml proteinase K (Sigma P4850) was added. The cell suspension was vortexed and incubated overnight shaking at 55°C and 800 rpm. The next day 85 µl of 5 M NaCl was added to the lysates and after inverting the tube

a few times, the sample was centrifuged at 16000 xg for 10 min at RT. The supernatant was transferred into a new Eppendorf tube without disturbing the pellet and was mixed with 250 µl isopropanol. After repeating the previous centrifugation step, the supernatant was discarded and the pellet was washed with 1 ml 70% EtOH. The sample was centrifuged and after discarding the supernatant, the pellet was air-dried for 20 minutes and then re-suspended in 50 µl dH_2O. DNA concentration was measured by using the NanoQuant Tecan Infinite M200Pro device.

DNA lysis buffer

Reagents	Final Concentration
NaCl	100 mM/L
EDTA	100 mM/L
Tris-HCl pH8	50 mM/L
SDS	1 %

Table 8. Composition of the DNA lysis buffer.

2.2.5 TIDE (Tracking of Indels by DEcomposition) sequencing

Clones were gradually expanded until they reached 90% confluency on a 6 cm petri dish. DNA was isolated as previously mentioned and the fragment bearing the mutation was amplified with primers (Table 9-10.) spanning the knock-out construct in two separate PCR reactions. The product from one reaction was used for gel-electrophoresis to check the size and efficiency of the PCR, the other PCR product was used to isolate the amplified DNA fragment using the Favorgen PCR clean-up mini-kit (Cat nu.: FAPCK001-2) according to manufacturer's instructions and sent for TIDE sequencing [141]. The sequencing mixture contained 1 µg DNA from the respective samples and 5 ug/ml of the forward TIDE sequencing primer in 20 µl.
To estimate the targeting efficiency and degree and nature of modification, we analyzed the sequencing data using the TIDE sequencing webtool http://shinyapps.datacurators.nl/tide/ which identifies small indels in the given sequence comparing to a control unmodified sequence.

Name of the primer	Sequence
sgRNA #2	CTCGGAACTTTAAATTCCGC
TIDE #2 fw	ATCAAGGCCTTAGCCAGCAA
TIDE #2 rev	GCTCAAAACTGATGGGAGGGA

Table 9. Guide RNAs and TIDE primer sequences used for targeted gene modification with CRISPR/Cas9

PCR reaction for TIDE sequencing:

temperature	time	cycle
94°C	2 min	
94°C	30 sec	x 40
58°C	40 sec	
72°C	50 sec	
72°C	10 min	
4°C	∞	

Table 10. PCR reaction for A20 TIDE sequencing.

2.2.6 RNA isolation from cells and tissues

Cells were seeded into 6 cm petri dishes at 50% confluency and stimulated with 1 ng/ml LPS or 30 ng/ml mouse TNF-α for 4 hours. The dishes were cooled on ice and washed 3 times with ice cold 1x PBS, then lysed by adding RNA lysis buffer (Qiagen) with 0.02% β-Mercaptoethanol to the cells. The lysate was collected in Eppendorf tubes and RNA was isolated using the RNeasy Mini kit 50 from Quiagen according to the protocol. 1 µg RNA was used from each sample for cDNA writing when samples were used for RT-qPCR.

The right upper lobe of the lungs were frozen in liquid nitrogen right after harvesting and stored on -80°C or in a liquid nitrogen tank until processed. The tissues were lysed in 5 ml tubes containing RNA lysis buffer with β-mercaptoethanol by using an electric tissue processing device and processed further using the RNeasy Mini kit 50 from Quiagen according to the protocol.

2.2.7 RNA sequencing

The NEBNext Ultra II RNA Library Prep was employed to prepare sequencing libraries, which were then sequenced using the Illumina NextSeq500 platform in a 75-base pair single-read configuration. The resulting sequencing data were aligned to the Mus musculus/mmc10 mouse genome assembly using the Spliced Transcripts Alignment to a Reference (STAR) aligner. Differential gene expression was subsequently assessed using DESeq2 [142,143]. The Gene Set Enrichment Analysis (GSEA) was executed as per the standard procedure, setting permutations at 1000 and sourcing hallmark gene sets from the Molecular Signature Database (www.gsea-msigdb.org/gsea/msigdb/). For the heatmap visualization, a single outlier per group, pinpointed through hierarchical clustering, was omitted, and the heatmapper.ca tool utilized [144].

2.2.8 cDNA synthesis

For quantitative Real Time PCR 1 µg RNA was used for reverse transcription to write cDNA using the iScript™ cDNA synthesis kit from Bio-Rad according to manufacturer's instructions and the indicated tables below (Table 11.-12).
The cDNA was diluted 10x with nuclease-free water to a final concentration of 5 ng/µl.

Reagents	Volume per reaction (µl)
1 µg RNA	variable
5x iScript Reaction mix	4 µl
iScript Reverse Transcriptase	1 µl
Nuclease-free water	to 20 µl final volume

Table 11. Reaction mix for cDNA synthesis.

Step	temperature	time
Primer binding	25°C	5 min
Reverse transcription	46°C	20 min
Enzyme Inactivation	95°C	1 min
	4°C	∞

Table 12. cDNA synthesis reaction.

2.2.9 Quantitative Real Time PCR analysis

The qPCR reaction was carried out by using the CFX Connect™ Real-Time PCR Detection System (Bio-Rad) using primers specific for TNFAIP3, IL-6, IL-1β, IFN-g, 28S, TBP, PD-L1 and MHC-1 (Table 13-15) and the relative gene expression was quantified according to the *Pfaffl* method [145] using mouse 28S or TBP as reference genes.

The relative expression of the target genes were calculated according to following equation: [146]

$$\text{Relative expression} = 2^{-\Delta\Delta CT}$$

$$\Delta CT = CT(\text{a target gene}) - CT(\text{a reference gene})$$

$$\Delta\Delta CT = \Delta CT(\text{a target sample}) - \Delta CT(\text{a reference sample})$$

Reagents	Volume per reaction (µl)
iTaq™ Universal SYBR ® Green Supermix Bio-Rad	7,5 µl
Primer mix (forward and reverse 10 µM)	0,75 µl
nuclease free water	1,75 µl
cDNA (5ng/ µl)	5 µl

Table 13. RT-qPCR reaction mixture.

temperature	time	cycle
95°C	30 sec	
95°C	5 sec	x 40
60°C	30 sec	
65°C	5 sec	
95°C	50 min	

Table 14. RT-qPCR reaction program.

Target gene	Forward primer sequences	Reverse primer sequences
28S	ATACCGGCACGAGACCGATAGTCA	GCGGACCCCACCCGTTTACCTC
TNFAIP3	AAACCAATGGTGATGGAAACTG	GTTGTCCCATTCGTCATTCC
IL-1β	ATGCCACCTTTTGACAGTGATG	TGTGCTGCTGCGAGATTTGA
IL-6	GACAAAGCCAGAGTCCTTCAGA	AGGAGAGCATTGGAAATTGGGG
IFN-γ	GCTACACACTGCATCTTGGC	TTTCAATGACTGTGCCGTGG
PD-L1	AACGCCACAGCGAATGATGT	ACAGGATGGATCCCAGAAGC
H2-Kb	CGGCGCTGATCACCAAACA	AGCGTCGCGTTCCCGTT

Table 15. List of used mouse specific RT-qPCR primers.

2.2.10 BCA assay and Western blot

20.000 Cells from the control KPr ($KRAS^{G12D/+}$:$p53^{\Delta/\Delta}$:dTomato) cell line and the KPAr ($KRAS^{G12D/+}$:$p53^{\Delta/\Delta}$:$A20^{\Delta/\Delta}$:dTomato) single clone were seeded in 4-4 wells of a 12 well plate on the previous day and treated with 20 ng/ml TNF-α. Technical quadruplicates of stimulated and untreated control cells were washed with ice-cold 1% PBS and harvested from 80% confluent 6 cm dishes in lysis buffer (Table 16.). The cell lysates were centrifuged at 14000 rcf on 4 °C and the supernatants were collected. The protein concentration of each sample was determined using the Pierce™ BCA Protein Assay Kit (Thermo Scientific™) according to manufacturer's instructions and using the NanoQuant Tecan Infinite M200Pro device.

After determining the protein concentrations 25 µg of total protein from each sample were boiled with 6x loading dye (Table 17.) at 95 °C for 5 minutes before loaded onto 8% polyacrylamide gels (Table 18-20.) and separated by SDS-PAGE. Protein samples were transferred onto a nitrocellulose membrane by semi-dry blotting using the BioRender semi-dry blotter machine and blotting solution (Table 21). Membranes were stained with a Poncoe red solution for 3 minutes to visualize the proteins and determine whether the transfer worked. Afterwards, the membranes were washed with distilled water to remove the stain and were blocked with TBS-T containing 5% BSA for 1 hour (Table 20). The membranes were washed 3 times for 5 minutes with TBS-T and were incubated with primary antibodies in TBS-T +5% BSA overnight at 4°C. The next day, the membranes were washed 3 times with TBS-T and incubated for 1 hour at room temperature with a horseradish peroxidase-conjugated secondary antibody diluted in 5 ml of blocking buffer. After washing steps the membrane was incubated for 1 minute with 500 µL working solution of SuperSignal™ West Femto Maximum Sensitivity Substrate and imaged using the ChemiDoc Touch Imaging System (Bio-Rad).

Reagents	Final concentration	Amount in 50 ml
1 M Tris pH 7.5	20 mM	1 ml
5 M NaCl	100 mM	1 ml
0,1 M Na_3VO_4	1 mM	0.5 ml
0,5 M NaF	100 mM	10 ml
0,2 M Glycerol-2-phosphate	20 mM	5 ml
0,25 M EDTA	2.4 mM	0.5 ml
0,25 mM EGTA	1 mM	0.2 ml
NP-40	1 %	0.5 ml
Phenylmethylsulfonyl Fluoride (PMSF)	1%	

Table 16. Composition of the Protein lysis buffer.

Reagents	Final concentration	Amount in 10 ml
1 M Tris base	375 mM	3.75 ml
10 % SDS	9 %	900 µl
99 % Glycerol	50 %	5 ml
β-mercaptoethanol	9 %	900 µl
Bromophenol blue	0,03 %	30 µl

Table 17. Composition of the loading dye, Laemli buffer.

Reagents	10 ml final volume
distilled water	4 ml
30 % Bis-acrylamide	3.3 ml
1.5 M tris-Cl pH 8.8	2.5 ml
10 % SDS	0.1 ml
10 % APS	0.1 ml
TEMED	4 µl

Table 18. Composition of the 12% stacking gel.

Reagents	2,5 ml final volume
distilled water	1,7 ml
30 % Bis-acrylamide	415 µl
1 M tris-Cl pH 6.8	315 µl
10 % SDS	25 µl
10 % APS	25 µl
TEMED	2,5 µl

Table 19. Reagents used for casting the separation gel.

Reagents	Amount in 1 liter
0,25 M Tris Base (121,4g/mol)	30,3g
1,92 M Glycine (75g/mol)	144g
1% SDS	10g

Table 20. Composition of the 10x Running buffer, adjusted to pH 8.3.

Reagents	Amount in 1 liter
0,48 M Tris Base (121,4g/mol)	58,1g
0,39 M Glycine (75g/mol)	29,3
0,375% SDS	3,75g

Table 21. Composition of the Blotting buffer

Reagents	Volume in 100ml
10% SDS	20ml
0,5M Tris HCl pH 6,8	12,5 ml
Ultra Pure H_2O	67,5ml

Table 22. Composition of the stripping buffer

750µl ml ß-mercaptoethanol per 100 ml were added to the stripping buffer freshly before use.

Reagents	Amount in 100ml
Tris Base (121,4g/mol)	12,114g
NaCl (58 g/mol)	43,83

Table 23. Composition of the 10x concentrated TBS buffer, pH 7.5.

Antibodies	Working dilution
Mouse HSC 70 (Santa Cruz Biotechnology sc-166692)	1:2000
Mouse A20 (Santa Cruz Biotechnology sc7298)	1:2000
Anti-mouse IgG, HRP-linked (Cell Signaling)	1:5000

Table 24. Primary and secondary antibodies used for Western blot.

2.2.11 Cell proliferation dye dilution assay

KPr and KPAr cells were collected and labeled with the CellTrace™ Violet Cell Proliferation Kit (Thermo Fisher, cat. no.: C34557) following the guidelines provided by the manufacturer. Both cell groups were stained simultaneously and plated in triplicate in 12-well plates for specified time intervals. Cells were then collected and subjected to FACS analysis 48 and 72 hours post-seeding.

2.2.12 Tissue harvesting

Isolation of lung cells

Mice were killed with cervical dislocation, pinched down to sterile surface and opened by cutting through the skin and the peritoneal wall from bottom up. The diaphragm and the ribcage were cut open and after cutting the vena cava and the trachea, the lungs were weighed and perfused with 2-3 mls of 1x PBS through the heart, using a 27G BD microlance needle. The upper right and the middle right lobes of the lungs were collected and snap-frozen in liquid nitrogen for subsequent RNA and protein isolation, respectively. The remaining parts of the lungs were kept in ice-cold 1x PBS and were further processed under a laminar hood. The collected lung tissues were cut into small pieces on a petri dish within 1 ml digestion reaction, which was prepared freshly, containing DNase 50 U/ml (Sigma Chemicals Co., Cat#DN25-100MG) and Collagenase I 150 U / ml (Gibco™, Invitrogen, Cat# 17100-017) in complete media (RPMI 1640 supplemented with 10% Fetal Bovine Serum (FBS, Invitrogen), 1% Penicillin/streptomycin (Pen/strep Gibco™) and 1% L-glutamine (GE Healthcare). The cutted pieces were transferred in a 14 ml falcon tube with an additional 4 ml of digestion reaction and were incubated at 37°C for one hour. The digested suspensions were filtered through 70 μm pore size cell strainers (BD Falcon, Ref 352350) using the plunger of a 2 ml syringe into a 50 ml falcon tube and supplemented with 10 ml complete medium. Cells were collected by centrifugation at 300 xg 5 minutes and the pellet was resuspended in 500 μl ACK Lysing Buffer (100 ml, Gibco™, Invitrogen, Cat# A1049201,) to lyse red blood cells. The reaction was stopped after 5 minutes of incubation by adding 5 ml complete media. The cells were collected by centrifugation, frozen and stored as described before until they were used for flow cytometric analysis.

Splenocyte isolation

Mice were killed by cervical dislocation, spayed with ethanol and fixed with needles. Using clean, sterilized scissors and forceps the spleens were taken out through a clean cut on the peritoneal wall. The spleens have been cleaned of fatty tissue, weighed and put into ice-cold 1x PBS and further processed under sterile conditions. Spleens were placed in a 70 µm pore size cell strainer within a petri dish containing 10 ml complete medium and smashed with the plunger of a 2 ml syringe. The cell suspension was aspirated 2-3 times using a 10-12 ml syringe and a 18 G needle to acquire a single cell suspension. The cell strainers were placed in 50 ml Falcon tubes and the cells were filtered once again. Subsequently the cells were collected by centrifugation (300 xg for 5 minutes at RT) and the cell pellet was resuspended in 1 ml ACK Lysing Buffer for 5 minutes to lyse red blood cells. The reaction was stopped by adding 5 ml complete medium and after centrifugation, the cells were frozen until flow cytometric analysis.

2.2.13 Flow cytometry / fluorescence activated cell sorting (FACS)

Single cell suspensions of lung cells or splenocytes from frozen aliquots were thawed and washed 2 times with 1 ml 1x PBS containing 5% FBS and 1 mM EDTA to remove residues of DMSO from the freezing medium. Cell suspensions were re-suspended in 100 µl of FACS buffer containing CD16/32 (Fc-γ block) in a 1:100 dilution and incubated on ice for 30 minutes. After the blocking step, cells were collected by centrifugation on 400 xg, 5 minutes and the pellet was resuspended in 100 µl of staining buffer, containing the respective antibodies for either the myeloid panel or lymphoid panel (Figure 16, Table 25). The cells were stained for 30 minutes at 4 °C and protected from light, washed three times with 1 ml FACS buffer afterwards and filtered through 35 µm pore size filters into 5 ml FACS tubes before loading into the machine.
Data was recorded using the FACSCanto II Flow Cytometer from BD Bioscience and events were recorded with the FACS Diva software. Data analysis was performed following exclusion of doublets using the FlowJo 10.7.1. analysis software.

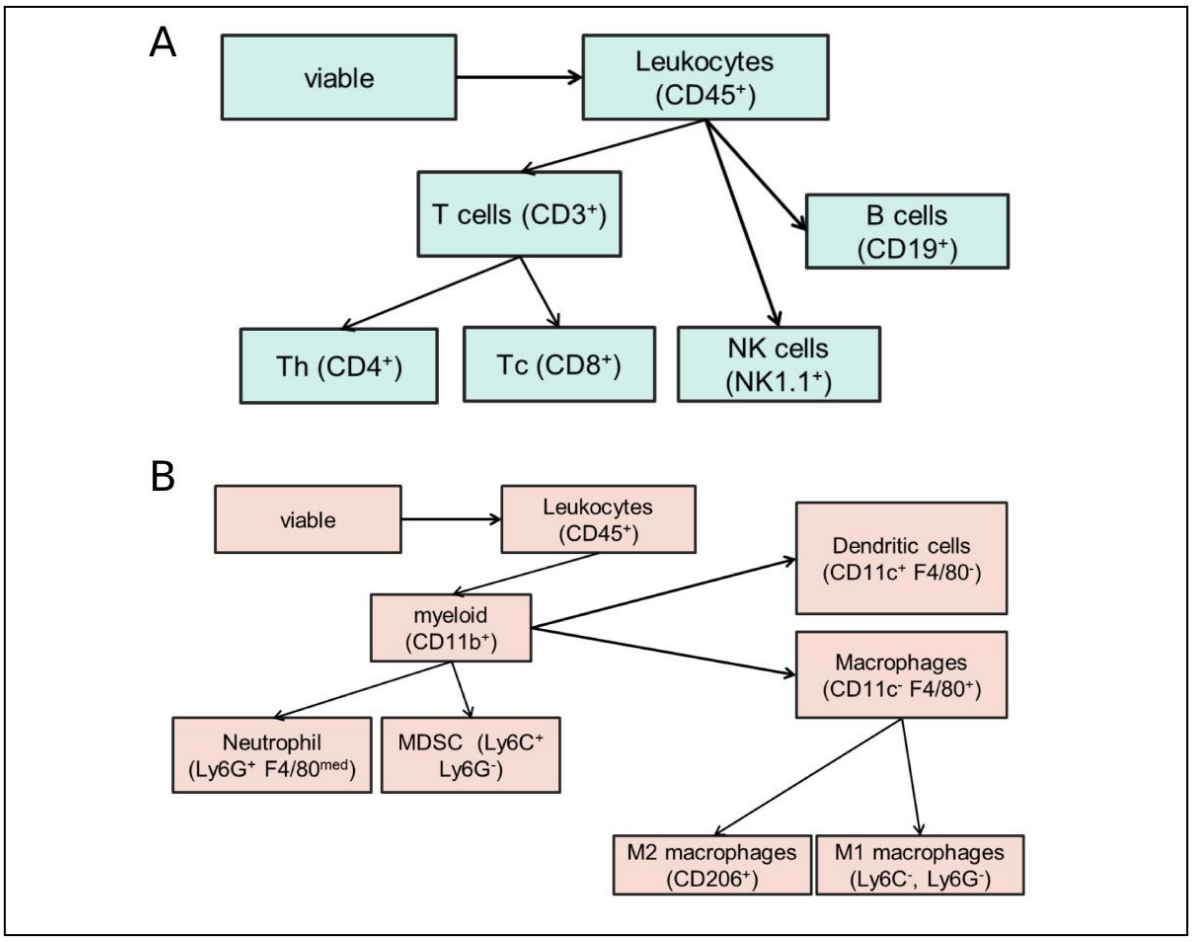

*Figure 16: Scheme depicting gating strategy for flow cytometry of **(A)** Lymphoid and **(B)** Myeloid cell populations.*

Target surface molecule	Fluorochrome	Company	Product Nu.
CD45	APC-Cy7	BD Biosciences	561037
CD8a	FITC	eBioscience™	11008182
CD4	PE	eBioscience™	12004182
CD3	APC	Invitrogen™	17003282
Nk1.1 (CD161b/c)	PE-Cy7	BD Biosciences	562062
CD19	PerCp-Cy5.5	eBioscience™	45019382
CD11c	FITC	Invitrogen™	11011482
CD206	PE	eBioscience™	141706
Ly6G	APC	eBioscience™	17966882
Ly6C	PE-Cy7	Invitrogen™	25593282
CD11b	PerCp-Cy5.5	Invitrogen™	45011282

CD274 (PD-L1)	BV-421	BioLegend®	124315
MHC-1	APC	BioLegend®	116518
Isotype Control	BV421	BioLegend®	400639
Isotype Control	APC	eBioscience™	17472481
CD16/CD32 Fcγ block	-	eBioscience™	14016185

Table 25. List of fluorochrome-conjugated primary antibodies

2.3 Statistical analysis

For statistical analysis of data GraphPad Prism 5.04 Graphpad Software has been used. Unpaired student's t-test was used for unequally distributed values within two groups. For Kaplan Meier survival analysis we used Tukey's post-hoc test.
All values are presented as standard deviation of mean values (SD) and two-sided p values below 0.05 were considered statistically significant *p<00.5 and **p<0.01; ***p<0.001.

3. Results

3.1 Results 1: Tumor intrinsic role of A20

In order to more thoroughly investigate the influence of A20 loss on tumorigenicity and immune evasion in KRAS-driven LUAD mouse models, we decided to generate A20 knockout cells within the $KRAS^{G12D/+}$ p53 deficient LUAD cell line, which also expresses the red fluorescent protein, dTomato. This allows us to identify and distinguish the tumor cells in orthotopic transplantation mouse models of LUAD. Additionally, the fluorescence in the tumor cells simplifies the analysis and recognition of surface markers on tumor cells, setting them apart from immune cells and other cell types. The $KRAS^{G12D/+}$ $p53^{\Delta/\Delta}$ dTomato (referred as KPr) cells were isolated from autochthonous tumors of mice at the endpoint.

3.1.1 Generation of A20 deficient KRAS mutant lung adenocarcinoma reporter cell line

For the deletion of A20 in KPr cells, we used CRISPR/Cas9 gene editing technology [147]. DNA was isolated from the pool of the CRISPR/Cas9 targeted KPr cells and unmodified cells, respectively and amplified with PCR using primers flanking the target site (Table 9). The amplified DNA fragments were purified from the PCR reactions and Sanger sequenced. The targeting efficiency and indel status was then determined based on the chromatograms using the TIDE (Tracking of Indels by Decomposition) sequencing free web-based tool.

The targeting efficiency of the cell pool was 53.1%, where 4 main modifications showed enrichment in the pool of cells; +1 insertions, and -5 base pair deletions were most abundant whereas -3 and -10 deletions were less abundant but still significant (Fig. 17A). Following this, we sorted single clones from the pool and 6 single clones were sent for sequencing. Among the 6 clones, clone number 2 had the highest (99,5%) targeting efficiency with +1 base pair insertion thus this clone has been chosen for further evaluation (Fig. 17B). Figure 17C shows DNA sequence alignment of the wild type and A20 mutant clone 2, which has +1 base insertion.

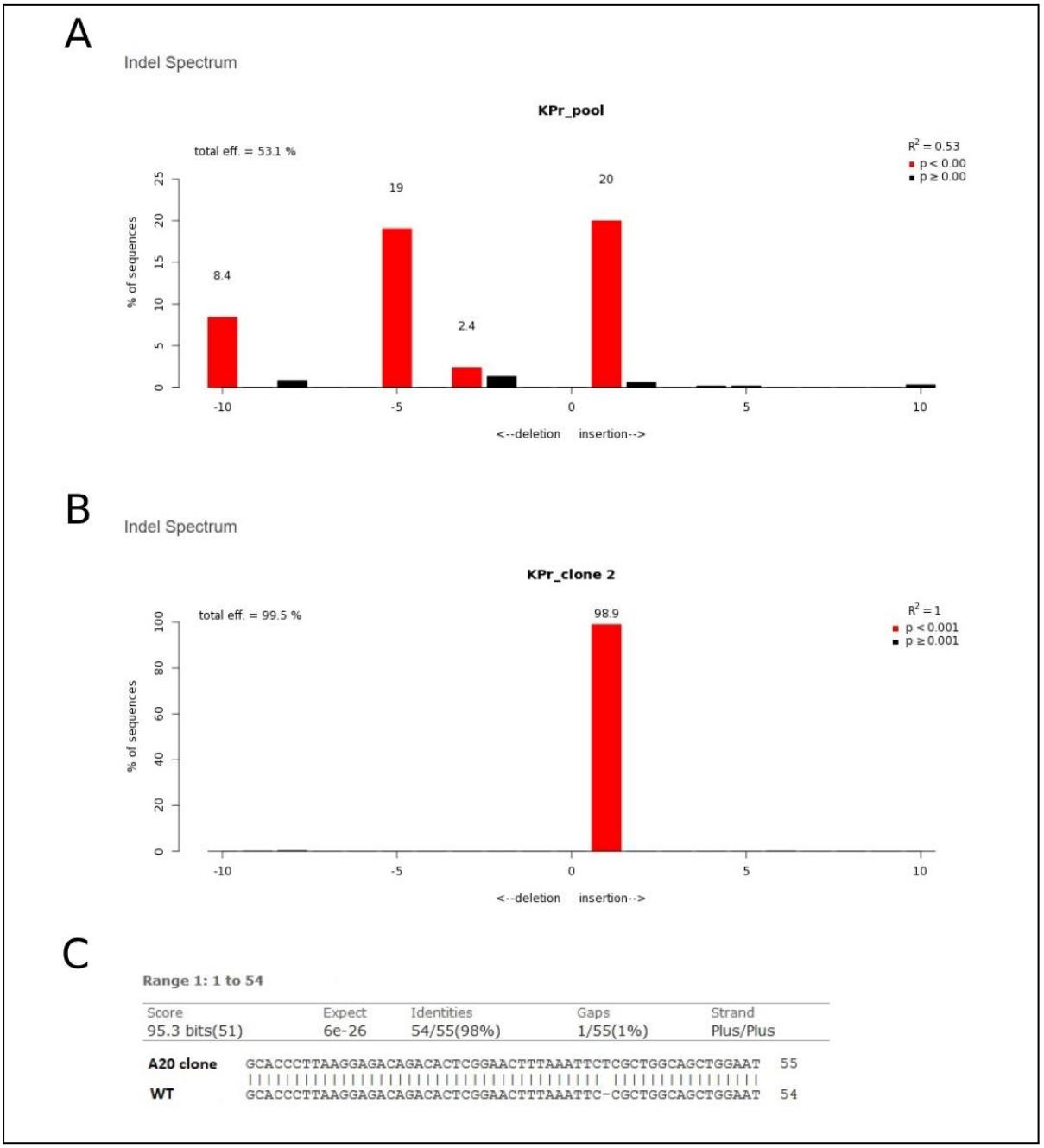

*Figure 17: Quantification of genome editing efficiency and Indel spectrum of **(A)** KPred cell pool and **(B)** KPred A20 clone 2. Genome editing efficiency was determined by TIDE sequencing. R provides a value for statistical significance of each indel. **(C)** Sequence alignment of WT pool and A20 mutant clone sequences.*

To verify that this frameshift mutation results in knockout of the TNFAIP3 and the mutant clone does not express the A20 protein, we treated cells with 10 ng/ml TNF-α for 4 hours and determined the mRNA expression level of TNFAIP3 gene which showed lower baseline expression levels and reduced levels upon stimulation (Fig. 18A). To test for the presence or the absence of a full size functional A20 protein after introducing the frameshift mutation we performed western blot analysis. For this we cultured the cells overnight in the presence of 10 ng/ml TNF-α to induce

expression of A20 which is normally not expressed or in very low levels in isolated KP tumor cells. The presence of a complete 90 kDa A20 protein in TNF-α-stimulated KPr cells, as opposed to its absence in KPAr cells, serves as confirmation that the knockout clone lacks functional A20 (Fig. 18B). The cytoskeletal protein β-actin (42 kDa) was used as a housekeeping gene, which is constitutively expressed in all samples of control and knockout cells. Overall, these data suggest that the frameshift mutation introduced in the second exon of A20 encoding gene leads to a functional knockout of the A20 protein.

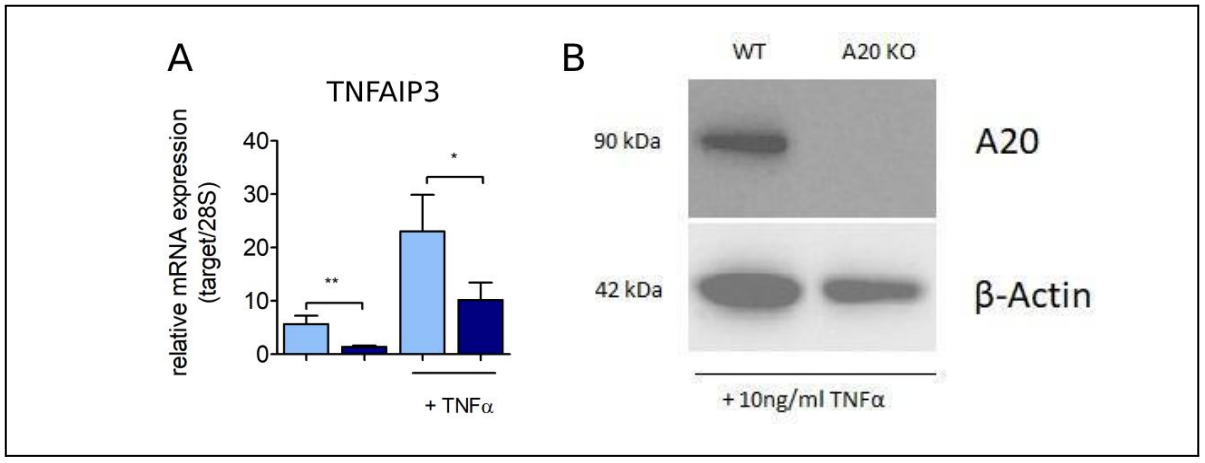

Figure 18: Verification of A20 knockout in KPr cells. ***(A)*** *Relative mRNA expression of TNFAIP3 in KPr and KPAr tumor cell lines.* ***(B)*** *Western blot analysis of WT and A20 knockout KPred cells stimulated with 10 ng/ml TNF-α overnight.*

3.1.2 A20 deficiency in KPr cells increases sensitivity to inflammatory cytokines and show higher PD-L1 and MHC-1 levels in vitro

To test whether the knockout of A20 has an effect on cell proliferation in the cancer cells, we performed cell proliferation assay by staining biological triplicates of KPr and KPAr cells with CellTrace violet dye and analyzed the cells by flow cytometry after 24, and 48 hours culturing. Unstained cells served as controls. The Violet proliferation dye attaches to proteins in the cell's cytoplasm, and with each subsequent cell division, the staining intensity reduces exponentially which is reflected as a shift in the peaks of the histogram. We did not observe faster dilution of the dye in either cell lines based on the histograms of the respective time points

between samples, thus we concluded that there are no differences in proliferation between KPr and KPAr cells in *in vitro* cultures (Fig. 19A).

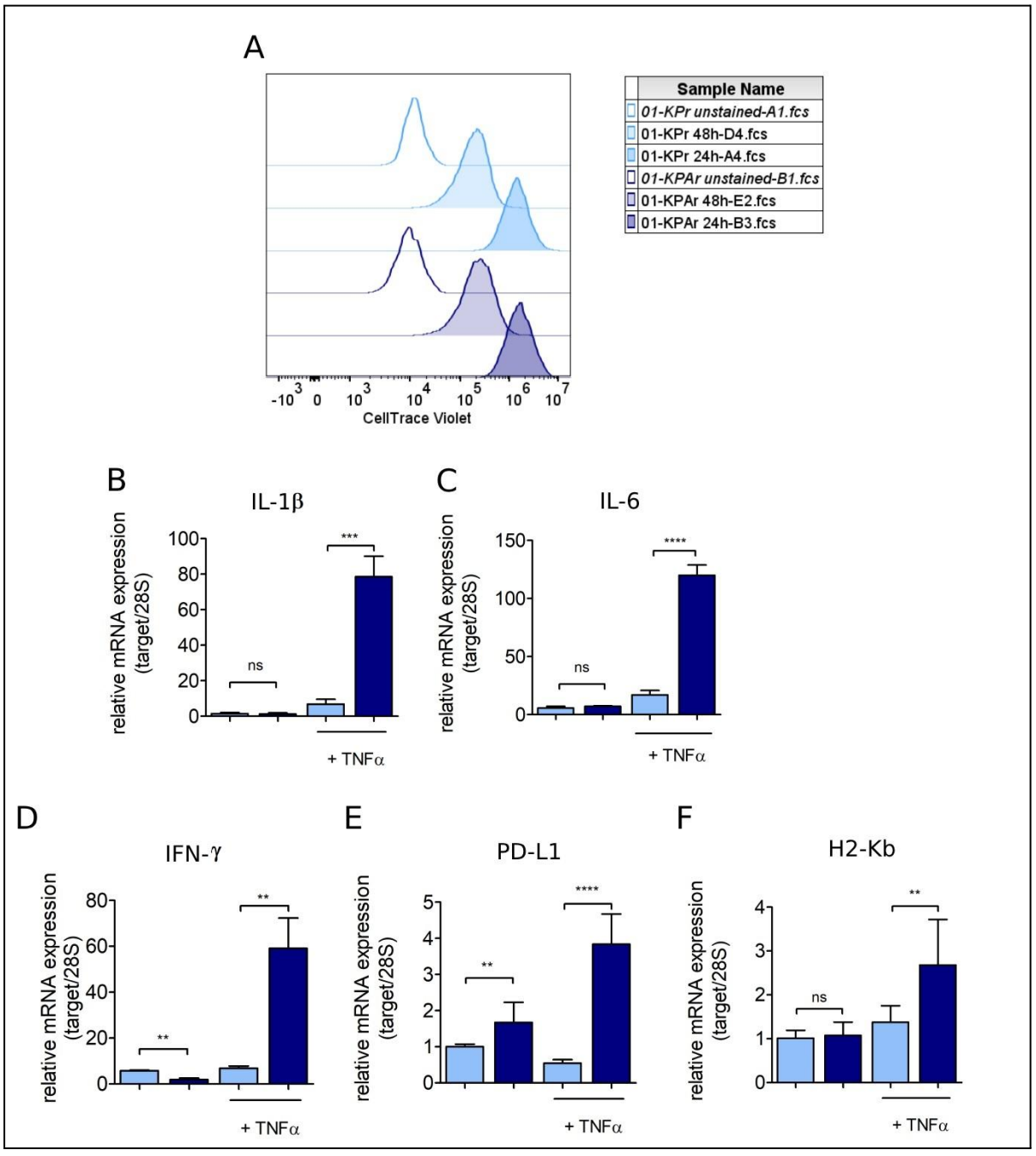

Figure 19: In vitro characterization of KPr and KPAr cell lines. ***(A)*** *Proliferation in KPr and KPAr cells was tracked using CellTrace Violet after 24 and 48 hours. The figure displays a sample cell population for each condition, serving as an example of the biological triplicates used in the assay. Gene expression levels for* ***(B)*** *IL-1β ,****(C)*** *IL-6 ,****(D)*** *IFN-γ ,* ***(E)*** *PD-L1 ,****(F)*** *and H2-Kb with and without TNF-α stimulation. Data are presented as the mean standard deviation (±SD), with duplicate sets of biological replicates per group. Significance levels are denoted as *p<0.05 and **p<0.01.*

We performed RT-qPCR to detect and assess the expression levels of NF-κB target genes following 4 hours of TNF-α stimulation in A20 knockout and WT cells. This

analysis unveiled a 60 to 120 fold increase in the expression of proinflammatory cytokines, IL-6, IL-1β, and IFN-γ (Fig. 19 B, C, D). Moreover, we noticed an elevated mRNA expression for PD-L1 and H2-Kb in KPAr cells, showing a 2 to 4 fold increase upon cytokine stimulation (Fig. 19 E, F).

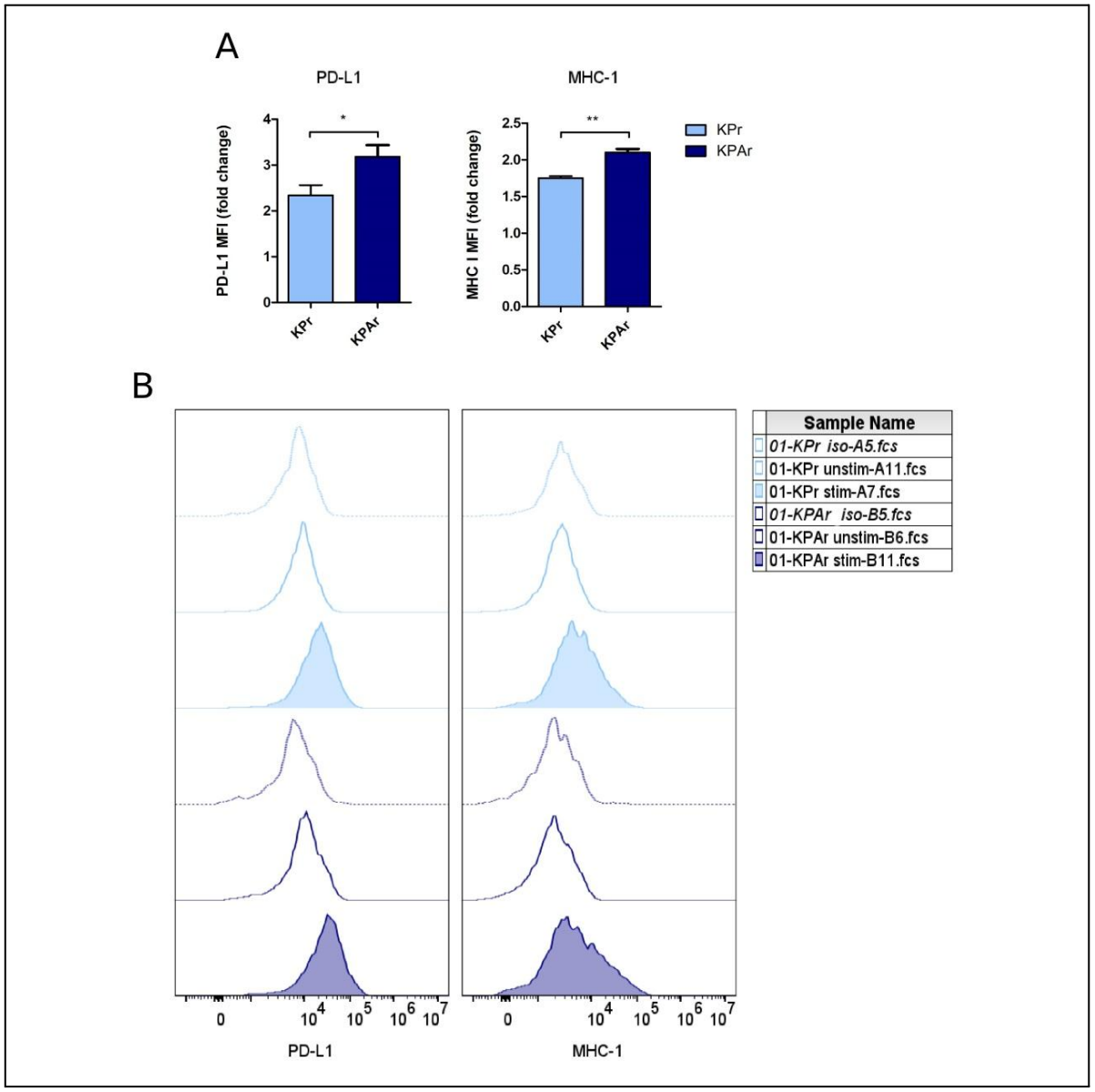

*Figure 20: Flow cytometric analysis of MHC-1 and PD-L1 expression on KPr and KPAr cells upon IFN-γ stimulation in vitro **(A)** shown by histograms (normalized to Mode) and **(B)** as mean fluorescent intensity (MFI), biological triplicates per group. Values are normalized to baseline levels of MHC-1 and PD-L1 of unstimulated cells. *p<00.5 and **p<0.01;*

As the gene expression data indicated potential changes in PD-L1 and H2-Kb mRNA levels in KPAr cells, we aimed to confirm this at protein level as well. To achieve this, we treated cells with 5 ng/ml of IFN-γ for a 24-hour period. Subsequently, we assessed the protein expression levels of MHC-1 and PD-L1 via flow cytometry, using the antibodies detailed in Table 25. Our observations indicated that KPAr cells exhibited a slightly elevated expression of MHC-1 and PD-L1 markers on their

surface compared to control cells, as evidenced by the mean fluorescence intensity (MFI) (Fig. 20A) of the respective markers and their corresponding histograms (Fig. 20B).

3.1.3 A20 deficient tumor cells escape immune surveillance by upregulating PD-L1 which leads to decreased $CD8^+$ T infiltration

To assess the impact of A20 knockdown on cancer cells *in vivo*, we performed Kaplan Meier survival analysis where the KPAr cells or their respective control KPr cells (1 million cells/ mouse) were orthotopically transplanted into immunocompetent C75BL/6 mice. Notably, the mice that received KPAr cells exhibited reduced survival compared to those that received wild-type tumor cells, as depicted in Figure 21 A. These findings align with our previous experiment without dTomato expressing tumor cells. This highlighted the association between A20 loss and heightened tumor aggressiveness and thus provides further evidence of A20's role as a tumor suppressor in mouse models of KRAS-driven lung adenocarcinoma.

To quantify alterations in tumor growth over time and gain a deeper understanding of the mechanisms through which A20-deficient tumors evade immune surveillance, we orthotopically transplanted 2.5 million KPr or KPAr cells into immunocompetent mice aged 8-10 weeks. The mice were euthanized at three distinct time points: 1, 2, and 3 weeks following transplantation (Fig. 21). The lungs were enzymatically digested and the single cell suspensions were stained with antibodies against CD45, CD8, and PD-L1 surface markers (Table 25) and analyzed by flow cytometry. There were no significant variations in the proportions of $CD45^+$ cells between KPr and KPAr groups, though a mild decrease was noticed in both by the third week (as shown in Fig. 21 B). The ratios of dTomato cells dramatically increased in the KPAr group on week 2 and week 3 while in the KPr group there was only a small increase in the ratios of tumor cells by week 3 (as depicted in Fig. 21 B). Concerning $CD8^+$ T cells, a sharp decline was observed in the KPAr group as early as the second week, which further dropped by the third week. In contrast, the KPr group showed a slight increase by the third week (Fig. 21 D). Additionally, the proportions of PD-L1-expressing dTomato tumor cells elevated in the KPAr lung tumors after two

weeks, but showed a decline after 3 weeks. This change aligns with the earlier noted decline in $CD8^+$ T cell ratios. These experiments were complementary to previous experiments we performed with KP and KPA cells without dTomato reporter and the findings from this thesis were included as a component of a larger published study.

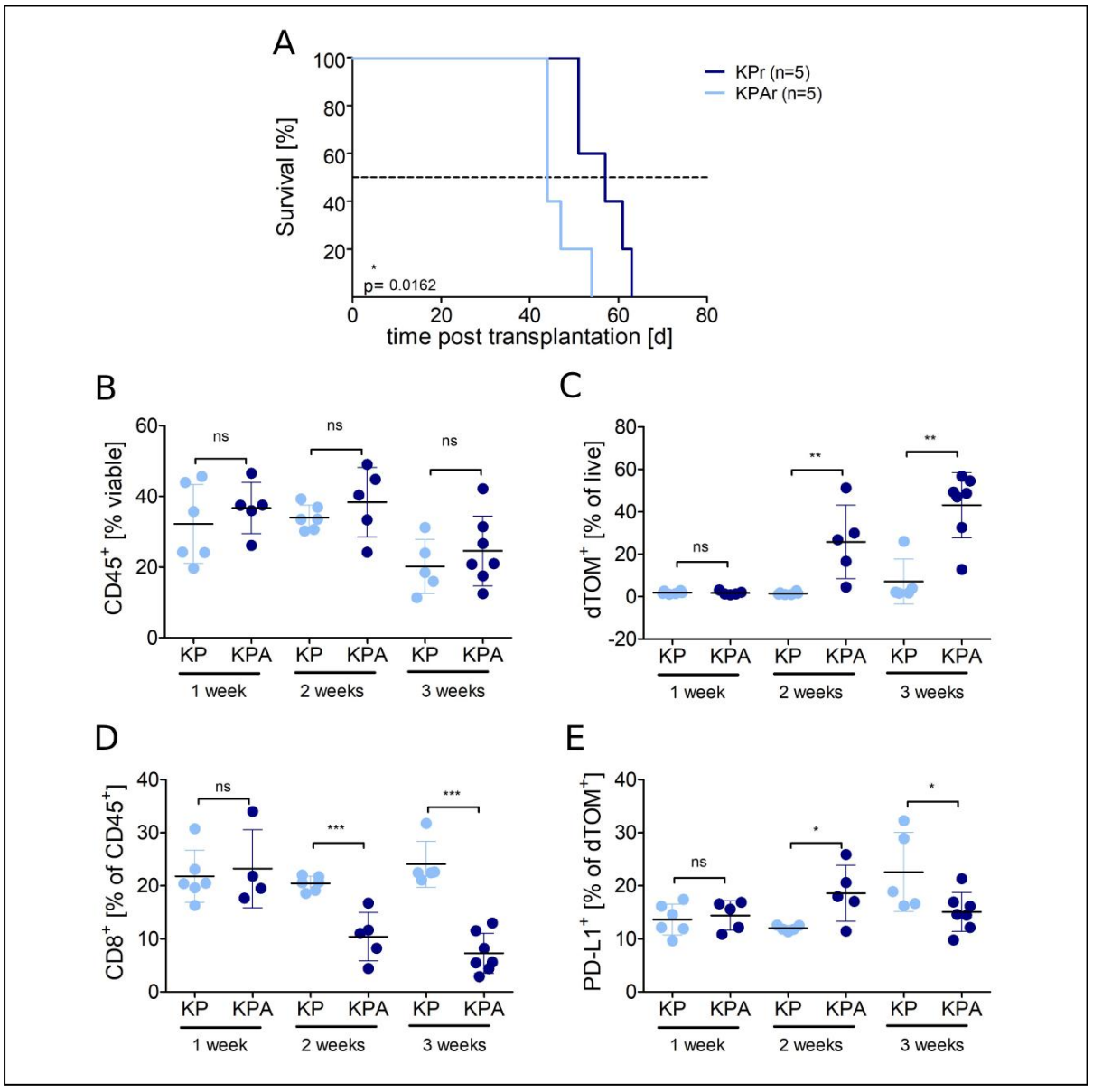

*Figure 21: **(A)** Kaplan Meier survival assay of orthotopically transplanted mice with 1 million of KPr or KPAr cell lines. „n" represents the number of experimental mice pre group. *p<00.5 Flow cytometric analysis of lung cells of KPr and KPAr tumor bearing mice 1, 2 and 3 weeks post transplantation. Changes in the tumor microenvironment demonstrated by alterations in the percentage of **(B)** CD45+ cells of viable cells **(C)** CD45+ CD8+ cells, **(D)** dTom+ cells and **(E)** PD-L1 expression on dTom+ tumor cells. The number of experimental mice pre group was 4-6. *p<00.5 **p<0.01;*

3.2 Results 2: Role of A20 in immune cells within the tumor microenvironment

Our preliminary findings indicate that partial systemic knockdown of A20, as observed in $A20^{\Delta/+}$ mice, induces a tumor-suppressive microenvironment. This discovery motivates further investigation into the physiological role of A20 in regulating tumor-stroma interactions. To understand the immunomodulatory properties of A20 within the tumor microenvironment, we aimed to elucidate its effects on immune cells in the stroma in mouse models of KRAS-driven lung adenocarcinoma. We hypothesize that knockdown of A20 expression in stromal cells can initiate a cascade of inter cellular effects, leading to further suppression of tumor growth.

Determining the key immune cells responsible for creating a tumor-suppressive milieu after A20 downregulation, and subsequently assessing their enhanced efficacy in tumor elimination, could offer significant insights into the advantages of using a synergistic combination of the most effective immune cells to enhance adoptive cell transfer-based immunotherapy.

3.2.1 Systemic knockdown of A20 leads to decreased $CD8^+$ and $CD4^+$ T cells within the lungs of experimental mice

The experimental approach involved initiating a systemic A20 knockdown in mice with established tumors, followed by the investigation of whether the elimination of the NF-κB negative regulatory influence leads to heightened immune cell activation. The primary objective was to ascertain whether this immune response induces a shift in the tumor microenvironment towards a state that inhibits tumor growth. For this purpose, we took advantage of the Tamoxifen/Cre^{ERT2} mouse model where the Cre recombinase is fused to the estrogen receptor mutated on the ligand binding domain allowing binding to tamoxifen [148]. The gene for this fusion protein is ubiquitously expressed from the ROSA26 locus (Fig. 22) and the protein is sequestered and kept inactive in the cytoplasm by the heat shock protein 90 (HSP90). Tamoxifen disrupts this interaction and allows the translocation of Cre^{ERT2}

to the nucleus which induces site specific recombination between the LoxP sites leading to the excision of the 2 exon in the A20 encoding gene [149].

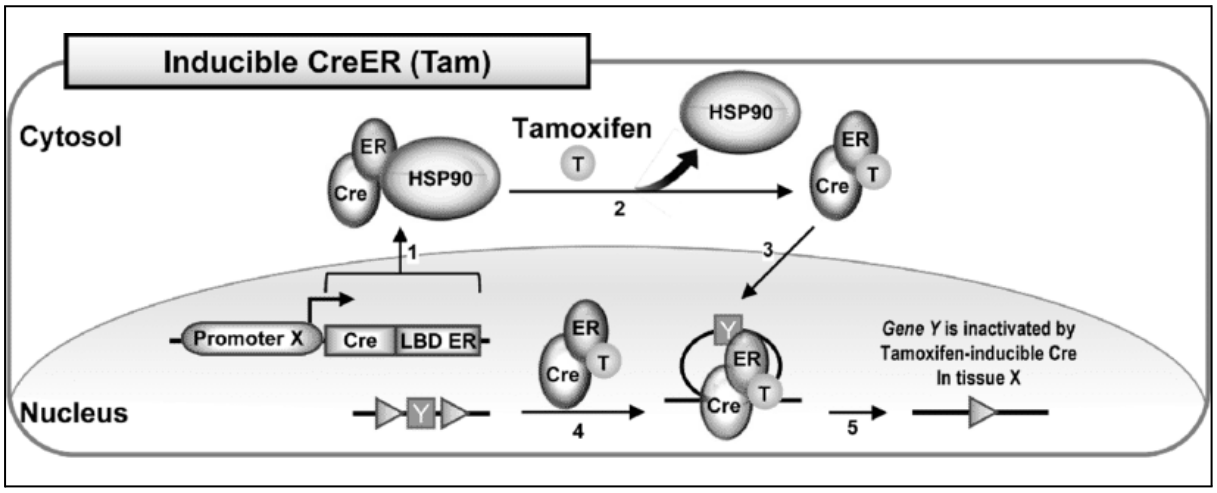

Figure 22: Inducible Cre^{ERT2} system. The Cre recombinase is fuzed to the mutated form of estrogen receptor and ubiquitously expressed under the ROSA26 promoter. Tamoxifen binding to Cre^{ERT2} allows translocation to the nucleus and activity of the recombinase [149].

Tamoxifen was diluted in sunflower oil and administered via gavage feeding of the mice. A20$^{fl/fl}$:Cre^{ERT2} mice were first treated with different doses of Tamoxifen to determine the ideal dose that induces recombination of the A20 exon 2 flanked by LoxP sites. Subsequently, DNA extracted from the lungs and spleen of treated mice was analyzed via PCR to determine the presence of wild-type, A20$^{fl/fl}$, A20$^{\Delta/fl}$, or A20$^{\Delta/\Delta}$ variants of the A20 gene (see Fig. 23). A20$^{fl/fl}$ mice were used as negative controls.

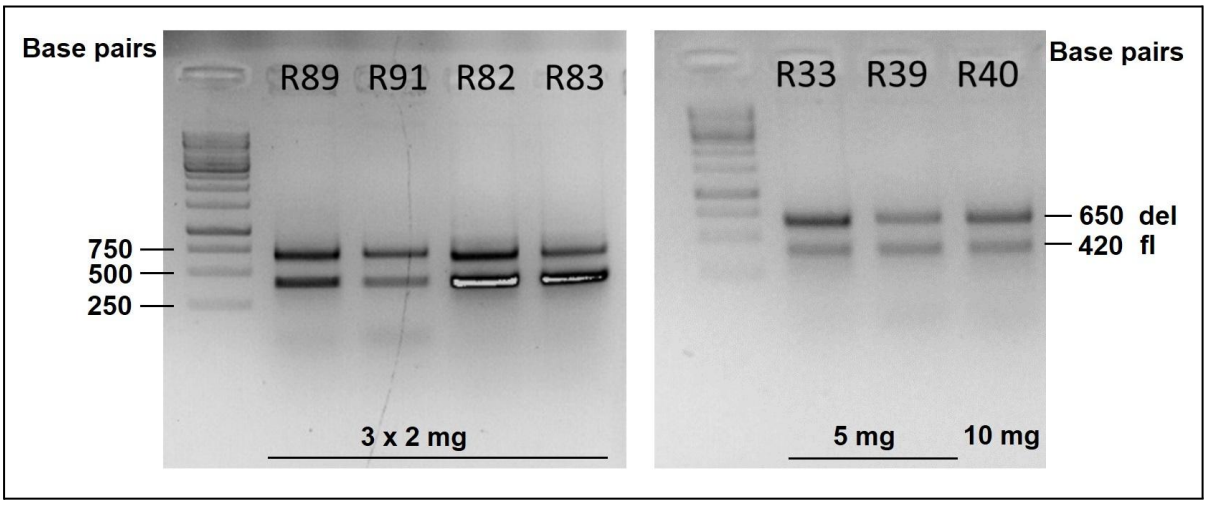

Figure 23: PCR reaction of Lung lysates of Tamoxifen treated A20$^{fl/fl}$:Cre^{ERT2} mice. Mice R89, R91, R82 and R83 were treated 3 times with 2 mg Tamoxifen while R33, R39 received 5 mg and R40 10 mg.

Although all A20$^{fl/fl}$:Cre^{ERT2} mice that were treated with highest doses of tamoxifen (5 or 10 mg) showed high recombination efficiency of A20 exon 2 (around or above 50% efficiency), they developed severe multiorgan inflammation rapidly and had to be euthanized within 5-7 days (Fig. 24). Lower doses with repeated treatment (3 x 2 mg) resulted in lower recombination of A20 exon 2 but these mice also developed severe inflammation in many organs later on in contrast to the control WT mice, which did not show any sign of inflammation.

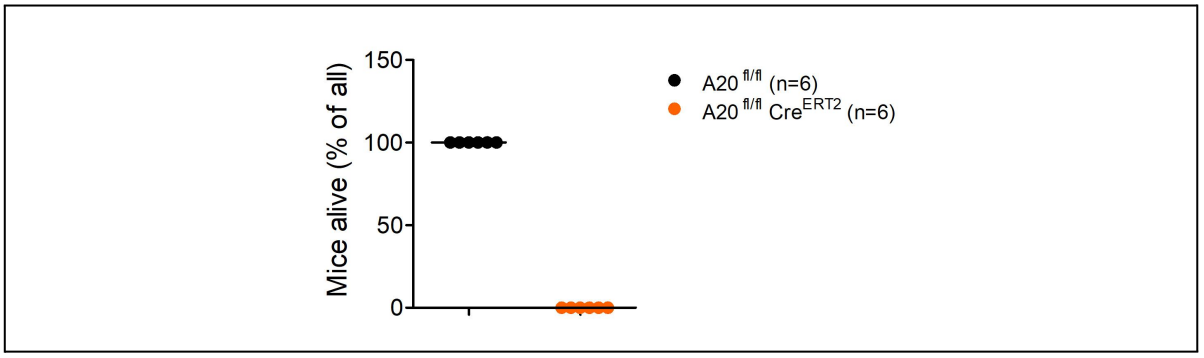

Figure 24: Viability of Tamoxifen treated A20$^{fl/fl}$ control and A20$^{fl/fl}$:Cre^{ERT2} mice after 7 days. Both groups contain all the mice that were treated with different concentrations of Tamoxifen.

To study the effect of A20 downregulation on antitumor response *in vivo* we used A20$^{fl/fl}$:Cre^{ERT2} and control A20$^{fl/fl}$ mice, which received 5 million of KPr tumor cells via orthotopic transplantation. These mice received oral gavage administration of 2 mg of Tamoxifen on day 9 and day 12 post-transplantation. The experimental cohort was sacrificed 5 days after the second Tamoxifen treatment, and subsequent analysis involved the harvesting of lungs and spleens. Lung cell lysates were subjected to flow cytometry to evaluate lymphoid immune cell markers.

Regrettably, the brief treatment did not yield favorable outcomes in terms of restraining tumor progression. We identified tumor cells based on the presence of the dTomato fluorescent protein; however, no noteworthy distinctions in tumor cell numbers were observed between the lungs of control and A20 knockdown mice (Fig. 25A). On the contrary, systemic *in vivo* knockdown of A20 drastically decreased the number of both CD4$^+$ and CD8$^+$ T cells in the lungs of experimental mice, while the number of CD45$^+$ leukocytes, NK cells and CD19$^+$ cells showed no significant differences compared to control (Fig. 25A and B).

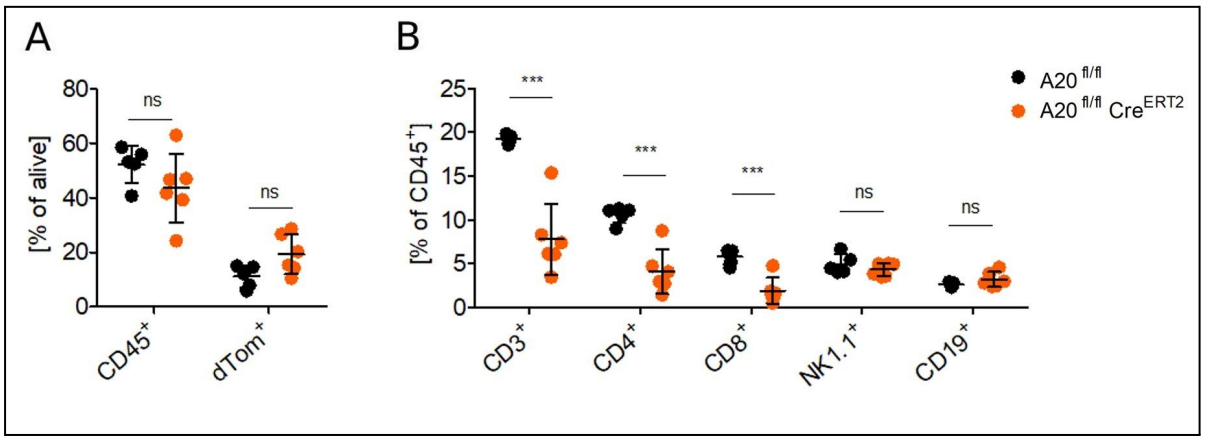

Figure 25: Immune cell composition of A20 proficient and A20 knockdown tumor bearing mice analyzed by flow cytometry. ***(A)*** *CD45⁺ leukocytes and dTomato⁺ tumor cells* ***(B)*** *Lymphoid cells shown in % of CD45⁺ cells.*

Our findings led us to the deduction that the systemic knockdown of A20 using the Cre^{ERT2} system results in a depletion of T cells within the lung tissue. This can be elucidated by a prior publication indicating that the expression of Cre in the thymus has an adverse impact on $CD4^+CD8^+$ immature cells, leading to apoptosis [150]. Since we were mainly interested in T cell responses this impedes the ability to assess how A20 loss influences immune cell activation and their capacity to eliminate tumors. As a result, we decided to alter our approach and utilize A20 heterozygous mice, which carry a deficiency in one allele of the gene. Unchallenged mice do not exhibit overt inflammatory phenotype, except for a mild cerebral inflammation, which is associated with regular levels of circulating TNF-α and IL-6 [102–104].

3.2.2 Systemic heterozygous downregulation of A20 enhances immune surveillance by increased T cells infiltration in the lungs of tumor bearing mice

In order to identify critical cell populations in the stroma of $A20^{\Delta/+}$ mice that are responsible for the tumor suppressive phenotype, the previously described KPr cells (5 million) were used and orthotopic transplanted into the lungs of 8 weeks old wild-type and $A20^{\Delta/+}$ mice. At 1 and 4 weeks post transplantation, we harvested the lungs and spleens of the experimental mice for flow cytometric analysis. Body and spleen weights were measured during the mice harvesting process and subsequently compared between the two experimental groups. Although there was no significant difference in body weights, the spleens of A20 heterozygous mice were enlarged (Fig. 26 A, B, C). Flow cytometric analysis unveiled an elevated ratio

of infiltrating $CD4^+$ and $CD8^+$ T cells in the lungs of $A20^{\Delta/+}$ mice compared to controls one week post-transplantation (Fig. 26 D). Conversely, there were no significant variations in NK cell populations and the myeloid cells, where $CD11b^+$ $Ly6C^+$ cells correspond to neutrophils, $CD11b^+$ $Ly6G^+$ are indicative of myeloid-derived suppressor cells, $CD11b^+$ $CD11c^+$ denote dendritic cells, and those marked by $CD11b^+$ $CD11c^+$ $CD206^+$ are representative of M2 macrophages (Fig 26 E).

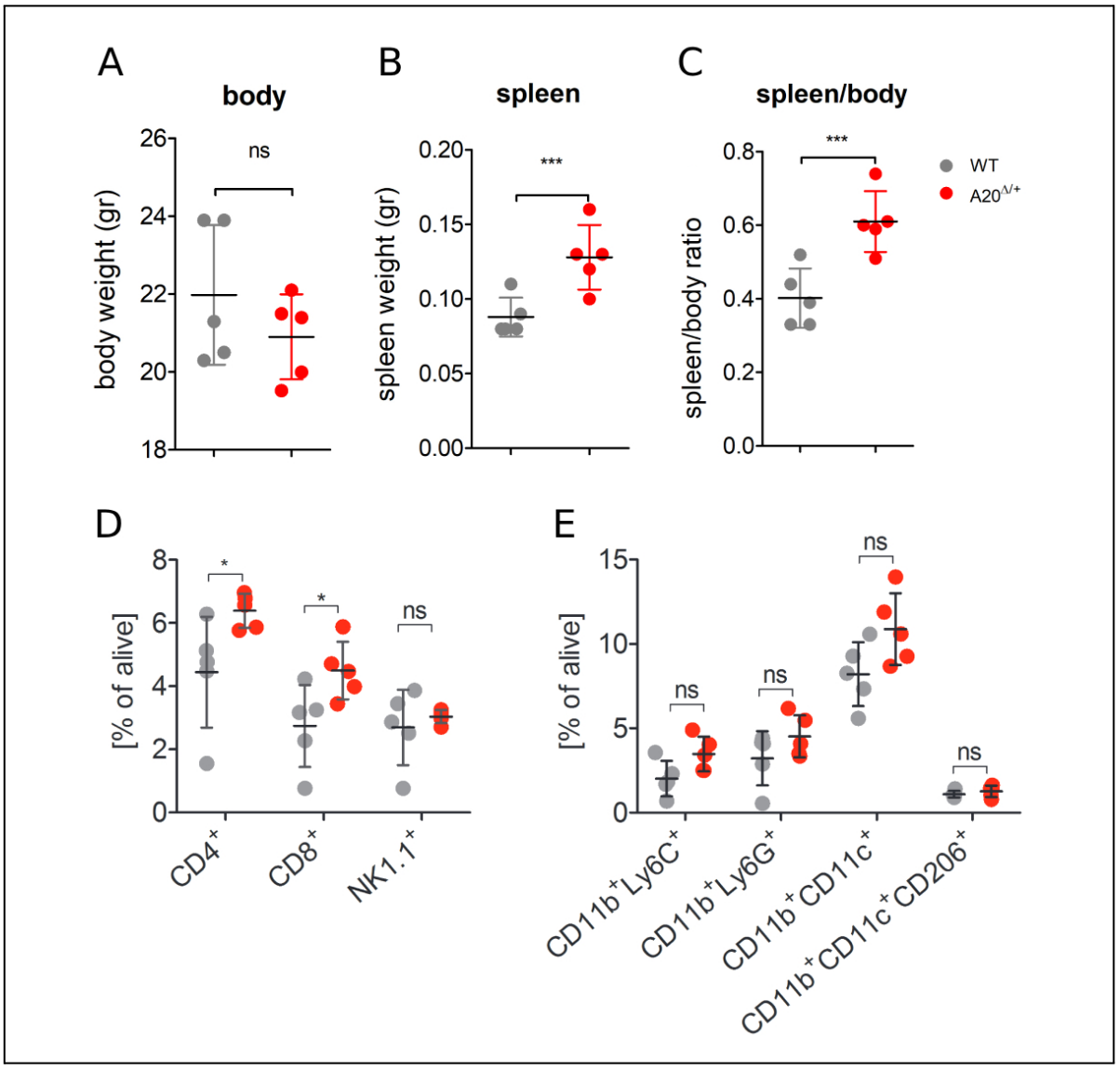

*Figure 26: **(A)** Body, **(B)** spleen and **(C)** spleen/body weight ratios of experimental mice after 1 and 4 weeks post tumor cell transplantation. Flow cytometric analysis of cell suspensions derived from tumor bearing lungs of wild-type versus $A20^{\Delta/+}$ mice (n= 5 per group) one week post transplantation. **(D)** $CD4^+$ $CD8^+$ and $NK1.1^+$ cells **(E)** $CD11b^+$ $Ly6C^+$ represent neutrophils, $CD11b^+$ $Ly6G^+$myeloid derived suppressor cells, $CD11b^+CD11c^+$ dendritic cells and $CD11b^+CD11c^+CD206^+$ represent M2 macrophages.*

3.2.3 Signaling pathways related to inflammation and immune response exhibit elevated levels in A20 heterozygous tumor bearing mice

To gain insights into *in vivo* processes and active cell populations, we conducted RNA sequencing. Samples from the lungs of tumor-bearing wild-type (WT) and $A20^{\Delta/+}$ mice from the 1 week time-point, along with their respective non-tumor-bearing controls, were collected for subsequent bulk RNA sequencing. Initially, the samples were subjected to RNA quality and integrity assessments before sequencing. Upon receiving the electronic data, we performed gene set enrichment analysis using the online tool Enricher, uncovering upregulated gene sets associated with specific signaling pathways in the A20 het mice compared to the control group. These findings indicate that tumor-bearing A20 heterozygous mice exhibit heightened activity in the JAK-STAT pathways, TNF signaling pathways, and inflammatory responses when compared to wild-type mice, as illustrated in the bar graph (Fig. 27 A).

Furthermore, heatmap illustrates elevated expression of genes linked to immune cell recruitment, including CCL5, CXCL9, CXCL10, and XCL1, in A20 het tumor-bearing mice (Fig. 27B). Moreover, heightened levels of T cell response markers such as CD8a, CD4, GZMB, IFN-γ, PRF1, TBX21, and EOMES are observed, along with increased presence of NCR1 and NKG7 associated with NK cell functions. Additionally, CLEC9A, linked to antigen presentation by dendritic cells, displays higher expression in $A20^{\Delta/+}$ tumor-bearing mice.

In summary, the RNA sequencing results reinforce the notion that A20 heterozygous mice display heightened inflammatory signaling. This observation lends additional support to our finding that systemic A20 downregulation may enhance the anti-tumorigenic characteristics of immune cells within the tumor microenvironment.

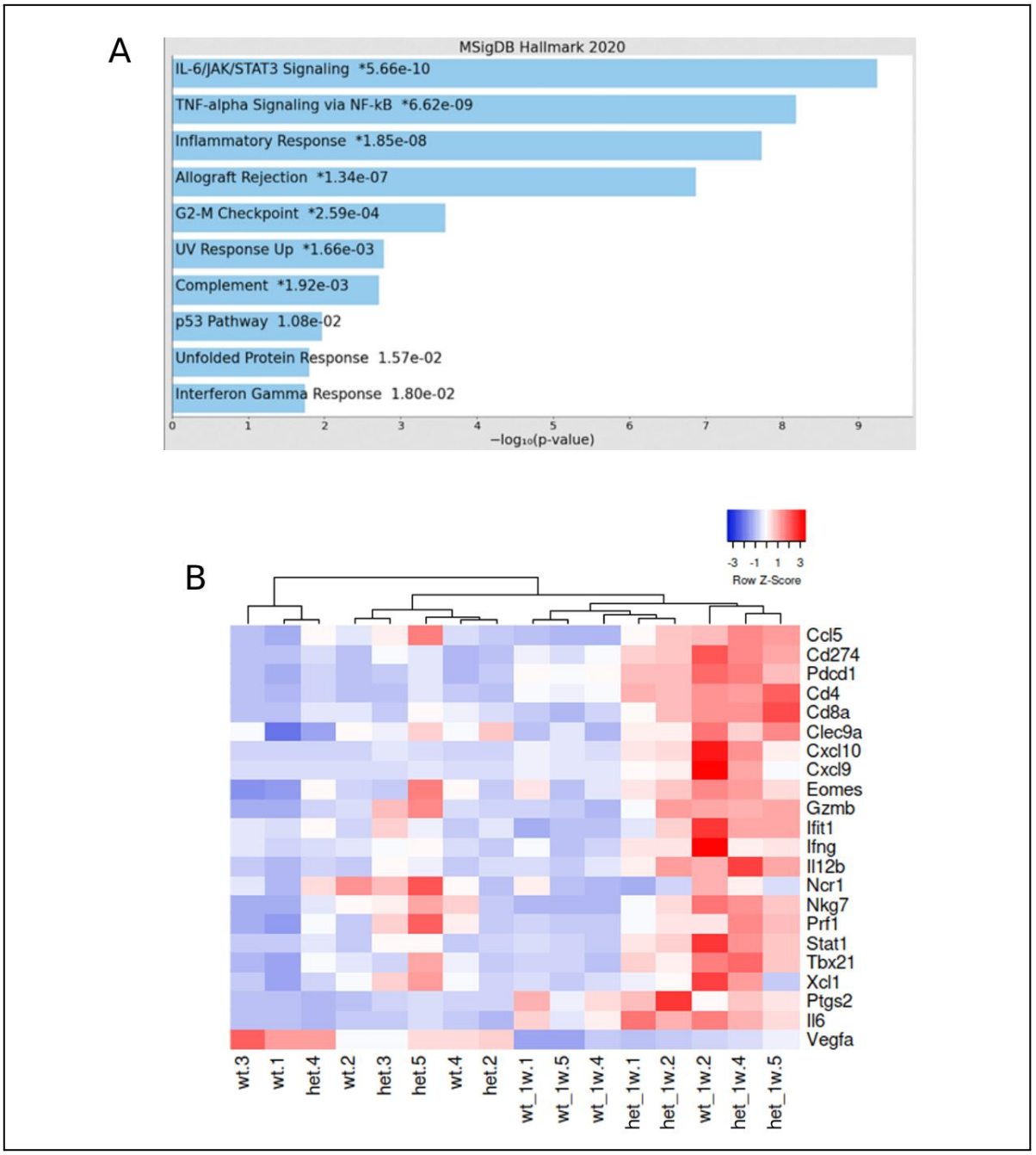

Figure 27: ***(A)*** *Gene set enrichment analysis of RNA sequencing data. Tumor bearing A20 heterozygous mice show increased activity of inflammatory pathways.* ***(B)*** *Heatmap of altered gene expression profiles of wild-type and A20 heterozygous tumor bearing mice versus tumor free control groups. Scale bar represents upregulated genes with red and downregulated genes with shades of blue.*

4. Discussion

Despite advances in treatment and prevention, lung cancer remains the predominant cause of cancer-associated deaths [2]. A frequent mutation driving this malignancy is found in the KRAS gene, linked to persistent inflammation and presenting significant treatment challenges [25,34]. Although research has made significant strides, and there are specific inhibitors targeting the G12C mutation of KRAS, there are currently no approved clinical inhibitors for other KRAS mutations [151]. Gaining a deeper insight into how KRAS mutant lung tumors influence the tumor microenvironment and elucidating their link to inflammation would provide crucial insights for enhancing current treatment strategies and exploring novel therapeutic approaches and combinations, ultimately aiming to enhance the quality of life for patients. Inflammation is recognized as a catalyst for tumorigenesis [63,64]. A key moderator of inflammatory stability is A20, which primarily acts as a counteractive agent for both canonical and non-canonical NF-κB signaling pathways, alongside other roles [85]. Within tumors, A20 can manifest dual roles, acting either as a tumor suppressor or an oncogene [81]. On the other hand, A20 as an NF-κB regulator has a crucial role in the regulation of immune cell activation as well [85].

This thesis aimed to delve deeper into the mechanisms underlying enhanced tumor growth and immune evasion resulting from the intrinsic loss of A20. To achieve this, we engineered an A20-deficient adenocarcinoma reporter cell line through CRISPR/Cas9 technology. We characterized this mutant using RT-qPCR and flow cytometry to assess the impact of A20 loss *in vitro.* Additionally, we conducted lung transplantation experiments in immunocompetent mice, implanting either control and A20-deficient tumor cells. Our investigation involved tracking tumor cell proliferation and profiling the evolving immune cell composition within the tumors at various time points. Furthermore, we studied the tumor suppressive effect of systemic A20 downregulation in orthotopic transplantation models of lung adenocarcinoma employing flow cytometry and RNA sequencing.

4.1 Discussion 1: Tumor suppressive role of A20

4.1.1 Genetic deletion of A20 in KP dTomato^{+} reporter cell line

With the aim of exploring the consequences of tumor-specific A20 loss both in vitro and in vivo, we employed the CRISPR/Cas9 system to genetically modify the KPr cell line. This modification involved introducing a frameshift mutation in the TNFAIP3 gene. To evaluate the effectiveness of our genome editing, we utilized the online tool TIDE (Tracking of Indels by DEcomposition) available at http://shinyapps.datacurators.nl/tide/. The results from TIDE confirmed the efficiency of gene editing in both pooled cells and single-cell clones.

Additionally, we conducted an analysis of TNFAIP3 gene expression at the mRNA level, revealing a significant reduction. Furthermore, our investigation included western blot analysis, which conclusively confirmed the absence of A20 protein expression. With all this serves as strong evidence for the successful knockout of A20.

4.1.2 A20 deficient KPr cell line shows increased sensitivity to cytokine stimulation

To assess the impact of A20 deficiency on tumor cell proliferation, we employed CellTrace Violet proliferation dye staining and conducted flow cytometry analysis. This experiment revealed no difference in proliferation between KPr and KPAr cells under standard culture conditions. As the proliferation assay was conducted under standard culture conditions where A20 exhibits its low baseline expression, any potential effect of A20 knockout on cell proliferation remains indistinguishable. To investigate whether the introduced mutation in A20/TNFAIP3 gene alters gene expression, we examined mRNA levels of NF-κB target genes following TNF-α stimulation. As anticipated, the absence of A20, resulted in a drastic increase of proinflammatory cytokines IL-6, IFN-γ, and IL-1β on mRNA level. This can indicate that KPAr cells could potentially release higher levels of inflammatory cytokines,

which might accelerate tumor progression. This could set up a feedback loop *in vivo*, where tumor cells further produce inflammatory cytokines in response to this inflammatory setting contributing to tumor progression. While it would be ideal to confirm cytokine production on protein level using ELISA in *in vitro* cultures, such verification was not part of the current study.

Additionally, we observed an upregulation of the PD-L1 checkpoint molecule and the H2-Kb (alpha chain of the MHC-I molecule found in mice) molecule on mRNA and protein level in KPAr cells, shown by RT-qPCR and flow cytometry. Higher MHC-1 expression on KPAr cells, which intensifies upon cellular stimuli to present self-antigens, indicates that the immune system might more effectively recognize and target these cells, especially if they exhibit aberrant molecules, compared to KPr cells. However, when combined with PD-L1 expression, this could rapidly neutralize T cells that might otherwise attack tumor cells presenting neoantigens.

Overall, our findings indicate that the intrinsic loss of A20 in tumors results in heightened responsiveness to inflammatory triggers and increased PD-L1 expression, which might enhance the aggressiveness of the tumors *in vivo*.

4.1.3 A20 deficient tumor cells upregulate PD-L1 and decrease survival of mice

Time point analysis of orthotopically transplanted KPr and KPAr cells showed that KPAr cells proliferate more rapidly over time than KPr and begin expressing the PD-L1 checkpoint molecule on week 2 while at the same time the ratios of $CD8^+$ T cells start decreasing from week 2. This pattern suggests that the initial rise in the checkpoint inhibitor PD-L1 on tumor cells required to escape from $CD8^+$ T cell recognition. By the third week, with the reduced presence of T cells, the need for heightened PD-L1 expression decreases, mirroring a diminished necessity for tumor cells to elude immune surveillance. In the control group featuring KPr cells, although there is some proliferation, it occurs at a slower rate. Additionally, the increase in PD-L1 expression on these tumor cells is not as marked, and the ratios of $CD8^+$ T cells remain relatively stable.

In summary, our findings confirm the previously reported findings that linked tumor-specific A20 deficiency to increased PD-L1 expression and a corresponding decrease in $CD8^+$ T cell infiltration in the tumor milieu, seen both in murine models of KRAS-driven lung adenocarcinoma and patients with KRAS mutant LUAD [121].

4.2 Discussion 2: The systemic effect of A20 downregulation

4.2.1 Induced Systemic knockdown of A20 using the inducible Tamoxifen/Cre^{ERT2} system

While prior studies have explored the impact of A20 knockdown in specific immune cells, the potential for heightened anti-tumor responses due to simultaneous A20 suppression in immune cell populations has not been extensively studied. To examine weather systemic A20 downregulation can lead to increased immune cell activation and better anti-tumorigenic responses, we bred ROSA26-Cre^{ERT2} $A20^{fl/fl}$ mice and treated them with different concentrations of Tamoxifen to induce Cre activation and subsequent A20 deletion. Since full knockout of A20 is incompatible with life as demonstrated by homozygous A20 knockout mice [101], we did not aim for full but only for partial heterozygous recombination. We noted a correlation between recombination efficiency in lung tissue and Tamoxifen dosage, accompanied by an escalation in multi-organ inflammation and a decline in survival rates. Consequently, we decided to use a lower dose of Tamoxifen, 2 mg, which achieved roughly 50% recombination in the lungs. This could still potentially enhance immune activation through lowered A20 levels and we decided to look at the short term changes within the tumor microenvironment. Following tumor cell transplantation, both ROSA26-Cre^{ERT2}: $A20^{fl/fl}$ mice and control $A20^{flfl}$ mice were administered Tamoxifen on days 9 and 12. Our hypothesis centered on the expectation that A20 reduction would amplify anti-tumor responses. However, flow cytometry data showed comparable tumor cell ratios between both groups, and a reduced T cell presence in the lungs of the A20-suppressed group. These observations suggest potential complications in T cell development, survival or maturation due to *in vivo* A20 knockdown in adult mice. In addition, a previous publication showed that Cre

recombinase expression in the thymus leads to apoptosis of $CD4^+CD8^+$ double positive immature T cells even in the absence of floxed allele [150]. While we assessed recombination efficiency primarily in lung tissues and spleens, variations across tissues and cells are plausible [152], complicating the systemic impact assessment. Although we didn't observe pronounced impacts on other examined cell types, this doesn't preclude potential alterations in their activity.

A plausible interpretation might be that the suppression of A20 in stromal cells triggered severe inflammation to the extent that it would promote tumor development. This widespread inflammation could essentially mask any beneficial effects on T-cell activation that might arise from A20 suppression.

4.2.2 A20 heterozygous mice show increased infiltration of T cells

To identify key stromal cells contributing to the tumor suppressive trait in A20 het mice, we transplanted 5 million KPr cells into 8-week-old wild-type and $A20^{\Delta/+}$ mice and analyzed the lung immune microenvironment via flow cytometry to determine if there are changes in the ratios of certain immune cell populations. We decided to focus on immune cells rather than stromal cells such as fibroblasts or other cells since immune cells are the main cell types mediating antitumor immune response and the NF-κB/IFN pathways that are regulated by A20 are crucial for immune cell activation.

We observed that A20 het mice had splenomegaly that can mean that lower levels of A20 leads to increased immune cell production and accumulation in the spleen although we did not look into this in more details and did not identify differences in immune cell populations in other tissues than the lungs. Flow cytometry analysis showed increased infiltration of $CD4^+$ and $CD8^+$ T cells in $A20^{\Delta/+}$ mouse lungs 1 week after transplantation but no significant differences in NK or other myeloid cell populations. These findings suggest that variations in T cell numbers may play a role in the observed phenotype and enhanced anti-tumorigenic properties. However, we cannot rule out the possibility of altered immune cell activity, or migration capacity of immune cells upon A20 downregulation as it was suggested by previous publications.

In conclusion, the heightened presence of T cells in the lungs of A20 heterozygous mice with tumors suggests that these T cells may either infiltrate more effectively or proliferate more rapidly. and we could utilize this knowledge to potentially improve effectiveness of T cell therapies. Harnessing this understanding could pave the way to enhancing the efficacy of T cell-based therapies.

4.2.3 Increased inflammatory signaling is observed in lung tissues of tumor-bearing $A20^{\Delta/+}$ mice

We conducted RNA sequencing on lung tissues from tumor-bearing wild-type and A20 heterozygous mice to gain insights into *in vivo* processes. However, gene set enrichment analysis confirmed our expectations, revealing heightened activity in inflammatory signaling pathways in the A20 heterozygous mice; this bulk RNA sequencing does not inherently differentiate between tumor and non-tumor tissue or identify the RNA source. We attempted to distinguish between favorable and unfavorable inflammatory markers using the RNA sequencing data, but we encountered substantial variations among the samples.

5. Conclusion and Outlook

This project highlights the dual roles of A20 in tumor cells versus immune cells in mouse models of lung adenocarcinoma.

We generated and assessed an A20-deficient KRAS mutant dTomato^{+} cell line, which exhibited heightened expression of proinflammatory cytokines such as IL-6, IL-1β, and INFγ-, along with elevated PD-L1 levels *in vitro*. Notably, these A20 knockout tumor cells displayed enhanced growth and increased PD-L1 expression when transplanted in immunocompetent mice, effectively evading T cell recognition. The experiments presented in this thesis were conducted as a complementary component of a larger study, which has already been published where we demonstrated that A20 acts as a tumor suppressor in KRAS-driven LUAD [121]. Tumor cells attempt to downregulate A20, resulting in accelerated growth and increased PD-L1 expression. This elevated PD-L1 expression, in turn, augments the effectiveness of anti-PD-L1 therapy for these tumors [121]. Our findings were confirmed through experiments conducted on mouse models of LUAD and data collected from melanoma patients, highlighting that individuals with lower A20 levels tend to exhibit more favorable responses to ICB (immune checkpoint blockade) therapy [121]. While our previous research provided insights into A20's role in the context of KRAS LUAD, our current focus is on examining the role of A20 in EGFR-mutated LUAD. This expansion of our research aims to broaden our understanding of A20's role beyond specific genetic mutations.

In the second part of this thesis, we demonstrated that A20$^{\Delta/+}$ mice exhibit a more anti-tumorigenic environment characterized by increased T cell infiltration and heightened inflammatory signaling. To gain deeper insights into the contributing cell types behind this phenotype, orthotopic transplantations can be repeated to identify immune cells in the lungs, spleens and tumor-draining lymph nodes of mice using flow cytometry and immunohistochemistry. Furthermore, a comprehensive characterization of immune cell populations and subpopulations, including Treg cells, as well as an assessment of the activation/exhaustion status of T cells, and the examination of specific antigen presentation cell populations in tumor-draining lymph nodes, would provide valuable insights into elucidating and comprehending the intricate interplay between stromal and tumor cells in A20$^{\Delta/+}$ mice. Performing RNA

sequencing on distinct immune cell populations would yield additional valuable insights and complement the findings obtained through flow cytometric analysis. This approach would enable us to pinpoint which immune cell subsets exhibit an enhanced antitumorigenic response due to A20 downregulation and identify the distinctions when compared to the previously published data on conditional homozygous A20 knockdown in immune cells. Additionally, isolating and characterizing specific immune cell populations *in vitro* may offer insights into how heterozygous A20 loss impacts immune cell function. Given our observation that $A20^{\Delta/+}$ mice have an increased T cell presence, investigating these cells *in vitro* becomes particularly relevant. While it is true that $A20^{\Delta/\Delta}$ $CD8^+$ T cells exhibit heightened efficiency as killers and can reduce tumor growth in mouse models [135], their hyperactivity poses a potential concern, warranting exploration of whether $A20^{\Delta/+}$ $CD8^+$ T cells can retain the benefits of $A20^{\Delta/\Delta}$ $CD8^+$ T cells without the associated negative effects. Moreover, the concept of co-transplanting $CD4^+$ and $CD8^+$ T cells is widely proposed as a potentially more effective therapy since $CD4^+$ T cells contribute significantly to antigen presentation, B cell activation, exhibit cytotoxic capabilities, and are a great source of IFN-γ [153,154].

To further advance our understanding of how manipulating A20 levels could enhance treatment options for KRAS mutant LUAD patients, extensive research in mouse models is essential.

6. Supplementary data

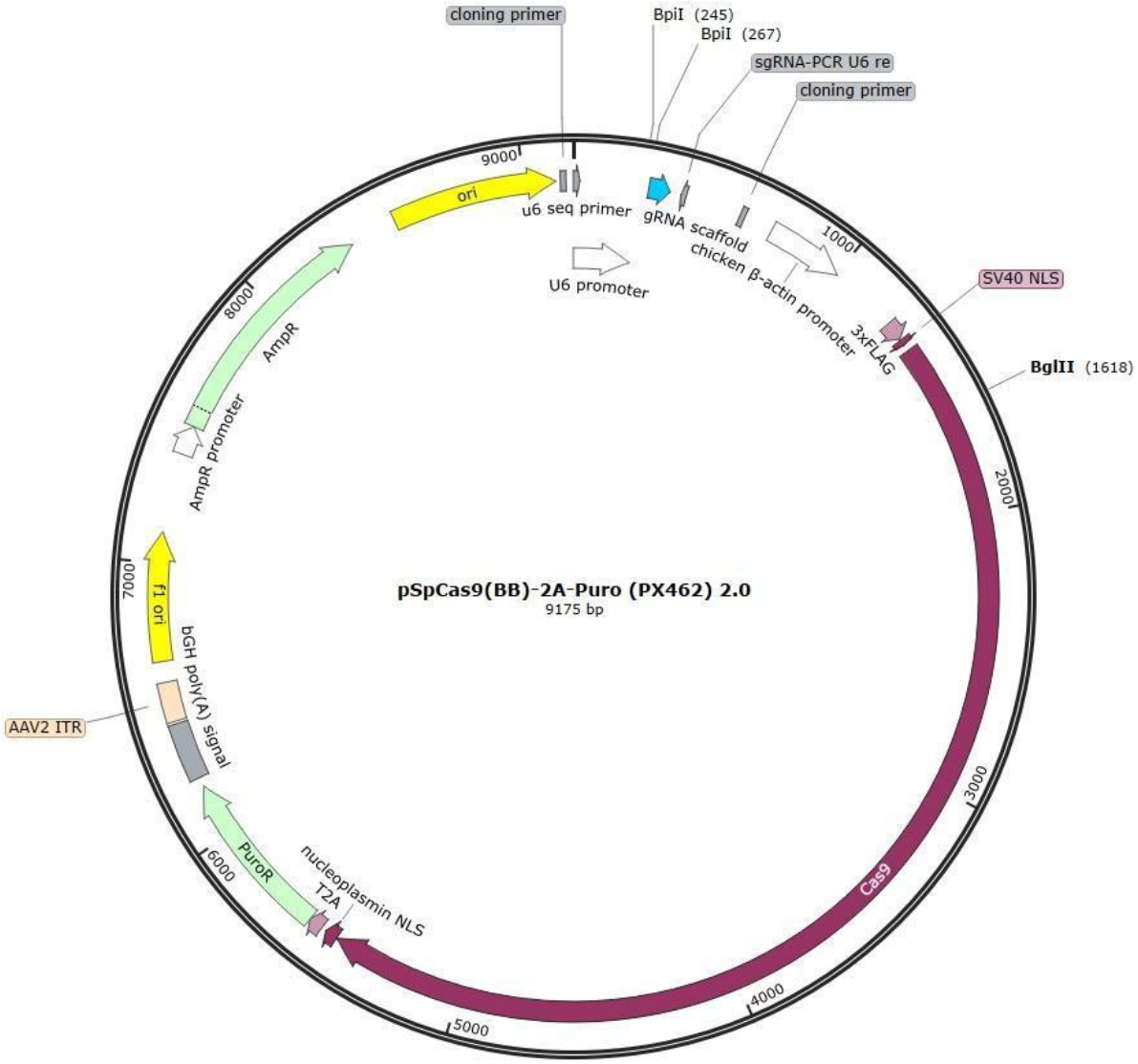

Fig S1. Gene map of pSpCas9(BB)-2A-Puro(pX462) 2.0 plasmid was used for the transfection of target cells with or without the sgRNA cloned into the indicated cloning site. Figure adapted from Snapgene.

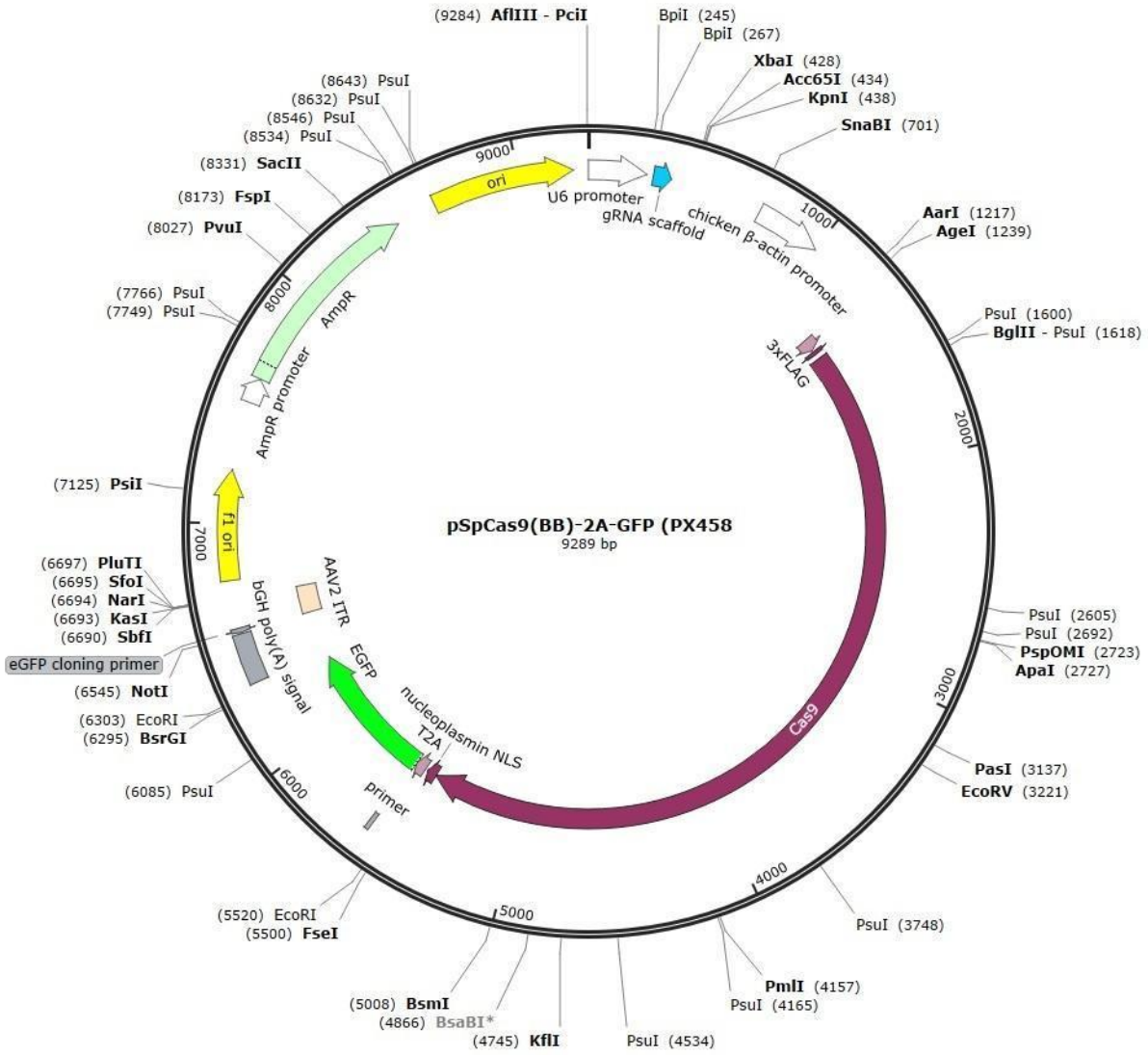

Fig S2. Gene map of pSpCas9(BB)-2A-GFP (pX458) plasmid without puromycin resistance encoding gene was used to transfect the cells and determine transfection efficiency. Figure adapted from Snapgene.

7. Bibliography

1. Sung H, Ferlay J, Siegel RL, et al. Global cancer statistics 2020: GLOBOCAN estimates of incidence and mortality worldwide for 36 cancers in 185 countries. *CA Cancer J Clin*. 2021;71(3):209-249. doi:10.3322/caac.21660
2. Siegel RL, Miller KD, Fuchs HE, Jemal A. Cancer statistics, 2022. *CA Cancer J Clin*. 2022;72(1):7-33. doi:10.3322/caac.21708
3. Bray F, Ferlay J, Soerjomataram I, Siegel RL, Torre LA, Jemal A. Global cancer statistics 2018: GLOBOCAN estimates of incidence and mortality worldwide for 36 cancers in 185 countries. *CA Cancer J Clin*. 2018;68(6):394-424. doi:10.3322/caac.21492
4. Cardona AF, Ricaurte L, Zatarain-Barrón ZL, Arrieta O. Squamous cell lung cancer: genomic evolution and personalized therapy. *Salud Publica Mex*. 2019;61(3):329-338. doi:10.21149/10115
5. Rodak O, Peris-Díaz MD, Olbromski M, Podhorska-Okołów M, Dzięgiel P. Current Landscape of Non-Small Cell Lung Cancer: Epidemiology, Histological Classification, Targeted Therapies, and Immunotherapy. *Cancers (Basel)*. 2021;13(18). doi:10.3390/cancers13184705
6. Rudin CM, Brambilla E, Faivre-Finn C, Sage J. Small-cell lung cancer. *Nat Rev Dis Primers*. 2021;7(1):3. doi:10.1038/s41572-020-00235-0
7. Sánchez-Ortega M, Carrera AC, Garrido A. Role of NRF2 in lung cancer. *Cells*. 2021;10(8). doi:10.3390/cells10081879
8. Girard L, Rodriguez-Canales J, Behrens C, et al. An Expression Signature as an Aid to the Histologic Classification of Non-Small Cell Lung Cancer. *Clin Cancer Res*. 2016;22(19):4880-4889. doi:10.1158/1078-0432.CCR-15-2900
9. Wang B-Y, Huang J-Y, Chen H-C, et al. The comparison between adenocarcinoma and squamous cell carcinoma in lung cancer patients. *J Cancer Res Clin Oncol*. 2020;146(1):43-52. doi:10.1007/s00432-019-03079-8
10. Zappa C, Mousa SA. Non-small cell lung cancer: current treatment and future advances. *Transl Lung Cancer Res*. 2016;5(3):288-300. doi:10.21037/tlcr.2016.06.07
11. Sui Q, Liang J, Hu Z, et al. Genetic and microenvironmental differences in non-smoking lung adenocarcinoma patients compared with smoking patients. *Transl Lung Cancer Res*. 2020;9(4):1407-1421. doi:10.21037/tlcr-20-276
12. Luo W, Tian P, Wang Y, et al. Characteristics of genomic alterations of lung adenocarcinoma in young never-smokers. *Int J Cancer*. 2018;143(7):1696-1705. doi:10.1002/ijc.31542
13. Bade BC, Dela Cruz CS. Lung cancer 2020: epidemiology, etiology, and prevention. *Clin Chest Med*. 2020;41(1):1-24. doi:10.1016/j.ccm.2019.10.001
14. Malhotra J, Malvezzi M, Negri E, La Vecchia C, Boffetta P. Risk factors for lung cancer worldwide. *Eur Respir J*. 2016;48(3):889-902. doi:10.1183/13993003.00359-2016
15. Gibbons DL, Byers LA, Kurie JM. Smoking, p53 mutation, and lung cancer. *Mol Cancer Res*. 2014;12(1):3-13. doi:10.1158/1541-7786.MCR-13-0539

16. Kanwal M, Ding X-J, Cao Y. Familial risk for lung cancer. *Oncol Lett*. 2017;13(2):535-542. doi:10.3892/ol.2016.5518

17. Li L, Shao M, He X, Ren S, Tian T. Risk of lung cancer due to external environmental factor and epidemiological data analysis. *Math Biosci Eng*. 2021;18(5):6079-6094. doi:10.3934/mbe.2021304

18. Shankar A, Dubey A, Saini D, et al. Environmental and occupational determinants of lung cancer. *Transl Lung Cancer Res*. 2019;8(Suppl 1):S31-S49. doi:10.21037/tlcr.2019.03.05

19. Lababede O, Meziane MA. The eighth edition of TNM staging of lung cancer: reference chart and diagrams. *Oncologist*. 2018;23(7):844-848. doi:10.1634/theoncologist.2017-0659

20. Detterbeck FC. The eighth edition TNM stage classification for lung cancer: What does it mean on main street? *J Thorac Cardiovasc Surg*. 2018;155(1):356-359. doi:10.1016/j.jtcvs.2017.08.138

21. McGranahan N, Swanton C. Clonal heterogeneity and tumor evolution: past, present, and the future. *Cell*. 2017;168(4):613-628. doi:10.1016/j.cell.2017.01.018

22. Skoulidis F, Heymach JV. Co-occurring genomic alterations in non-small-cell lung cancer biology and therapy. *Nat Rev Cancer*. 2019;19(9):495-509. doi:10.1038/s41568-019-0179-8

23. Wang Z, Xing Y, Li B, Li X, Liu B, Wang Y. Molecular pathways, resistance mechanisms and targeted interventions in non-small-cell lung cancer. *Mol Biomed*. 2022;3(1):42. doi:10.1186/s43556-022-00107-x

24. Lei Y, Lei Y, Shi X, Wang J. EML4-ALK fusion gene in non-small cell lung cancer. *Oncol Lett*. 2022;24(2):277. doi:10.3892/ol.2022.13397

25. Hamarsheh S, Groß O, Brummer T, Zeiser R. Immune modulatory effects of oncogenic KRAS in cancer. *Nat Commun*. 2020;11(1):5439. doi:10.1038/s41467-020-19288-6

26. Cox AD, Fesik SW, Kimmelman AC, Luo J, Der CJ. Drugging the undruggable RAS: Mission possible? *Nat Rev Drug Discov*. 2014;13(11):828-851. doi:10.1038/nrd4389

27. Yang Y, Zhang H, Huang S, Chu Q. KRAS mutations in solid tumors: characteristics, current therapeutic strategy, and potential treatment exploration. *J Clin Med*. 2023;12(2). doi:10.3390/jcm12020709

28. Indini A, Rijavec E, Ghidini M, Cortellini A, Grossi F. Targeting KRAS in solid tumors: current challenges and future opportunities of novel KRAS inhibitors. *Pharmaceutics*. 2021;13(5). doi:10.3390/pharmaceutics13050653

29. Moore AR, Rosenberg SC, McCormick F, Malek S. RAS-targeted therapies: is the undruggable drugged? *Nat Rev Drug Discov*. 2020;19(8):533-552. doi:10.1038/s41573-020-0068-6

30. Huang L, Guo Z, Wang F, Fu L. KRAS mutation: from undruggable to druggable in cancer. *Signal Transduct Target Ther*. 2021;6(1):386. doi:10.1038/s41392-021-00780-4

31. Ferrer I, Zugazagoitia J, Herbertz S, John W, Paz-Ares L, Schmid-Bindert G. KRAS-Mutant non-small cell lung cancer: From biology to therapy. *Lung Cancer*.

2018;124:53-64. doi:10.1016/j.lungcan.2018.07.013

32. Zhu C, Guan X, Zhang X, et al. Targeting KRAS mutant cancers: from druggable therapy to drug resistance. *Mol Cancer*. 2022;21(1):159. doi:10.1186/s12943-022-01629-2

33. Alsulaiman AS, Alharthi SB, Albariqi AS, et al. KRAS G12C-Mutant Non-Small-Cell Lung Adenocarcinoma: First Documented Report in the Arabian Gulf. *Cureus*. 2022;14(7):e27090. doi:10.7759/cureus.27090

34. Salgia R, Pharaon R, Mambetsariev I, Nam A, Sattler M. The improbable targeted therapy: KRAS as an emerging target in non-small cell lung cancer (NSCLC). *Cell Rep Med*. 2021;2(1):100186. doi:10.1016/j.xcrm.2020.100186

35. O'Sullivan É, Keogh A, Henderson B, Finn SP, Gray SG, Gately K. Treatment Strategies for KRAS-Mutated Non-Small-Cell Lung Cancer. *Cancers (Basel)*. 2023;15(6). doi:10.3390/cancers15061635

36. Walser T, Cui X, Yanagawa J, et al. Smoking and lung cancer: the role of inflammation. *Proc Am Thorac Soc*. 2008;5(8):811-815. doi:10.1513/pats.200809-100TH

37. Varghese AM, Sima CS, Chaft JE, et al. Lungs don't forget: Comparison of the KRAS and EGFR mutation profile and survival of collegiate smokers and never smokers with advanced lung cancers. *J Thorac Oncol*. 2013;8(1):123-125. doi:10.1097/JTO.0b013e31827914ea

38. Riely GJ, Kris MG, Rosenbaum D, et al. Frequency and distinctive spectrum of KRAS mutations in never smokers with lung adenocarcinoma. *Clin Cancer Res*. 2008;14(18):5731-5734. doi:10.1158/1078-0432.CCR-08-0646

39. Zhang J, Fujimoto J, Zhang J, et al. Intratumor heterogeneity in localized lung adenocarcinomas delineated by multiregion sequencing. *Science*. 2014;346(6206):256-259. doi:10.1126/science.1256930

40. Holderfield M. Efforts to develop KRAS inhibitors. *Cold Spring Harb Perspect Med*. 2018;8(7). doi:10.1101/cshperspect.a031864

41. Nakajima EC, Drezner N, Li X, et al. FDA Approval Summary: Sotorasib for KRAS G12C-Mutated Metastatic NSCLC. *Clin Cancer Res*. 2022;28(8):1482-1486. doi:10.1158/1078-0432.CCR-21-3074

42. Jänne PA, Riely GJ, Gadgeel SM, et al. Adagrasib in Non-Small-Cell Lung Cancer Harboring a KRASG12C Mutation. *N Engl J Med*. 2022;387(2):120-131. doi:10.1056/NEJMoa2204619

43. Dhillon S. Adagrasib: First Approval. *Drugs*. 2023;83(3):275-285. doi:10.1007/s40265-023-01839-y

44. Wang Y, Zhang H, Li J, Niu M-M, Zhou Y, Qu Y. Discovery of potent and noncovalent KRASG12D inhibitors: Structure-based virtual screening and biological evaluation. *Front Pharmacol*. 2022;13:1094887. doi:10.3389/fphar.2022.1094887

45. Kemp SB, Cheng N, Markosyan N, et al. Efficacy of a Small-Molecule Inhibitor of KrasG12D in Immunocompetent Models of Pancreatic Cancer. *Cancer Discov*. 2023;13(2):298-311. doi:10.1158/2159-8290.CD-22-1066

46. Hyun S, Shin D. Small-Molecule Inhibitors and Degraders Targeting KRAS-Driven

Cancers. *Int J Mol Sci*. 2021;22(22). doi:10.3390/ijms222212142

47. Tomasini P, Walia P, Labbe C, Jao K, Leighl NB. Targeting the KRAS Pathway in Non-Small Cell Lung Cancer. *Oncologist*. 2016;21(12):1450-1460. doi:10.1634/theoncologist.2015-0084

48. Alam M, Hasan GM, Eldin SM, et al. Investigating regulated signaling pathways in therapeutic targeting of non-small cell lung carcinoma. *Biomed Pharmacother*. 2023;161:114452. doi:10.1016/j.biopha.2023.114452

49. Ghimessy A, Radeczky P, Laszlo V, et al. Current therapy of KRAS-mutant lung cancer. *Cancer Metastasis Rev*. 2020;39(4):1159-1177. doi:10.1007/s10555-020-09903-9

50. Ramalingam SS, Vansteenkiste J, Planchard D, et al. Overall Survival with Osimertinib in Untreated, EGFR-Mutated Advanced NSCLC. *N Engl J Med*. 2020;382(1):41-50. doi:10.1056/NEJMoa1913662

51. O'Rourke N, Roqué I Figuls M, Farré Bernadó N, Macbeth F. Concurrent chemoradiotherapy in non-small cell lung cancer. *Cochrane Database Syst Rev*. 2010;(6):CD002140. doi:10.1002/14651858.CD002140.pub3

52. Nagasaka M, Gadgeel SM. Role of chemotherapy and targeted therapy in early-stage non-small cell lung cancer. *Expert Rev Anticancer Ther*. 2018;18(1):63-70. doi:10.1080/14737140.2018.1409624

53. Reita D, Pabst L, Pencreach E, et al. Direct Targeting KRAS Mutation in Non-Small Cell Lung Cancer: Focus on Resistance. *Cancers (Basel)*. 2022;14(5). doi:10.3390/cancers14051321

54. Kwan AK, Piazza GA, Keeton AB, Leite CA. The path to the clinic: a comprehensive review on direct KRASG12C inhibitors. *J Exp Clin Cancer Res*. 2022;41(1):27. doi:10.1186/s13046-021-02225-w

55. Walsh RJ, Soo RA. Resistance to immune checkpoint inhibitors in non-small cell lung cancer: biomarkers and therapeutic strategies. *Ther Adv Med Oncol*. 2020;12:1758835920937902. doi:10.1177/1758835920937902

56. Shen Y, Chen J, Li X-P. Research advances in immune checkpoint drugs for non-small cell lung cancer. *J Drug Target*. July 7, 2023:1-44. doi:10.1080/1061186X.2023.2235098

57. Dantoing E, Piton N, Salaün M, Thiberville L, Guisier F. Anti-PD1/PD-L1 Immunotherapy for Non-Small Cell Lung Cancer with Actionable Oncogenic Driver Mutations. *Int J Mol Sci*. 2021;22(12). doi:10.3390/ijms22126288

58. Baghban R, Roshangar L, Jahanban-Esfahlan R, et al. Tumor microenvironment complexity and therapeutic implications at a glance. *Cell Commun Signal*. 2020;18(1):59. doi:10.1186/s12964-020-0530-4

59. Polyak K, Haviv I, Campbell IG. Co-evolution of tumor cells and their microenvironment. *Trends Genet*. 2009;25(1):30-38. doi:10.1016/j.tig.2008.10.012

60. Anichini A, Perotti VE, Sgambelluri F, Mortarini R. Immune escape mechanisms in non small cell lung cancer. *Cancers (Basel)*. 2020;12(12). doi:10.3390/cancers12123605

61. Quail DF, Joyce JA. Microenvironmental regulation of tumor progression and

metastasis. *Nat Med*. 2013;19(11):1423-1437. doi:10.1038/nm.3394

62. Hanahan D. Hallmarks of cancer: New Dimensions. *Cancer Discov*. 2022;12(1):31-46. doi:10.1158/2159-8290.CD-21-1059

63. Mantovani A, Allavena P, Sica A, Balkwill F. Cancer-related inflammation. *Nature*. 2008;454(7203):436-444. doi:10.1038/nature07205

64. O'Callaghan DS, O'Donnell D, O'Connell F, O'Byrne KJ. The role of inflammation in the pathogenesis of non-small cell lung cancer. *J Thorac Oncol*. 2010;5(12):2024-2036. doi:10.1097/jto.0b013e3181f387e4

65. Oeckinghaus A, Ghosh S. The NF-kappaB family of transcription factors and its regulation. *Cold Spring Harb Perspect Biol*. 2009;1(4):a000034. doi:10.1101/cshperspect.a000034

66. Sun S-C, Chang J-H, Jin J. Regulation of nuclear factor-κB in autoimmunity. *Trends Immunol*. 2013;34(6):282-289. doi:10.1016/j.it.2013.01.004

67. Beinke S, Ley SC. Functions of NF-kappaB1 and NF-kappaB2 in immune cell biology. *Biochem J*. 2004;382(Pt 2):393-409. doi:10.1042/BJ20040544

68. Liu T, Zhang L, Joo D, Sun S-C. NF-κB signaling in inflammation. *Signal Transduct Target Ther*. 2017;2:17023. doi:10.1038/sigtrans.2017.23

69. Zhang H, Sun S-C. NF-κB in inflammation and renal diseases. *Cell Biosci*. 2015;5:63. doi:10.1186/s13578-015-0056-4

70. Sun S-C. Non-canonical NF-κB signaling pathway. *Cell Res*. 2011;21(1):71-85. doi:10.1038/cr.2010.177

71. Cildir G, Low KC, Tergaonkar V. Noncanonical NF-κB Signaling in Health and Disease. *Trends Mol Med*. 2016;22(5):414-429. doi:10.1016/j.molmed.2016.03.002

72. Taniguchi K, Karin M. NF-κB, inflammation, immunity and cancer: coming of age. *Nat Rev Immunol*. 2018;18(5):309-324. doi:10.1038/nri.2017.142

73. Krappmann D, Vincendeau M. Mechanisms of NF-κB deregulation in lymphoid malignancies. *Semin Cancer Biol*. 2016;39:3-14. doi:10.1016/j.semcancer.2016.05.002

74. Pak C, Miyamoto S. A new alpha in line between KRAS and NF-κB activation? *Cancer Discov*. 2013;3(6):613-615. doi:10.1158/2159-8290.CD-13-0193

75. Mizumoto Y, Kyo S, Kiyono T, et al. Activation of NF-kappaB is a novel target of KRAS-induced endometrial carcinogenesis. *Clin Cancer Res*. 2011;17(6):1341-1350. doi:10.1158/1078-0432.CCR-10-2291

76. Meylan E, Dooley AL, Feldser DM, et al. Requirement for NF-kappaB signalling in a mouse model of lung adenocarcinoma. *Nature*. 2009;462(7269):104-107. doi:10.1038/nature08462

77. Bassères DS, Ebbs A, Levantini E, Baldwin AS. Requirement of the NF-kappaB subunit p65/RelA for K-Ras-induced lung tumorigenesis. *Cancer Res*. 2010;70(9):3537-3546. doi:10.1158/0008-5472.CAN-09-4290

78. Bassères DS, Ebbs A, Cogswell PC, Baldwin AS. IKK is a therapeutic target in KRAS-Induced lung cancer with disrupted p53 activity. *Genes Cancer*. 2014;5(1-2):41-55. doi:10.18632/genesandcancer.5

79. Opipari AW, Boguski MS, Dixit VM. The A20 cDNA induced by tumor necrosis factor alpha encodes a novel type of zinc finger protein. *J Biol Chem*. 1990;265(25):14705-14708.

80. Opipari AW, Hu HM, Yabkowitz R, Dixit VM. The A20 zinc finger protein protects cells from tumor necrosis factor cytotoxicity. *J Biol Chem*. 1992;267(18):12424-12427. doi:10.1016/S0021-9258(18)42292-2

81. Shi Y, Wang X, Wang J, Wang X, Zhou H, Zhang L. The dual roles of A20 in cancer. *Cancer Lett*. 2021;511:26-35. doi:10.1016/j.canlet.2021.04.017

82. Wertz I, Dixit V. A20--a bipartite ubiquitin editing enzyme with immunoregulatory potential. *Adv Exp Med Biol*. 2014;809:1-12. doi:10.1007/978-1-4939-0398-6_1

83. Malynn BA, Ma A. A20: A multifunctional tool for regulating immunity and preventing disease. *Cell Immunol*. 2019;340:103914. doi:10.1016/j.cellimm.2019.04.002

84. Das T, Chen Z, Hendriks RW, Kool M. A20/Tumor Necrosis Factor α-Induced Protein 3 in Immune Cells Controls Development of Autoinflammation and Autoimmunity: Lessons from Mouse Models. *Front Immunol*. 2018;9:104. doi:10.3389/fimmu.2018.00104

85. Lin S-C, Chung JY, Lamothe B, et al. Molecular basis for the unique deubiquitinating activity of the NF-kappaB inhibitor A20. *J Mol Biol*. 2008;376(2):526-540. doi:10.1016/j.jmb.2007.11.092

86. Komander D, Barford D. Structure of the A20 OTU domain and mechanistic insights into deubiquitination. *Biochem J*. 2008;409(1):77-85. doi:10.1042/BJ20071399

87. Bosanac I, Wertz IE, Pan B, et al. Ubiquitin binding to A20 ZnF4 is required for modulation of NF-κB signaling. *Mol Cell*. 2010;40(4):548-557. doi:10.1016/j.molcel.2010.10.009

88. Verhelst K, Carpentier I, Kreike M, et al. A20 inhibits LUBAC-mediated NF-κB activation by binding linear polyubiquitin chains via its zinc finger 7. *EMBO J*. 2012;31(19):3845-3855. doi:10.1038/emboj.2012.240

89. Malynn BA, Ma A. A20 takes on tumors: tumor suppression by an ubiquitin-editing enzyme. *J Cell Biol*. 2009;185(3):i3-i3. doi:10.1083/JCB1853OIA3

90. Heyninck K, Beyaert R. A20 inhibits NF-kappaB activation by dual ubiquitin-editing functions. *Trends Biochem Sci*. 2005;30(1):1-4. doi:10.1016/j.tibs.2004.11.001

91. Bellail AC, Olson JJ, Yang X, Chen ZJ, Hao C. A20 ubiquitin ligase-mediated polyubiquitination of RIP1 inhibits caspase-8 cleavage and TRAIL-induced apoptosis in glioblastoma. *Cancer Discov*. 2012;2(2):140-155. doi:10.1158/2159-8290.CD-11-0172

92. Onizawa M, Oshima S, Schulze-Topphoff U, et al. The ubiquitin-modifying enzyme A20 restricts ubiquitination of the kinase RIPK3 and protects cells from necroptosis. *Nat Immunol*. 2015;16(6):618-627. doi:10.1038/ni.3172

93. De Valck D, Heyninck K, Van Criekinge W, Contreras R, Beyaert R, Fiers W. A20, an inhibitor of cell death, self-associates by its zinc finger domain. *FEBS Lett*. 1996;384(1):61-64. doi:10.1016/0014-5793(96)00283-9

94. Martens A, van Loo G. A20 at the crossroads of cell death, inflammation, and autoimmunity. *Cold Spring Harb Perspect Biol*. 2020;12(1).

doi:10.1101/cshperspect.a036418

95. Duong BH, Onizawa M, Oses-Prieto JA, et al. A20 restricts ubiquitination of pro-interleukin-1β protein complexes and suppresses NLRP3 inflammasome activity. *Immunity*. 2015;42(1):55-67. doi:10.1016/j.immuni.2014.12.031

96. Vande Walle L, Van Opdenbosch N, Jacques P, et al. Negative regulation of the NLRP3 inflammasome by A20 protects against arthritis. *Nature*. 2014;512(7512):69-73. doi:10.1038/nature13322

97. Shao L, Oshima S, Duong B, et al. A20 restricts wnt signaling in intestinal epithelial cells and suppresses colon carcinogenesis. *PLoS ONE*. 2013;8(5):e62223. doi:10.1371/journal.pone.0062223

98. Nakamura BN, Glazier A, Kattah MG, et al. A20 regulates canonical wnt-signaling through an interaction with RIPK4. *PLoS ONE*. 2018;13(5):e0195893. doi:10.1371/journal.pone.0195893

99. Parvatiyar K, Barber GN, Harhaj EW. TAX1BP1 and A20 inhibit antiviral signaling by targeting TBK1-IKKi kinases. *J Biol Chem*. 2010;285(20):14999-15009. doi:10.1074/jbc.M110.109819

100. Shi C-S, Kehrl JH. TRAF6 and A20 regulate lysine 63-linked ubiquitination of Beclin-1 to control TLR4-induced autophagy. *Sci Signal*. 2010;3(123):ra42. doi:10.1126/scisignal.2000751

101. Lee EG, Boone DL, Chai S, et al. Failure to regulate TNF-induced NF-kappaB and cell death responses in A20-deficient mice. *Science*. 2000;289(5488):2350-2354. doi:10.1126/science.289.5488.2350

102. Guedes RP, Csizmadia E, Moll HP, Ma A, Ferran C, da Silva CG. A20 deficiency causes spontaneous neuroinflammation in mice. *J Neuroinflammation*. 2014;11:122. doi:10.1186/1742-2094-11-122

103. Studer P, da Silva CG, Revuelta Cervantes JM, et al. Significant lethality following liver resection in A20 heterozygous knockout mice uncovers a key role for A20 in liver regeneration. *Cell Death Differ*. 2015;22(12):2068-2077. doi:10.1038/cdd.2015.52

104. Moll HP, Lee A, Minussi DC, et al. A20 regulates atherogenic interferon (IFN)-γ signaling in vascular cells by modulating basal IFNβ levels. *J Biol Chem*. 2014;289(45):30912-30924. doi:10.1074/jbc.M114.591966

105. Yu M-P, Xu X-S, Zhou Q, Deuitch N, Lu M-P. Haploinsufficiency of A20 (HA20): updates on the genetics, phenotype, pathogenesis and treatment. *World J Pediatr*. 2020;16(6):575-584. doi:10.1007/s12519-019-00288-6

106. Aeschlimann FA, Batu ED, Canna SW, et al. A20 haploinsufficiency (HA20): clinical phenotypes and disease course of patients with a newly recognised NF-kB-mediated autoinflammatory disease. *Ann Rheum Dis*. 2018;77(5):728-735. doi:10.1136/annrheumdis-2017-212403

107. Duncan CJA, Dinnigan E, Theobald R, et al. Early-onset autoimmune disease due to a heterozygous loss-of-function mutation in TNFAIP3 (A20). *Ann Rheum Dis*. 2018;77(5):783-786. doi:10.1136/annrheumdis-2016-210944

108. Rajamäki K, Keskitalo S, Seppänen M, et al. Haploinsufficiency of A20 impairs protein-protein interactome and leads into caspase-8-dependent enhancement of

NLRP3 inflammasome activation. *RMD Open*. 2018;4(2):e000740. doi:10.1136/rmdopen-2018-000740

109. Shimizu M, Matsubayashi T, Ohnishi H, et al. Haploinsufficiency of A20 with a novel mutation of deletion of exons 2-3 of TNFAIP3. *Mod Rheumatol*. 2021;31(2):493-497. doi:10.1080/14397595.2020.1719595

110. Zhou Q, Wang H, Schwartz DM, et al. Loss-of-function mutations in TNFAIP3 leading to A20 haploinsufficiency cause an early-onset autoinflammatory disease. *Nat Genet*. 2016;48(1):67-73. doi:10.1038/ng.3459

111. Adrianto I, Wen F, Templeton A, et al. Association of a functional variant downstream of TNFAIP3 with systemic lupus erythematosus. *Nat Genet*. 2011;43(3):253-258. doi:10.1038/ng.766

112. Boonyasrisawat W, Eberle D, Bacci S, et al. Tag polymorphisms at the A20 (TNFAIP3) locus are associated with lower gene expression and increased risk of coronary artery disease in type 2 diabetes. *Diabetes*. 2007;56(2):499-505. doi:10.2337/db06-0946

113. Graham RR, Cotsapas C, Davies L, et al. Genetic variants near TNFAIP3 on 6q23 are associated with systemic lupus erythematosus. *Nat Genet*. 2008;40(9):1059-1061. doi:10.1038/ng.200

114. Sokhi UK, Liber MP, Frye L, et al. Dissection and function of autoimmunity-associated TNFAIP3 (A20) gene enhancers in humanized mouse models. *Nat Commun*. 2018;9(1):658. doi:10.1038/s41467-018-03081-7

115. Catrysse L, Vereecke L, Beyaert R, van Loo G. A20 in inflammation and autoimmunity. *Trends Immunol*. 2014;35(1):22-31. doi:10.1016/j.it.2013.10.005

116. Ma A, Malynn BA. A20: linking a complex regulator of ubiquitylation to immunity and human disease. *Nat Rev Immunol*. 2012;12(11):774-785. doi:10.1038/nri3313

117. Kato M, Sanada M, Kato I, et al. Frequent inactivation of A20 in B-cell lymphomas. *Nature*. 2009;459(7247):712-716. doi:10.1038/nature07969

118. Braun FCM, Grabarczyk P, Möbs M, et al. Tumor suppressor TNFAIP3 (A20) is frequently deleted in Sézary syndrome. *Leukemia*. 2011;25(9):1494-1501. doi:10.1038/leu.2011.101

119. Bavi P, Abubaker J, Al-Sanea N, et al. Clinico-pathological significance of TNF alpha-induced protein3 (TNFAIP3) in Middle Eastern colorectal carcinoma. *Clin Epigenetics*. 2011;2(2):417-418. doi:10.1007/s13148-011-0049-z

120. Chen H, Hu L, Luo Z, et al. A20 suppresses hepatocellular carcinoma proliferation and metastasis through inhibition of Twist1 expression. *Mol Cancer*. 2015;14:186. doi:10.1186/s12943-015-0454-6

121. Breitenecker K, Homolya M, Luca AC, et al. Down-regulation of A20 promotes immune escape of lung adenocarcinomas. *Sci Transl Med*. 2021;13(601). doi:10.1126/scitranslmed.abc3911

122. Langsch S, Baumgartner U, Haemmig S, et al. miR-29b Mediates NF-κB Signaling in KRAS-Induced Non-Small Cell Lung Cancers. *Cancer Res*. 2016;76(14):4160-4169. doi:10.1158/0008-5472.CAN-15-2580

123. Vendrell JA, Ghayad S, Ben-Larbi S, Dumontet C, Mechti N, Cohen PA.

A20/TNFAIP3, a new estrogen-regulated gene that confers tamoxifen resistance in breast cancer cells. *Oncogene*. 2007;26(32):4656-4667. doi:10.1038/sj.onc.1210269

124. Yoon CI, Ahn SG, Bae SJ, et al. High A20 expression negatively impacts survival in patients with breast cancer. *PLoS ONE*. 2019;14(8):e0221721. doi:10.1371/journal.pone.0221721

125. Wisnieski F, Santos LC, Calcagno DQ, et al. The impact of DNA demethylation on the upregulation of the NRN1 and TNFAIP3 genes associated with advanced gastric cancer. *J Mol Med*. 2020;98(5):707-717. doi:10.1007/s00109-020-01902-1

126. Guo Q, Dong H, Liu X, et al. A20 is overexpressed in glioma cells and may serve as a potential therapeutic target. *Expert Opin Ther Targets*. 2009;13(7):733-741. doi:10.1517/14728220903045018

127. Codd JD, Salisbury JR, Packham G, Nicholson LJ. A20 RNA expression is associated with undifferentiated nasopharyngeal carcinoma and poorly differentiated head and neck squamous cell carcinoma. *J Pathol*. 1999;187(5):549-555. doi:10.1002/(SICI)1096-9896(199904)187:5<549::AID-PATH278>3.0.CO;2-O

128. Wang L, Hong B, Jiang X, Jones L, Chen S-Y, Huang XF. A20 controls macrophage to elicit potent cytotoxic CD4(+) T cell response. *PLoS ONE*. 2012;7(11):e48930. doi:10.1371/journal.pone.0048930

129. Shao B, Wei X, Luo M, et al. Inhibition of A20 expression in tumor microenvironment exerts anti-tumor effect through inducing myeloid-derived suppressor cells apoptosis. *Sci Rep*. 2015;5:16437. doi:10.1038/srep16437

130. Vetters J, van Helden MJ, Wahlen S, et al. The ubiquitin-editing enzyme A20 controls NK cell homeostasis through regulation of mTOR activity and TNF. *J Exp Med*. 2019;216(9):2010-2023. doi:10.1084/jem.20182164

131. Song X-T, Evel-Kabler K, Shen L, Rollins L, Huang XF, Chen S-Y. A20 is an antigen presentation attenuator, and its inhibition overcomes regulatory T cell-mediated suppression. *Nat Med*. 2008;14(3):258-265. doi:10.1038/nm1721

132. Hannani D, Leplus E, Laurin D, et al. A New Plasmacytoid Dendritic Cell-Based Vaccine in Combination with Anti-PD-1 Expands the Tumor-Specific CD8+ T Cells of Lung Cancer Patients. *Int J Mol Sci*. 2023;24(3). doi:10.3390/ijms24031897

133. Stevens D, Ingels J, Van Lint S, Vandekerckhove B, Vermaelen K. Dendritic Cell-Based Immunotherapy in Lung Cancer. *Front Immunol*. 2020;11:620374. doi:10.3389/fimmu.2020.620374

134. Düwel M, Welteke V, Oeckinghaus A, et al. A20 negatively regulates T cell receptor signaling to NF-kappaB by cleaving Malt1 ubiquitin chains. *J Immunol*. 2009;182(12):7718-7728. doi:10.4049/jimmunol.0803313

135. Giordano M, Roncagalli R, Bourdely P, et al. The tumor necrosis factor alpha-induced protein 3 (TNFAIP3, A20) imposes a brake on antitumor activity of CD8 T cells. *Proc Natl Acad Sci USA*. 2014;111(30):11115-11120. doi:10.1073/pnas.1406259111

136. Zhou S, Yang H. Immunotherapy resistance in non-small-cell lung cancer: From mechanism to clinical strategies. *Front Immunol*. 2023;14:1129465. doi:10.3389/fimmu.2023.1129465

137. DuPage M, Dooley AL, Jacks T. Conditional mouse lung cancer models using adenoviral or lentiviral delivery of Cre recombinase. *Nat Protoc*.

2009;4(7):1064-1072. doi:10.1038/nprot.2009.95

138. Moll HP, Mohrherr J, Breitenecker K, Haber M, Voronin V, Casanova E. Orthotopic Transplantation of Syngeneic Lung Adenocarcinoma Cells to Study PD-L1 Expression. *J Vis Exp*. 2019;(143). doi:10.3791/58101

139. Arguello M, Paz S, Ferran C, Moll HP, Hiscott J. Anti-viral tetris: modulation of the innate anti-viral immune response by A20. *Adv Exp Med Biol*. 2014;809:49-64. doi:10.1007/978-1-4939-0398-6_4

140. Abe T, Fujimori T. Reporter mouse lines for fluorescence imaging. *Dev Growth Differ*. 2013;55(4):390-405. doi:10.1111/dgd.12062

141. Brinkman EK, Chen T, Amendola M, van Steensel B. Easy quantitative assessment of genome editing by sequence trace decomposition. *Nucleic Acids Res*. 2014;42(22):e168. doi:10.1093/nar/gku936

142. Dobin A, Davis CA, Schlesinger F, et al. STAR: ultrafast universal RNA-seq aligner. *Bioinformatics*. 2013;29(1):15-21. doi:10.1093/bioinformatics/bts635

143. Love MI, Huber W, Anders S. Moderated estimation of fold change and dispersion for RNA-seq data with DESeq2. *Genome Biol*. 2014;15(12):550. doi:10.1186/s13059-014-0550-8

144. Babicki S, Arndt D, Marcu A, et al. Heatmapper: web-enabled heat mapping for all. *Nucleic Acids Res*. 2016;44(W1):W147–W153. doi:10.1093/nar/gkw419

145. Pfaffl MW. A new mathematical model for relative quantification in real-time RT-PCR. *Nucleic Acids Res*. 2001;29(9):e45. doi:10.1093/nar/29.9.e45

146. Rao X, Huang X, Zhou Z, Lin X. An improvement of the 2ˆ(-delta delta CT) method for quantitative real-time polymerase chain reaction data analysis. *Biostat Bioinforma Biomath*. 2013;3(3):71-85.

147. Ran FA, Hsu PD, Wright J, Agarwala V, Scott DA, Zhang F. Genome engineering using the CRISPR-Cas9 system. *Nat Protoc*. 2013;8(11):2281-2308. doi:10.1038/nprot.2013.143

148. Garcia-Gonzalez I, Benedito R. Intricacies of conditional genetics in vascular biology. *Curr Opin Hematol*. 2021;28(3):189-197. doi:10.1097/MOH.0000000000000646

149. Kim H, Kim M, Im S-K, Fang S. Mouse Cre-LoxP system: general principles to determine tissue-specific roles of target genes. *Lab Anim Res*. 2018;34(4):147-159. doi:10.5625/lar.2018.34.4.147

150. Shi J, Petrie HT. Activation kinetics and off-target effects of thymus-initiated cre transgenes. *PLoS ONE*. 2012;7(10):e46590. doi:10.1371/journal.pone.0046590

151. Hanahan D, Weinberg RA. Hallmarks of cancer: the next generation. *Cell*. 2011;144(5):646-674. doi:10.1016/j.cell.2011.02.013

152. Hameyer D, Loonstra A, Eshkind L, et al. Toxicity of ligand-dependent Cre recombinases and generation of a conditional Cre deleter mouse allowing mosaic recombination in peripheral tissues. *Physiol Genomics*. 2007;31(1):32-41. doi:10.1152/physiolgenomics.00019.2007

153. Ben Khelil M, Godet Y, Abdeljaoued S, Borg C, Adotévi O, Loyon R. Harnessing antitumor CD4+ T cells for cancer immunotherapy. *Cancers (Basel)*. 2022;14(1). doi:10.3390/cancers14010260

154. Ostroumov D, Fekete-Drimusz N, Saborowski M, Kühnel F, Woller N. CD4 and CD8 T lymphocyte interplay in controlling tumor growth. *Cell Mol Life Sci*. 2018;75(4):689-713. doi:10.1007/s00018-017-2686-7